van Belle, Gerard T., Angular Size Measurements of Highly Evolved Stars, Ph.D., Department of Physics and Astronomy, December, 1996.

This dissertation describes (i) development of hardware and software for the Infrared Optical Telescope Array (IOTA) interferometer, (ii) use of IOTA to study highly evolved stars. IOTA is a two telescope Michelson stellar interferometer capable of measuring the angular sizes of bright stars down to 4.5 milliarcseconds. During the course of the dissertation research, angular diameters were obtained for over 80 stars in late stages of stellar evolution, such as giants, supergiants, carbon stars and Mira variables. From these diameters, effective temperatures and linear sizes were calculated for oxygen-rich, S-type and carbon stars, for both Mira variables and non-Miras. For oxygen-rich giants and carbon stars, the effective temperatures were correlated with spectral types. For oxygen-rich Mira variables, the periodic behavior of their linear sizes and effective temperatures was established. Utilization of these basic parameters opened the door to more complicated investigations of stellar physics, including: oxygen-rich Mira variable pulsation mode, and relative mass loss rates between the chemical abundance types.

ANGULAR SIZE MEASUREMENTS OF HIGHLY EVOLVED STARS

by
Gerard T. van Belle

A dissertation
submitted to The Department of Physics and Astronomy
and The Graduate School of the University of Wyoming in Partial Fulfillment of
Requirements for the Degree of

DOCTOR OF PHILOSOPHY
in
PHYSICS

Laramie, Wyoming
December, 1996

TO THE GRADUATE SCHOOL:

The members of the Committee approve the dissertation of Gerard T. van Belle presented on October 29, 1996.

_____

H. M. Dyck, Chairman

_____

R.W. Canterna

_____

R.R. Howell

_____

S.T. Ridgway

_____

E.J. Spillar

_____

D. E. Walrath

APPROVED:

_____

Lee H. Schick, Head, Department of Physics and Astronomy

_____

Donald S. Warder, Dean of Graduate School

TABLE OF CONTENTS

LIST OF TABLES

LIST OF FIGURES

ACKNOWLEDGMENTS

Many people played a part in substantially improving the quality of this dissertation, both directly and indirectly. I would like to thank David Ciardi for insightful comments & conversations; Jim Benson and Bob Thompson for productive observing runs; and Ron Canterna for generous use of computer resources.

This thesis benefitted greatly from fruitful discussions with Chris Haniff, Peter Hauschildt, Michael Scholz, Peter Tuthill, and Lee Anne Willson. Many thanks to the staffs of the F.L. Whipple Observatory and of the IOTA project office, particularly Wes Traub and Marc Lacasse. My appreciation to the Santa Barbara Instrument Group for its swift and cordial product support. In this research, we have used, and acknowledge with thanks, data from the AAVSO International Database, and the SIMBAD/AFOEV databases at the CDS in Strasbourg, France. Funding for this research was provided in part by NASA Grant NGT-40050 to Wyoming Planetary and Space Science Center, and NSF grant AST-9021181.

Most of all, I would like to acknowledge a deep debt of gratitude to my advisor, Mel Dyck. His expertise, instruction and trust are all reflected in any merit that this dissertation might possess.

PREFACE

This dissertation describes high resolution astronomical research conducted at the IR Optical Telescope Array (IOTA). During the course of dissertation research, four refereed publications were produced, and have been included here in their entirety. University regulations require that manuscripts rather than reprints be used, and that the manuscripts be presented without their original title pages or abstracts. Chapters IV thru VII are the manuscripts to van Belle *et al.* (1997), Dyck *et al*. (1996a), Dyck *et al*. (1996b), and van Belle *et al*. (1996) respectively.

Astronomy compels the soul to look upwards and leads us from this world to another. - Plato, *The Republic.*

Pulsing with brightness as with some unbearable pain or pleasure, clustered in pathless and countless multitudes, dreamlike in clarity, blazing in perfect blackness, the stars seized all his attention, troubled him, excited him, and drew him up... - C.S. Lewis, *Out of the Silent Planet.*

CHAPTER I

INTRODUCTION

1.1 Introduction

This dissertation describes research performed at the Infrared Optical Telescope Array (IOTA). IOTA is an interferometric telescope providing roughly two orders of magnitude improvement in spatial resolution over traditional single aperture telescopes. The unique capabilities of this instrument have been utilized over the course of this dissertation to explore the basic parameters of highly evolved stellar objects.

The first three chapters of this dissertation will introduce the topic of interferometry, both in general and as specifically applied at IOTA. The appropriate historical context which frames this research is given in §1, along with an outline of the accomplishments of the dissertation. Some pertinent interferometric theory is given in §2, and a description of the instrument is presented in §3.

1.2 Historical Background

1.2.1 Single Aperture Telescopes

In order to cast the accomplishments of this dissertation in proper context, it would be instructive to briefly examine the history of the telescope, paying particular attention to developments in telescope technology. The first telescopes turned to astronomical use were those of Galileo Galilei, who in 1609 began a revolution in astronomy through the application of telescope technology. At the turn of the present century, telescope technology had advanced such that the largest telescope in the world was a the Yerkes 40" refractor. This instrument was brought into being by George

Ellery Hale, who over the course of his life initiated three subsequent projects resulting in what was at the time the world's largest telescope (Abell, Morrison & Wolff 1987). The completion of the 5m Hale telescope on Mount Palomar in 1948 represented the culmination of classical telescope design, and the realistic upper limit to aperture size in the lack of advanced technologies. A more complete discussion of the history of classical telescopes can be found in King (1979).

The last two decades have seen significant advances in technologies pertinent to telescope construction and operation. Manufacturing advances have allowed for the construction of enormous mirrors; design advances have solved long-standing problems in mirror support and dome construction; and advances in electronics technology have improved telescope control and detector technology. Truly giant telescopes have become not only practical but also cost effective; as a result, a new generation of 8-10m class telescopes is coming on line (Angel 1990).

As the size of telescopes grows, their ability to collect light from the skies increases as the square of the aperture radius. In the absence of atmospheric distortion, the larger the telescope, the better its ability to resolve finer detail. The theoretical resolution limit of a telescope is classically defined by the Airy pattern resulting from its size, D, and the wavelength λ at which it is operating:

$$\theta\,[arcsec] = A x \frac{\lambda\,[\mu m]}{D\,[m]},$$

where A is on the order of one-half (Born & Wolf 1980). However, in the absence of sophisticated techniques, the *actual* limit of a telescope's resolving power is defined by

atmospheric seeing. This phenomenon limits a telescope of any size to typically a resolution of 1".0, with the best nights at the best sites no better than 0".25 (Dyck & Howell 1983). For a review on seeing, see Coulman (1985).

The limitations of the atmosphere were investigated by Fried (1966), who characterized the turbulent atmosphere in an effort to define atmospheric resolution limits. Speckle interferometry was proposed by Laberyrie (1970) as a means to recover at least some of the spatial frequency information afforded by large apertures; application of the technique demonstrated its viability (Gezari, Labeyrie & Stachnik 1972). Discussions of the merits and limitations of speckle interferometry can be found in Korff (1973) and Labeyrie (1978); a bibliography of speckle papers can be found in Dainty (1981). As is discussed in Korff (1973), speckle is limited in that it does not recover phase information of the object being observed; that is to say, a full reconstruction of the original image is not possible due to the fact that information has been lost.

As such, giant and even moderate aperture telescopes are significantly limited in their ability to resolve small objects or fine structure in larger ones. Furthermore, even in the absence of the atmosphere, even the largest telescopes are only barely of sufficient resolving power to begin to tackle many problems of astrophysical interest: angular sizes of stars, stellar surface brightness distribution, extrasolar planet detection, galactic & extragalactic distances, to name a few.

1.2.2 Interferometry

As a means to overcome the resolution limitations of single aperture telescopes, interferometry has come to be utilized in the last ten years as a viable approach to achieve extremely high spatial resolution in the optical and infrared wavelength regimes. Just as with giant aperture telescopes, the technique of utilizing arrays of telescopes has also benefited from the recent advances in technology. Interferometry has been used in the radio for a number a decades, and many techniques are well-defined at this point.

The resolution of a simple two-element interferometer can be estimated by using an equation similar to (1); rather than the diameter aperture D being the significant factor, it is the separation B of the two apertures:

$$\theta\,[arcsec] = Ax\frac{\lambda\,[\,\mu m]}{B\,[m]}.$$

Since it can be possible to work in a regime that surpasses the Airy criterion, the value of A is on order of one tenth. This resolution regime is dependent upon certain assumptions about the source being observed, which are quite straightforward (e.g. stars are generally round). The specific assumptions invoked in this dissertation will be discussed in detail in subsequent chapters.

Use of separated apertures to achieve increased spatial resolution was first suggested by Fizeau (1868); the first unsuccessful attempts at applying the technique were made shortly thereafter (Stèephan 1873,1874). Michelson (1890) reexamined the method as an approach for measuring stellar angular diameters; a year later he had successfully utilized it in measuring the diameters of the Galilean moons (Michelson

1891). A hiatus in the use of the technique ensued; thirty years later, stellar fringes were first detected by Merrill & Anderson (1920). Within a year, Michelson & Pease (1921), in a landmark paper, had used interferometry to establish the diameter of α Orionis (Betelgeuse) at 0".047. After seven further angular diameters had been measured by Pease (1931), the technique once again languished for decades. Hanbury Brown & Twiss began the modern revival of the technique with a series of papers (1954, 1957a, 1957b, 1958) and actual measurements for the intensity interferometer at Narrabri Observatory (1956, Hanbury Brown *et al.* 1974).

As interferometry has matured into a modern technique, two approaches have been utilized. The simplest approach to obtaining multiple apertures in proper alignment is to mask off a single aperture telescope with subapertures. The approach has been applied over the past three decades (Elliot & Glass 1970, Kulagin 1970, Glass & Elliot 1972, Currie, Knapp & Liewer 1974, McCarthy & Low 1975, McCarthy, Low & Howell 1977a, McCarthy, Low & Howell 1977b, Davis & Tango 1979, Haniff *et al.* 1987, Nakajima 1989, Haniff & Buscher 1992), although the resulting spatial resolution still suffers from the fact that the aperture-to-aperture baseline B tends to be less than telescope diameter D.

The second approach has been development of true multiple aperture interferometers. In pursuit of technology development, quite a number of prototype instruments have been built (Twiss & Tango 1977, Tango 1979, Shao & Staelin 1980, Davis & Tango 1986, Shao, Colavita & Staelin 1986, Townes *et al.* 1986, Gay &

Mekarnia 1988, Dyck, Benson & Ridgway 1993). This decade has seen the construction and initial operation of facility-class instruments capable of milliarcsecond resolution observations: IOTA (Carleton *et al.* 1994, Dyck *et al.* 1995), COAST (Baldwin *et al.* 1996), SUSI (Davis 1994), NPOI (Hutter *et al.* 1993), the CHARA Array (McAlister 1992), and the Keck & VLT interferometers (Barr 1990). Further development of interferometric technology promises a generation of space-based instruments, delivering results in the microarcsecond regime (Shao 1992, Black 1995, Shao *et al.* 1995, Weiler *et al.* 1995).

1.3 Dissertation Accomplishments

Over the course of this dissertation, a number of goals were achieved. First of all, the IOTA interferometer system has been developed to the point where a substantial body of data may be obtained in a single observing run. A wide variety of upgrades were added to the system over the duration of this research, including a redesign of the IR beam recombination table, installation and calibration of baseline stations, and development of improved data collection hardware. Along with the improvements, routine maintenance and repairs were of course necessary as well (e.g. mirror realuminization). Secondly, software needed to be developed to support the operation of the system and to assist in the interpretation of the data collected. Lastly, and most importantly, with these hardware and software tools a considerable amount of ground-breaking research was accomplished with IOTA over the course of this dissertation. Four papers were produced as a result of this research; these manuscripts shall make up

the bulk of this dissertation and may be found in §4 - §7. It is worth noting that while the manuscript found in §4 was the last one to be produced over the course of the dissertation, it serves to provide context for the subsequent chapter and as such is presented first.

CHAPTER II

INTERFEROMETRIC BASICS

2.1 Interferometry

Optical interference is defined by Hecht (1990) as *an interaction of two or more lightwaves yielding a resultant irradiance that deviates from the sum of the component irradiances.* In order to gain some insight into the nature of how interferometers operate, a simple exploration of the behavior of these instruments is in order. (It is worthy to note that a more complicated Fourier approach can also be applied to deriving the response of an interferometer; this approach is quite powerful, particularly with regards to multiple aperture interferometers where $N_{APERTURES} > 2$. For a discussion of this approach, see Steward 1983.) A.A. Michelson proposed in 1890 the *stellar interferometer* as a device of great potential in measuring the small angular dimensions of distant astronomical bodies. The merits of the Michelson interferometer are such that its invention earned Michelson the Nobel Prize in Physics in 1907.

Light from an extremely distant point source (e.g. an unresolved star) is collected by two interferometer apertures, widely separated by a distance D. Each of the two beams are focused onto a detector centered at point P_0 in such a fashion that the total optical paths traveled by the two beams from the illuminating star are equal. In doing so, the beams will add coherently and a series of fringes will form about P_0. The visibility of interference fringes can be measured by the maximum and minimum light intensity of the fringes resulting from constructive and destructive interference, respectively:

$$V \equiv \frac{I_{max} - I_{min}}{I_{max} + I_{min}}.$$

For a point source passing through a system of perfect response, V will be unity.

Assume now that light from a second point source, at some small angular distance θ from the original point source, is also passing through our optical system. Since the two beams from our original point have a zero path difference, the two beams from the second point source are delayed relative to one another by a time shift $D\theta/c$, such that fringes will form about a second point, P_1. The resulting irradiance pattern detected will be the superposition of the two fringe patterns.

A star resolved by the interferometer can be seen as a collection of incoherent point sources, each illuminating the two apertures of the interferometer. For a star of uniform circular surface brightness distribution, its visibility can be expressed as

$$V = 2\left| \frac{J_1(\pi D \theta / \overline{\lambda_0})}{\pi D \theta / \overline{\lambda_0}} \right|,$$

where J_1 is the first order Bessel function, D is the separation of the interferometer apertures, θ is the angular diameter of the source, and $\__0$ is the mean wavelength of the light (Hecht 1990). Hence, a measurement of the visibility V can be utilized in obtaining an estimate of a star's angular size θ.

2.2 Stellar Surface Brightness Distribution

A straightforward application of interferometry can be the detection of deviations from a uniform surface brightness distribution. From angular diameter, the next highest order spatial frequency phenomenon presented by a surface brightness distribution is

limb darkening. Limb darkening is an apparent dimming of the stellar surface from center to limb of projected disk, due to the temperature gradient in the atmospheres. For many cases, limb darkening can be simply represented in a linear fashion by the equation

$$I_\lambda(\mu) = I_\lambda(1)[1 - u_\lambda(1 - \mu)].$$

where $I_\lambda(\mu)$ is the brightness of a point on the disk at wavelength λ, μ is the cosine of the angle between the normal to the surface at that point and the line of sight from star to observer, and u_λ is the limb-darkening coefficient. As derived by Hanbury Brown *et al.* (1974), this intensity distribution results in a visibility that can be expressed as

$$V = \left| \frac{\alpha \frac{J_1(x)}{x} + \beta \left(\frac{\pi}{2} \right)^{1/2} \frac{J_{3/2}(x)}{x^{3/2}}}{\alpha/2 + \beta/3} \right|$$

where $\alpha = 1 - u_\lambda$, $\beta = u_\lambda$, $x = \pi\theta_{LD}D / \_0$, θ_{LD} is the true angular diameter of the limb-darkened star. In the case of a well-sampled visibility curve, unique solutions for θ_{LD} and u_λ can be found.

After limb darkening, the next expected surface brightness distribution phenomenon expected would be spotting. Spotting has the potential to manifest itself in a wide variety of manners, including number, size and relative contrast of spots. Hence this phenomenon does not lend itself to a simple mathematical characterization, as does limb darkening. *Practical* image reconstruction of spotted stellar surfaces will in all likelihood require concurrent sampling at multiple baselines - hence, a three or more element interferometer - in order to provide enough spatial frequency information to uniquely solve for the source brightness distribution.

CHAPTER III

THE IOTA INTERFEROMETER

3.1 Description of the Instrument

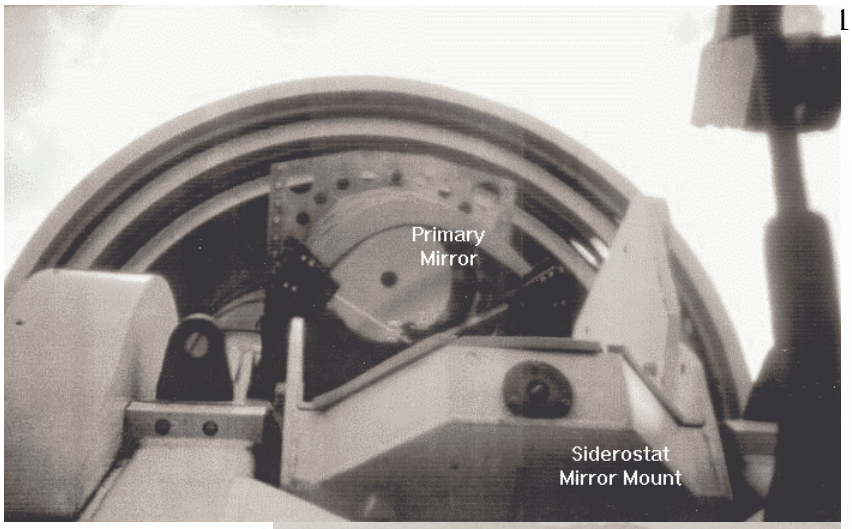

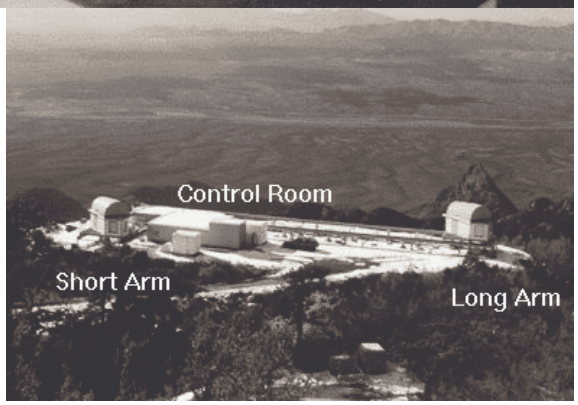

The IR Optical Telescope Array (IOTA) is situated at the Fred Lawrence Whipple Observatory on Mount Hopkins, which is located approximately 45 minutes south of Tucson, AZ, near Green Valley, AZ. During the course of the research presented in this dissertation, IOTA was a two aperture interferometer; future plans include expansion of IOTA to include a third aperture. The overall layout of the site may be seen in Figure 3.1; at the right is the long arm aperture housing, at its 35m station, to the left is the short arm aperture housing, at its 15m station. For scale, at the center of the image is a small car. Each arm has stations at every 5m and 7m for locating the apertures.

To understand the operation of the interferometer, it is instructive to follow the light path from sky to detector. Starlight from a given object is tracked by a flat siderostat mirror; this light is directed into a Cassegrain telescope, whose 45 cm primary

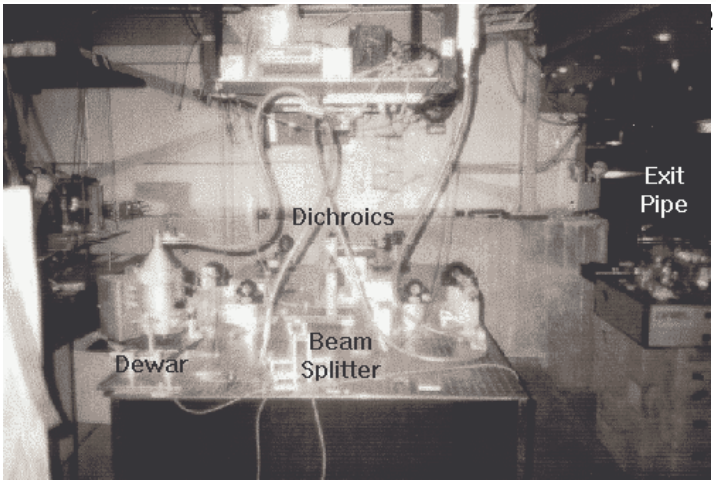

mirror collects the beam, with the secondary mirror directing the beam through the hole in the primary. The secondary also serves to make the beam afocal, maintaining a 2" diameter throughout the system until just before the system detectors. Just after passing the primary and secondary mirrors, the beam reflects off a tertiary mirror and down into the interferometer vacuum system. The tertiary mirror is mounted on a piezoelectric stack that allows for rapid steering of the mirror and hence compensation for wavefront tilt errors introduced by the turbulent atmosphere. The siderostat and primary mirror assembly can be seen in Figure 3.2; the large semicircle in the background of the picture is the aperture housing roof, which has been rolled back to expose the siderostat to the sky.

As the beam passes through the vacuum system, two movable retroreflector mirrors are available to change the length of optical path in the two arms of the interferometer. The long delay runs the 35m length of the long arm, and operates in a 'move and clamp' fashion; the retroreflector is locked into place for static operation. The

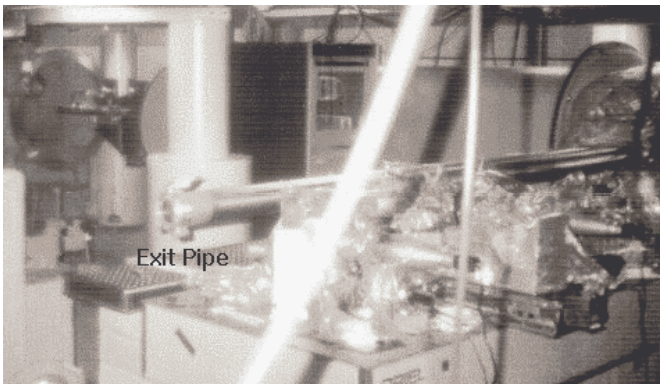

short delay is a retroreflector on a 2.3m electromagnetic induction track; it floats on an air bearing and is operated dynamically during data acquisition, being capable of position accuracies good to 10nm due to closed loop laser interferometric metrology. As the interferometer beams pass through the vacuum system, the delays can be adjusted such that the optical path difference (OPD) between the two beams from star to beam recombiner is zero. When the OPD is zero, interference will occur. The exit pipe of the vacuum system, with the vacuum itself in the background, may be seen in Figure 3.3.

Upon exiting the vacuum system, each beam passes through a dichroic flat, allowing the visible light to pass through while the infrared light is reflected off of the surface. Each beam of infrared light is directed at opposite sites of a 50/50 beam splitter flat, allowing for recombination of the two beams. Each recombined beam is then focused onto an InSb detector, mounted inside a dewar and held at liquid nitrogen temperatures during observing. The IR table may be seen in Figure 3.4. Each beam of visible light passes over the IR table and over the visible light table, where the still-separated visible light from each arm is focussed onto a high-speed CCD camera. Correction of atmospheric errors is accomplished by sampling the CCD cameras at 100 Hz and compensating through driving the tip/tilt tertiary mirrors in each arm. A view of the cameras, in addition to the tip/tilt correction computer, may be seen in Figure 3.5.

3.2 Target Selection

When selecting objects to be observed at IOTA, there are three selection criteria

to be considered:

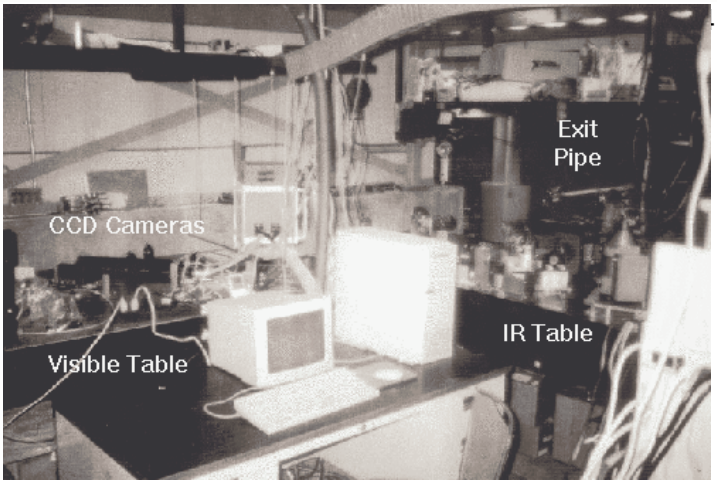

Brightness. In order to detect fringes for an object at IOTA, it must be bright enough for both the visible light CCD tracking cameras, and for the IR detectors. Since the response of the CCD cameras is quite good at longer wavelengths (e.g. 800-950 nm), where coincidentally many of our objects are bright, it has been more useful for us to characterize the limiting magnitude in terms of an object's I band (900 nm) brightness, rather than V band (550 nm); this system limit is approximately I _ 7 mag. For the IR dewars, which operate in the K band (2200 nm), the system limit is approximately K _ 2.5 mag. Both the I and K band limitations are subject to nightly seeing conditions; for example, fringe detection at K _ 4.0 mag is possible on the best of nights, but this is not a consistently achievable goal.

Sky position. The right ascension (RA) of an object determines the availability of an object. RA can dictate if an object is above the horizon at anytime during the night for a given time of year; for those nights when the object is available, RA will dictate when that time is. The declination (dec) of an object plays a large role in dictating the optical path difference between the interferometer's two arms; typically for a given evening, the location of the long delay line will dictate an accessible dec range of 15-30° in width on the sky.

Expected angular size. For an object to be of scientific interest to IOTA, it needs to be able to be resolved by the instrument. For the maximum 38m baseline, arising from use of the [35m,15m] system configuration, objects needed to be in excess of 4.5mas in order to be resolved by the interferometer. Also of concern are objects that are too large. The amplitude of the visibility sampled for these objects will be quite small, resulting in a very low signal-to-noise, and the visibility will be sampled in a non-monotonic region of the visibility curve. Objects that the interferometer cannot resolve are actually of great use to an observing program, allowing for a sampling of the interferometer's point response and consequently, a calibration of the instrument. Interleaving unresolved calibration sources with resolved target sources is necessary for nominal data reduction.

Within the constraints of these considerations, a large number of objects are available to the IOTA interferometer. Given the ease with which the array can observe angularly large, IR bright objects, highly evolved stellar objects lend themselves for study by IOTA, including all variations of giant and supergiant stars: variable and non-variable stars; oxygen-rich, carbon-rich and S-type stars. Keeping in mind these selection criteria, examination of the visible and infrared brightnesses available in *The Bright Star Catalog* (Hoffliet 1982) and the *Catalog of Infrared Observations* (Gezari *et al.* 1993) leads to an estimate of the total number of each type of star available for observation at IOTA; a list of the target populations by type may be seen in Table 3.1.

Table 3.1. Number of highly evolved stellar objects observable by IOTA.

Stellar Type	Number
oxygen-rich giants	400
supergiants	40
S-type stars	15
Carbon stars	50
oxygen-rich Mira variables	70
S-type Mira variables	15
Carbon Mira variables	10
Calibration stars	500

On the other end of stellar evolution, young stellar objects present themselves as targets of great potential for IOTA as well. However, these objects are at present just out of reach of the interferometer's K band sensitivity, and completely out of reach of the V band limit of the device. Future upgrades to IOTA, for both IR InSb science detectors and an IR guiding system, will allow for investigation of these equally interesting objects.

3.3 Fringe Finding

One of the keys for use of interferometric data is the location of fringes in the presence of noise. The ease with which this is accomplished is of course dictated by the

signal-to-noise ratio (S/N) of a given fringe in the raw data. The S/N can be reduced for two reasons: First, as stellar flux is reduced for dimmer and dimmer sources, the signal strength drops; and Second, for well-resolved sources, the fringe amplitude drops and the resulting S/N can be quite low. Development of fringe finding routines were an integral aspect of this dissertation and allowed for rapid, accurate reduction of the interferometric data.

The most complete approach to locating fringes in noisy data is to cross-correlate the raw data with a model white light fringe. However, this technique, while effective, can prove to be computationally intensive, particularly when considering reducing 20,000 to 50,000 scans for an observing run, each containing 1,500 to 4,000 points. A less demanding but equally effective approach has been developed over the course of this thesis, and can typically reduce an entire evening's data in about 5-20 minutes, depending on the total amount of data collected and computer speed.

Consider a white light fringe of expected frequency ν_f; as it passes the single element detector, the detector is being sampled at a frequency of ν_s, resulting in a string of raw data points x_i. For a filter centered at wavelength λ of bandwidth $\Delta\lambda$, the number of fringes N_f in the central lobe is expected to be

$$N_f = \frac{\lambda}{\Delta\lambda} x2.$$

For a single fringe, the number of samples peak-to-peak (N_{pp}) will be dictated by the fringe frequency and the sampling frequency:

$$N_{pp} = \frac{\nu_s}{\nu_f}.$$

We may establish a 'find value' for a single fringe, by looking for both the falling edge of the fringe (the 'descendant') and the rising edge of the fringe (the 'ascendant'):

$$\begin{aligned} FV(i) &= fv(descendant) \\ &+ fv(ascendant) \\ &= (x_i - x_{i+1}) + (x_{i+1} - x_{i+2}) + \ldots + (x_{i+l-1} - x_{i+l}) \\ &+ (x_{i+l+1} - x_{i+l}) + (x_{i+l+2} - x_{i+l+1}) + \ldots + (x_{i+N_{pp}} - x_{i+N_{pp}-1}) \end{aligned}$$

where $l = 0.5 * N_{pp}$ is the halfway point of the fringe (the location of the fringe trough). To locate the central lobe, a total find value can be calculated:

$$FV_{TOT}(i) = FV(i) + FV(i + N_{pp}) + \ldots + FV(i + (N_f - 1) x N_{pp}).$$

By scanning through the entire raw data string and locating the peak FV_{TOT}, the position of the white light fringe may be obtained. Assuming each data point x_i has a certain amount of noise Δx_i associated with it, we may estimate the error in FV_{TOT} by a simple propagation of errors:

$$\Delta FV_{TOT} = \sqrt{2 x N_{pp} x N_f x \Delta x_i^2}.$$

Hence, for the IOTA system, we can get an estimate of FV_{TOT} and ΔFV_{TOT} for a nominal reduction. Typically $\lambda = 2.2$ μm, $\Delta\lambda = 0.4$ μm, $\nu_s = 500$ Hz, and $\nu_f = 100$ Hz. Thus $N_{pp} = 5$, $N_f \_ 10$; assuming a fringe packet peak-to-peak strength of ±10 and a peak-to-peak noise of $\Delta x_i = \pm 2$ leads to and estimated $FV_{TOT}(fringe) \_ 100$ with $\Delta FV_{TOT} \_ 20$.

Aside from the white light fringe position indicated by FV_{TOT}, other *a priori* information can also be incorporated in the data reduction to gain confidence in fringe location. For a typical data set consisting of multiple scans, the fringes will typically be located in roughly the same spot from scan to scan, within the spread of arrival time

introduced by atmospheric error. The actual shape of a fringe packet could also be utilized in further refining an estimate of FV_{TOT}, although this has not been necessary within the scope of this thesis.

CHAPTER IV

CARBON MIRAS AND S-TYPE STARS

4.1 Introduction

Using the Infrared Optical Telescope Array (IOTA, see Carleton *et al*. 1994 and Dyck *et al.* 1995) we have been carrying out a program of interferometric high-resolution observations of highly evolved stars. In previous papers (van Belle *et al.* 1996, Dyck *et al.* 1996a, Dyck *et al.* 1996b) we detail the results from IOTA of oxygen-rich Mira variables, giant/supergiant stars and carbon stars; in this paper we shall discuss interferometric observations of carbon Miras, and S-type Miras and non-Miras and compare them to our previous results. Using previously compiled stellar catalogs (e.g. Kholopov *et al.* 1988, Gezari *et al.* 1993), observed fluxes and estimates of surface temperatures allowed us to estimate blackbody angular diameters for these stars; more than dozen carbon Mira variables and two dozen S-type stars (both Miras and non-Miras) have angular diameters in excess of 5 milliarcseconds (mas), easily resolvable by IOTA. Although this is in contrast to the 70+ oxygen-rich Mira variables and the few hundred oxygen-rich giant/supergiant stars in excess of IOTA's resolution limit, this is still enough of a sample to begin characterizing the differences between the oxygen-rich, S-type and carbon stars. Presented in this paper are angular sizes for 5 carbon Miras and 4 S-type Miras, in addition to angular sizes for 4 out of 7 non-Mira S-type stars observed (the latter three being observed but unresolved), along with analyses comparing Mira variable and non-Mira stars of the three abundance types.

S stars exhibit an envelope enriched in carbon and heavy elements, indicative of the s-process (Smith & Lambert 1990). Optical surveys of stars have turned up few of these stars, e.g. the *Bright Star Catalog* (Hoffleit & Jaschek 1982) has only ~0.1% S type stars (Jura 1988). Infrared studies are more successful, e.g. the *Two Micron Sky Survey* (Neugebauer & Leighton 1969, henceforth TMSS) has proportionately an order of magnitude more stars, indicating the cooler nature of these stars; the *TMSS* indicates roughly a 3:1 ratio of carbon stars to S stars (Wing & Yorka 1977). Two classes of S stars are thought to exist, as suggested by Iben & Renzini (1983) and subsequently supported by a number of observational studies. *Extrinsic* S stars includes stars with altered elemental abundances, through the mechanism of mass transfer from a companion (e.g. Jorissen & Mayor 1992). *Intrinsic* S stars are thought to be high luminosity stars lying upon the AGB (e.g. Little *et al*. 1987, Smith & Lambert 1988). The presence of technetium in the spectra of S stars allows for the differentiation of the two classes; intrinsic S stars exhibit Tc, while in extrinsic S stars Tc is absent. (Tc is an s-process element with no stable isotope; its presence in a spectrum is a sign of recent convective mixing within an intrinsic S star.) The S stars addressed in this paper are all intrinsic S stars.

The evolutionary status of these stars has been thought to be that of an intermediate stage between the two other types: M - S - C (Iben & Renzini 1983). This hypothesis is supported by observation that S stars bridge an abundance gap between oxygen-rich and carbon stars, being within 1.05 of [O] = [C] (Scalo & Ross 1976). This

interpretation, however, has been called into question with the discovery of carbon stars with 60 μm excesses (Willems & de Jong 1986, Thronson *et al*. 1987), and oxygen-rich circumstellar shells (Little-Marenin 1986, Willems & de Jong 1986). A lively debate on the nature of this aspect of stellar evolution has ensued (cf. de Jong 1989, Zuckerman & Maddalena 1989). In analysis of these observations, it has been suggested (e.g. Willems & de Jong 1986, 1988, Chan & Kwok 1988, Kwok & Chan 1993) that the M to C transition occurs on very short timescales (< 100 yr), with mass loss ceasing during the transition from O-rich to C-rich surface abundances. In contrast to these conclusions, Jura (1988), using *TMSS* and *IRAS* data, and Bieging & Latter (1994), using millimeter CO emission data, both infer continuing mass loss over much longer time scales (10^4 yr).

Independent of *how* stars become carbon stars, there is common agreement that these objects represent stars evolving off of the AGB (cf. Groenewegen *et al*. 1992, Zuckerman *et al.* 1978). A great deal of mass loss is associated with carbon stars, as inferred from *IRAS* data (e.g. Claussen *et al.* 1987, Jura 1988) and CO emission data (e.g. Knapp & Morris 1985). For non-Mira carbon stars, as investigated in one of our previous papers (Dyck *et al*. 1996b), the mean temperature was measured to be 3000±200K, the mean radius was estimated to be 400 $R_{\odot}$, making them more comparable to oxygen-rich Miras than to giant and supergiant stars. Two of the carbon stars (S Aur and CIT 13) were found to have significant effects of circumstellar shells on their temperature determinations.

In §4.2 we introduce the interferometric observations taken at IOTA. The data

reduction and ancillary data is presented in §4.3; analysis of the derived parameters and trends is discussed in §4.4. There are two aspects to the results presented in this paper. First, there are the results specifically obtained herein; the carbon-rich and S-type Mira variables, and the S-type non-Miras. Second, the overall context cast by the results of this paper and those of our three previous papers (Dyck *et al.* 1996a, 1996b, van Belle *et al.* 1996) is examined, particularly with regards to the implications for relative stages of stellar evolution. A potential for insight into the progression of these late stages of stellar evolution due to the rather unique nature of our data presented over the course of these four papers; to our knowledge, this is the first presentation of a complete body of effective temperatures and linear radii for these objects.

4.2 Observations

The data reported in this paper were obtained in the *K* band (λ = 2.2 μm, $\Delta\lambda$ = 0.4 μm) at IOTA, using the telescopes at the [15m, 15m], [35m, 5m] and [35m, 15m] stations, providing 21m, 35m, and 38m baselines, respectively. Use of IOTA at 2.2 μm to observe Mira variables offers three advantages: First, effects of interstellar reddening are reduced, relative to the visible (A_K = 0.11 A_V; see Mathis 1990); Second, the effects of circumstellar emission are reduced shortward of 10 μm (Rowan-Robinson & Harris 1983a), and; Third, the *K* band apparent uniform-disk diameter of Mira variables is expected to be close to the Rosseland mean photospheric diameter (see the discussion in §4.3.1). The interferometer, detectors and general data reduction procedures are described more fully in Carleton *et al.* (1994) and Dyck *et al.* (1995), with procedures

relating specifically to Mira variables in van Belle *et al*. (1996). As was previously reported in these papers, starlight collected by the two 0.45 m telescopes is combined on a beam splitter and detected by two single element InSb detectors, resulting in two complementary interference signals. The optical path delay is mechanically driven through the white light fringe position to produce an interferogram with fringes at a frequency of 100 Hz. Subsequent data processing locates the fringes in the raw data and filters out the low and high frequency noise with a square filter 50 Hz in width.

Observations of target objects are alternated with observations of unresolved calibration sources to characterize slight changes in interferometer response, due to both seeing and instrumental variations. Calibration sources were selected from *V* band data available in *The Bright Star Catalog, 4th Revised Edition* (Hoffleit & Jaschek 1982) and *K* band data in the *Catalog of Infrared Observations* (Gezari *et al.* 1993), based upon angular sizes calculated from estimates of bolometric flux and effective temperature; calibration source visibility was selected to be at least 90% and ideally greater than 95%, limiting the effect of errors in calibrator visibility to a level substantially below measurement error. Mira variables observed were selected upon three criteria: First, the stars needed to fall within IOTA's sensitivity limits; Second, the stars needed to be accessible to IOTA's observational setup for a given evening (specifically, optical delay); and Third, the stars needed to be of sufficient estimated angular size to be resolved by IOTA. Phase was not a selection criterion. The selection criteria for the Mira variables are more fully described in van Belle *et al*. (1996).

Five carbon and four S-type Mira variable stars were resolved at IOTA during five observing runs between June 1995 and June 1996, in addition to four non-Mira S-type stars, out of a total of seven observed. The visibility data for the two detector

Table 4.1. IOTA observations of carbon Miras & S-type stars.

Star	Date	φ	B_p [m]	Visibility	θ_{UD} [mas]
Carbon Miras:					
S CEP	96 Jun 06	0.22	27.32	0.3672	13.67 ± 0.76
V CRB	96 May 29	0.08	37.32	0.6708	7.37 ± 0.59
V CRB	96 May 29		37.42	0.6374	
V CRB	96 May 30		37.50	0.5562	
V CRB	96 May 30		37.39	0.5919	
V CRB	96 Jun 06		35.41	0.5847	
V CRB	96 Jun 07		35.52	0.6790	
U CYG	95 Jul 09	0.57	37.43	0.6260	7.17 ± 0.58
U CYG	95 Oct 05	0.76	36.38	0.6859	6.75 ± 0.63
U CYG	95 Oct 05		36.29	0.6754	
U CYG	96 May 29	0.28	37.10	0.6576	7.27 ± 0.61
U CYG	96 May 29		37.04	0.6218	
U CYG	96 May 31		36.08	0.5874	
U CYG	96 Jun 01		35.27	0.6565	
U CYG	96 Jun 06		34.36	0.6898	
V CYG	95 Oct 05	0.25	36.88	0.0470	15.98 ± 2.00
V CYG	96 May 31	0.81	36.07	0.1846	12.54 ± 0.64
R LEP	95 Oct 06	0.99	32.45	0.8888	11.50 ± 0.64
R LEP	95 Oct 07		32.40	0.3694	
S-Type Miras:					
R AND	95 Jul 09	0.43	37.22	0.5307	8.26 ± 0.56
R AND	95 Oct 04	0.65	36.19	0.5644	7.78 ± 0.57
R AND	95 Oct 04		35.98	0.5756	
R AND	95 Oct 05		36.73	0.6063	
R AND	95 Oct 05		36.88	0.6003	
R AND	95 Oct 08		38.21	0.5703	
R AND	95 Oct 08		38.21	0.5537	
W AOL	96 Jun 04	0.98	31.06	0.4064	11.13 ± 0.66
W AOL	96 Jun 04		30.79	0.4729	
R CYG	95 Jul 09	0.41	37.07	0.7188	6.16 ± 0.64
R CYG	95 Oct 05	0.62	37.04	0.7495	5.64 ± 0.68
R CYG	95 Oct 05		37.02	0.7720	
R CYG	96 May 29	0.18	36.80	0.6705	6.94 ± 0.63
R CYG	96 May 29		36.83	0.6613	
R CYG	96 May 31		36.10	0.6518	
R CYG	96 Jun 01		34.70	0.7196	
R CYG	96 Jun 06		34.46	0.6637	
R LYN	95 Oct 04	0.75	34.71	0.8510	4.99 ± 0.85
R LYN	95 Oct 04		34.83	0.8879	
R LYN	95 Oct 04		34.76	0.8300	
R LYN	95 Oct 04		34.87	0.7505	
R LYN	96 Mar 13	0.17	35.91	0.7585	5.84 ± 0.70
S-Type non-Miras:					
NZ GEM	96 Mar 11	?	36.07	0.8413	Unresolved
NZ GEM	96 Mar 11		35.94	1.1030	
HR 8062	95 Jul 10	?	37.64	1.0400	Unresolved
IRC 40458	96 May 29	?	36.82	0.9383	Unresolved
IRC 40458	96 Jun 01		35.85	0.9668	
RS CNC	96 Mar 07	0.46	21.21	0.4825	15.73 ± 0.96

RS CNC	96 Mar 07		21.20	0.5576	
RS CNC	96 Mar 07		21.18	0.4124	
RS CNC	96 Mar 07		21.21	0.4372	
RS CNC	96 Mar 07		21.21	0.4401	
AA CYG	96 May 29	?	36.94	0.8143	5.13 ± 0.78
AA CYG	96 Jun 06		34.61	0.8057	
AD CYG	96 May 29	?	37.43	1.1180	Unresolved
OP HER	95 Jun 04	?	37.55	0.7869	5.14 ± 0.72
OP HER	95 Jun 04		37.59	0.8202	
OP HER	95 Jun 04		37.34	0.7955	
OP HER	95 Jun 04		37.28	0.7900	
OP HER	95 Jun 05		37.48	0.7844	
OP HER	95 Jun 05		37.54	0.7843	
OP HER	96 May 28	?	37.26	0.7314	6.00 ± 0.65
OP HER	96 May 28		37.20	0.7270	
ST HER	95 Jun 03	?	36.93	0.5073	9.15 ± 0.55
ST HER	95 Jun 03		36.86	0.4653	
ST HER	95 Jun 04		36.93	0.4378	
ST HER	95 Jun 04		36.86	0.4262	
ST HER	95 Jun 05		36.90	0.4552	
ST HER	95 Jun 05		36.84	0.4462	
ST HER	96 May 29	?	36.75	0.4197	9.32 ± 0.56
ST HER	96 May 30		36.96	0.4718	
ST HER	96 May 30		37.00	0.4485	
ST HER	96 Jun 01		35.64	0.4510	

channels have been averaged and are listed in Table 4.1, along with the date of the observation, the interferometer projected baseline, the stellar phase and the derived uniform disk angular size; the latter two points are discussed further in §4.3. Our experience with the IOTA interferometer (Dyck *et al.* 1996a) has demonstrated that the night-to-night RMS fluctuations in visibility data generally exceed the weighted statistical error from each set of interferograms; we have characterized these fluctuations and use the empirical formula $\varepsilon_V = \pm 0.0509 / \sqrt{number\ of\ nights}$ to assign the "external" error. The interested reader should see Dyck *et al.* (1996a) for a more complete discussion. Finally, visibility data were fit to uniform disk models to obtain an initial angular size θ_{UD}. These uniform disk diameters and their estimated errors, derived from the uncertainty in

the visibilities, are also listed in Table 4.1.

We note that typically visibility points in a single range of baselines were utilized in calculating the uniform disk diameter θ_{UD}. For the stars in our sample, the visibility data were all at spatial frequencies, x, shortward of the first zero of the uniform disk model, $|2 J_1(x)/x|$. Haniff, Scholz & Tuthill (1995) noted that the uniform disk model was not a particularly good model for visible-light data for Mira variables; rather, the data were a better fit to a simple Gaussian. Although we do not currently have multiple spatial frequency data for any Mira variables, we expect that the departures from a uniform disk model will not be as great at 2.2 μm as it is at visible wavelengths. This expectation is based upon our unpublished 2.2 μm data for α Her, a supergiant star expected to have the same order of atmospheric extension as do the Mira variables. A comparison of our data with visible α Her data (Tuthill 1994) indicates that the departures from a uniform disk visibility curve are present in the visible but not the infrared. Thus we assume that to first order, a uniform disk model will also fit the Mira data; a slight correction to the derived angular sizes to account for this assumption will be discussed in §4.3.1. In this case, a single spatial frequency point will uniquely and precisely determine the angular diameters for visibilities in the approximate range $0.25 \leq V \leq 0.75$. If there are significant differences between the brightness profiles for supergiants and for Mira variables then this assumption will be invalid; this point may only be addressed by detailed multiple spatial frequency observations of the visibility curves.

4.3 Data

Many of the data reduction procedures utilized in this investigation are similar if not identical to those described in van Belle *et al*. (1996, henceforth Paper I); hence, for the sake of brevity we shall direct the interested reader to more complete descriptions of the procedures are contained within that paper, noting in this section similarities and detailing only the significant deviations. As was noted in §4.1, the objects presented in this paper are part of an ongoing observational program to observe evolved stars at IOTA. Previous papers have already been presented, discussing results from oxygen-rich K and M giants and supergiants (Dyck *et al*. 1996a), non-Mira carbon stars (Dyck *et al*. 1996b), and oxygen-rich Mira variable stars (Paper I); effective temperatures and linear radii from these papers will be utilized in the analysis of §4.4. We note that the three parameters established to investigate mass loss - luminosity, the P_r / P_g pressure ratio and *K - [60]* color - were not determined in our previous papers and as such these sections (§4.3.2 - 3.4) are unique to this paper.

4.3.1 Phase, Spectral Type, Effective Temperature

As in Paper I, rough Mira variable phases were initially established from data contained within *The General Catalog of Variable Stars, 4th Edition* (Kholopov *et al.* 1988, GCVS); more precise values (particularly for recent zero phase date) were subsequently determined from recent visual brightness data available from the Association Francaise des Observateurs d'Etoiles Variables (AFOEV) (Schweitzer 1996). Fourier analysis of the AFOEV data (Scargle 1982, Horne & Baliunas 1986) provided a cross-check of the GCVS periods; the periods agreed at the 1% level, corresponding to an average difference in period of 1.1^{d}. Zero phase estimate was the larger uncertainty in phase determination, though still small, averaging 6^{d}.

Spectral types were established from the GCVS. In contrast to Paper I, we do not establish phase-dependent spectral types; the papers by Lockwood & Wing (1971) and Lockwood (1972) we used previously for the M-type Miras include observations of S-type stars, but phase-dependent spectral types are not determined for these stars. However, the need for determining phase-dependent spectral types is relaxed as we are not using the spectral-type dependent $log\ F_{TOT}/F_K$ relationship of Dyck, Lockwood & Capps (1974) to determine bolometric fluxes (see the next section).

The stellar effective temperature, T_{EFF}, is defined in terms of the star's luminosity and radius by $L = 4\pi\sigma R^2 T_{EFF}^4$. Rewriting this equation in terms of angular diameter θ_R and bolometric flux F_{TOT}, a value of T_{EFF} was calculated from the flux and Rosseland diameter using $T_{EFF} = 2341(F_{TOT} / \theta_R^{\ 2})^{1/4}$; the units of F_{TOT} are 10^{-8} erg/cm^{2}s, and θ_R is in

mas. The error in T_{EFF} is calculated from the usual propagation of errors.

As in Paper I, we have used the model atmospheres of Scholz & Takeda (1987) to evaluate the effects of limb darkening, adopting as they do the surface where the Rosseland mean opacity equals unity as the appropriate surface for computing an effective temperature. Although Scholz & Takeda's models do not address carbon or S-type stars directly, we shall use them as sufficient approximations of the marginal effect of limb darkening at this wavelength. Following the treatment of Paper I, we have adopted a phase-averaged multiplicative factor relating the Rosseland angular size to the uniform disk angular size: $\theta_R = 1.045\ \theta_{UD}$. We note that Tsuji (1981) has suggested that carbon stars have lower temperatures and higher luminosities than the normal M giant sequence, such that atmospheric extension may be more important than calculated by $\theta_R = 1.045\ \theta_{UD}$. Our investigation of Scholz & Takeda's atmospheric models indicates that the limb-darkening corrections could be no more than 10% different from the correction factors we calculate, leading to a systematic error of no greater than 5% in effective temperature scale. We also note that for the non-Mira stars, we use a correction of 1.022 rather than 1.045, following Dyck *et al.* (1996a, 1996b).

Another potential source of error for the angular size measurements of the greatly extended Mira variable stars is departures from spherical symmetry. We have a small amount of unpublished data on S CrB that indicates the potential for variation in angular size (12.2 mas - 13.7 mas) over a range of projected baseline angles ($\Delta\theta = 19°$). Although further evidence for and characterization of this effect needs to obtained to

firmly establish its effect on , we conservatively adopt a 10% error in angular size, which we added in quadrature. Similar data for non-Mira stars (γ Leo, RS Cnc) gives no indication of this effect.

To compute the stellar bolometric flux for these stars, we have made use of data from a number of sources. Most importantly, contemporaneous measurements of incoherent K band fluxes were made during each interferometric scan. We obtained our standard star photometric calibrations using the K band measurements found in the *Two Micron Sky Survey* (Neugebauer & Leighton 1969) for our non-variable point-response calibration sources. No airmass corrections were applied since the calibrators were observed at nearly identical airmasses as the target objects. Contemporaneous V band measurements were obtained from the available AFOEV visual data for the variable stars (Schweitzer 1996). From Gezari *et al*. (1993), measures of the L band flux were taken, and the *IRAS Point Source Catalog* (IPAC 1986) provided 12, 25, 60 and 100 μm flux measurements; we note that data from these two sources were not contemporaneous and shall consider their temporal variations when we calculate the error in F_{TOT}. The photometry for each source is listed in Table 4.2.

For the carbon stars in the sample, estimates of the K band reddening were taken from Claussen *et al*. (1987); A_V was estimated from A_K using the relation $A_K = 0.11\ A_V$ from Mathis (1990). Reddening data were not readily available for the S stars and were not considered. However, since both types of objects are at roughly the same distances, we expect that reddening would be on the same order of magnitude as A_V and A_K for the

carbon stars; since the K band photometry had the greatest effect on the computed F_{TOT}, with A_K of marginal effect on m_K ($\underline{A}_K$ 0.06), we do not expect this to be significant. Nevertheless, we have included reddening consideration for completeness with the carbon stars, and will include lack of compensation for this effect in our estimation of error in F_{TOT} for the S-type stars.

Once the fluxes between 0.55 μm to 100 μm had been established, a Planck curve was fit to the data by means of a χ^2 minimization, and the bolometric flux calculated from a numeric integration of that curve. We note that such a curve is a poor fit, particularly at the longer wavelengths; however, the majority of the bolometric flux is contributed about the K band, the wavelengths of which (V, K, L bands) held the majority of the weight in the fit.

Error in the estimation of F_{TOT} was calculated from a number of potential sources: K, V, L band photometry errors, long wavelength excess, and for the S-type

Table 4.2. Phase, spectral type & photometry.

Star	Date	φ	Spectral Type	V [mag]	K [mag]	L [mag]	m_{12} [mag]	m_{25} [mag]	m_{60} [mag]	K-m_{60} [mag]
Carbon Miras:										
S CEP	96 Jun 06	0.21	C7.4e(N8e)	9.50	-0.07 ± 0.15	-1.47	-2.83	-3.24	-3.47	3.40
V CRB	96 May 29	0.05	C6.2e(N2e)	8.50	1.22 ± 0.06	0.71	-1.42	-1.70	-1.81	3.03
U CYG	95 Jul 09	0.57	C7.2e-C9.2(NPe)	9.75	1.01 ± 0.11	0.05	-1.50	-1.81	-2.13	3.15
U CYG	95 Oct 05	0.76	C7.2e-C9.2(NPe)	8.00	0.89 ± 0.08	0.05	-1.50	-1.81	-2.13	3.02
U CYG	96 May 29	0.27	C7.2e-C9.2(NPe)	9.00	0.77 ± 0.04	0.05	-1.50	-1.81	-2.13	2.90
V CYG	95 Oct 05	0.23	C5.3e-C7.4e(NPe)	11.00	0.38 ± 0.48	-1.28	-3.43	-3.85	-4.04	4.42
V CYG	96 May 31	0.79	C5.3e-C7.4e(NPe)	11.50	0.50 ± 0.21	-1.28	-3.43	-3.85	-4.04	4.54
R LEP	95 Oct 06	0.99	C7.6e(N6e)	9.50	0.43 ± 0.15	-0.60	-2.82	-3.09	-3.36	3.79
S-Type Miras:										
R AND	95 Jul 09	0.43	S3.5e-S8.8e(M7e)	13.50	0.48 ± 0.02	-1.17	-2.66	-3.49	-3.27	3.75
R AND	95 Oct 04	0.65	S3.5e-S8.8e(M7e)	15.00	1.11 ± 0.02	-1.17	-2.66	-3.49	-3.27	4.38
W AOL	96 Jun 04	0.94	S3.9e-S6.9e	7.50	0.05 ± 0.08	-0.84	-4.36	-4.99	-4.93	4.98
R CYG	95 Jul 09	0.43	S2.5.9e-S6.9e(Tc)	12.00	1.05 ± 0.04	0.20	-1.42	-2.22	-2.50	3.55
R CYG	95 Oct 05	0.64	S2.5.9e-S6.9e(Tc)	14.00	1.49 ± 0.05	0.20	-1.42	-2.22	-2.50	3.99
R CYG	96 May 29	0.20	S2.5.9e-S6.9e(Tc)	9.00	0.66 ± 0.05	0.20	-1.42	-2.22	-2.50	3.16
R LYN	95 Oct 04	0.72	S2.5.5e-S6.8e:	10.50	2.30 ± 0.23	1.06	0.49	0.19	-0.13	2.43
R LYN	96 Mar 13	0.15	S2.5.5e-S6.8e:	8.50	2.21 ± 0.90	1.06	0.49	0.19	-0.13	2.34
S-Type non-Miras:										
RS CNC	96 Mar 07	NA	M6eIb-II(S)	5.95	-1.67 ± 0.10	-2.00	-3.07	-3.73	-3.59	1.92
AA CYG	96 May 29	?	S7.5-S7.5.6(MPTc)	8.40	0.65 ± 0.11		-0.37	-0.90	-1.62	2.27
OP HER	95 Jun 04	?	M5IIb-IIIa(S)	6.32	0.03 ± 0.02	-0.15	-0.70	-1.01	-1.12	1.23
OP HER	96 May 28	?	M5IIb-IIIa(S)	6.32	0.16 ± 0.21	-0.15	-0.70	-1.01	-1.12	1.36
ST HER	95 Jun 03	?	M5IIb-IIIa(S)	6.70	-0.78 ± 0.01	-0.83	-2.12	-2.90	-2.87	2.07
ST HER	96 May 29	?	M6-7IIIaS	6.70	-0.58 ± 0.10	-0.83	-2.12	-2.90	-2.87	2.27

Table 4.3. Derived stellar parameters.

Star	Date	F_{TOT}	error	Model	θ_R [mas]	T_{EFF} [K]	*D1* [pc]	*D2* [pc]	*D3* [pc]	*D* [pc]	R [$R_\odot$]	L [$10^4 L_\odot$]
Carbon Miras:												
S CEP	96 Jun 06	140.80 ± 11.59	K	1.045	14.29 ±	2133 ± 73	560	404		482 ± 96	740 ± 154	1.013
V CRB	96 May 29	47.70 ± 6.52	V	1.045	7.70 ± 0.61	2217 ± 116		732		732 ± 146	606 ± 130	0.793
U CYG	95 Jul 09	57.20 ± 8.08	K=V	1.045	7.50 ± 0.61	2351 ± 126		629		629 ± 126	507 ± 109	0.702
U CYG	95 Oct 05	76.30 ± 14.17	V	1.045	7.05 ± 0.65	2606 ± 171		629		629 ± 126	477 ± 105	0.938
U CYG	96 May 29	75.60 ± 8.19	V	1.045	7.60 ± 0.64	2504 ± 125		629		629 ± 126	514 ± 111	0.928
V CYG	95 Oct 05	105.70 ± 13.40	K=L	1.045	16.70 ±	1837 ± 129	580	510		545 ± 109	978 ± 231	0.973
V CYG	96 May 31	101.20 ± 12.53	L	1.045	13.10 ±	2051 ± 82	580	510		545 ± 109	767 ± 158	0.930
R LEP	95 Oct 06	86.00 ± 12.73	K	1.045	12.02 ±	2056 ± 95	410	508		459 ± 92	593 ± 123	0.562
S-Type Miras:												
R AND	95 Jul 09	85.80 ± 5.87	L	1.045	8.63 ± 0.58	2424 ± 92	240	609	746	532 ± 106	493 ± 104	0.750
R AND	95 Oct 04	68.20 ± 9.35	L	1.045	8.13 ± 0.60	2359 ± 118	240	609	746	532 ± 106	464 ± 99	0.596
W AOL	96 Jun 04	129.40 ± 21.39	V=R	1.045	11.63 ±	2315 ± 118		427	832	629 ± 126	786 ± 164	1.586
R CYG	95 Jul 09	47.20 ± 5.48	R	1.045	6.43 ± 0.67	2419 ± 144	420	689	661	590 ± 118	408 ± 92	0.509
R CYG	95 Oct 05	33.50 ± 2.26	K=L	1.045	5.89 ± 0.72	2320 ± 146	420	689	661	590 ± 118	373 ± 87	0.360
R CYG	96 May 29	71.20 ± 6.10	R	1.045	7.25 ± 0.66	2525 ± 127	420	689	661	590 ± 118	459 ± 101	0.765
R LYN	95 Oct 04	17.00 ± 2.91	K	1.045	5.22 ± 0.89	2081 ± 199		1178	832	1005 ±	564 ± 148	0.533
R LYN	96 Mar 13	19.50 ± 10.63	K=V	1.045	6.10 ± 0.74	1991 ± 297		1178	832	1005 ±	659 ± 154	0.610
S-Type non-Miras:												
RS CNC	96 Mar 07	676.90 ± 9.62	K	1.022	16.08 ±	2977 ± 92	170		245	208 ± 42	359 ± 75	0.905
AA CYG	96 May 29	74.00 ± 9.79	V=K=	1.022	5.25 ± 0.80	2997 ± 250		550	759	654 ± 131	369 ± 93	0.982
OP HER	95 Jun 04	147.70 ± 1.29	V	1.022	5.25 ± 0.74	3560 ± 250			291	291 ± 58	164 ± 40	0.386
OP HER	96 May 28	145.90 ± 2.74	V	1.022	6.13 ± 0.66	3285 ± 178			291	291 ± 58	192 ± 44	0.384
ST HER	95 Jun 03	279.20 ± 23.87	V	1.022	9.35 ± 0.57	3129 ± 116			347	347 ± 69	348 ± 73	1.037
ST HER	96 May 29	235.90 ± 29.70	K=V	1.022	9.52 ± 0.57	2973 ± 129			347	347 ± 69	355 ± 74	0.880

Distance references: carbon Miras: 1 Rowan-Robinson & Harris (1983b), 2 Claussen *et al.* (1987) (M_K = -8.1); S Miras 1 Rowan-Robinson & Harris (1983a), 2 Jura (1988) (M_K = -8.1), 3 Yorka & Wing (1977) (M_K = -1.6); S non-Miras 1 Rowan-Robinson & Harris (1983a), 2 Jura (1988), 3 Yorka & Wing (1977) (M_K = -1.0).

stars, lack of reddening consideration. Given that estimates of V band data came from visual AFOEV data, Δm_V was estimated to be ±1.0 mag; since L band data were from the non-contemporaneous data in Gezari (1993), Δm_L was estimated to be ±0.25 mag. Long wavelength excesses were found to contribute a negligible amount of error to the estimate of F_{TOT}. Given the reddening for the carbon stars found in Claussen *et al*. (1987), an average reddening of $\underline{A_K}$ ±0.06 was considered as an additional source of error for the S-type stars. Errors in the estimation of F_{TOT} were added in quadrature to obtain a final F_{TOT} error value. The estimates of F_{TOT} were compared to those obtained from the $log\ F_{TOT}/F_K$ relationship of Dyck, Lockwood & Capps (1974), and found to be consistent (typically well within a single ΔF_{TOT}) with M8-M9 spectral class stars. The final F_{TOT} established for each star is listed in Table 4.3, along with primary source of error in F_{TOT}.

4.3.2 Linear Radius & Luminosity

Determination of linear radii from angular sizes necessitated an estimate of distance to these stars. A variety of inferential methods exist in the literature, exhibiting agreement within our sample at the 20% level, which is consistent with the spread in values of the previous investigation of a similar nature by Claussen *et al.* (1987). Where possible, we attempted to utilize two or more estimates of the stellar distances in order to gain confidence in these indirectly determined values; the values listed can be found in Table 4.3. For the carbon Miras, Rowan-Robinson & Harris (1983b) estimated distances from the luminosities calculated by Cohen (1979) as a function of temperature index.

Claussen *et al.* (1987) calculated the distances to these stars using the assumption M_K = -8.1, an assumption we also employed in estimating distance moduli; for our data, where more than one measurement of m_K was available, an average $\underline{m}_K$ was taken as a reasonable estimate for computation of the distance modulus. For the S Miras, Rowan-Robinson & Harris (1983a) used estimates of the luminosities for distance determination. For these stars Jura (1988) also assumed M_K = -8.1; m_K was again averaged in the presence of more than one measurement. Finally, for both Mira and non-Mira S stars, Yorka & Wing (1977) suggest that maximum light M_V = -1.6 and -1, respectively. Maximum light M_V's were obtained from the AFOEV visual light curves discussed earlier. Since reddening was not measured or estimated for these stars, we have assumed an average $\underline{A}_V$ _ 0.5, calculated from the A_V's estimated for the carbon stars.

As an estimate of the error in these distances, we compared the different distance values obtained for individual stars, where more than one value was available. The average standard deviation of the distances was 17%; hence, we have adopted a conservative 20% error as a reasonable uncertainty in the determined distances, noting that this consistent with typical errors in estimated distances to these objects (e.g. Celis 1980, Wyatt & Cahn 1983, Claussen *et al.* 1987, Feast *et al.* 1989). We note that the distances determined from the Yorka & Wing (1977) M_V assumption change by only roughly 1/3 of an error estimate with the change in M_V's due to the assumed reddening of $\underline{A}_V$ _ 0.5.

Linear radii for oxygen-rich giants and supergiants were obtained by utilizing

distances found in the *General Catalog of Trigonometric Stellar Parallaxes* (GCTP, van Altena *et al*. 1991). For the radii of the giants not in the GCTP, we used the spectral type-linear radii relation given in Dyck *et al*. (1996a) as a rough measure of linear radius.

We note that three S stars were unresolved by IOTA. The most distant S star resolved by the interferometer is AA Cyg at 759 pc; the distance of AD Cyg is inferred to be 1047 pc and unsurprisingly was not resolved. HR 8062 and IRC+40458, however, are indicated to be at distances of 274 pc and 459 pc, respectively. Using the average non-Mira S star radius of 298 $R_{\odot}$ (see Table 4.4 and the discussion in §4.4.1), these objects should be 10 and 6 mas in angular diameter, resolvable by IOTA. Alternatively, we may estimate the expected angular size using the average non-Mira S star temperature of approximately 3100K (see Table 4.4) and the measured bolometric flux of these objects. HR 8062, at $K = 0.97$, and IRC+40458, at $K = 1.29$, are estimated via this method to be 4.6 and 4.0 mas in size, at and below the resolution limit of the interferometer, respectively. These two approaches illustrate the greater precision of the temperature estimate versus the radius estimate for these stars.

From the linear radii and the effective temperatures calculated from angular size and bolometric flux, we may determine stellar luminosity from $L = 4\pi\sigma R^2 T_{EFF}^4$. As mass loss is expected to be affected by radiation pressure (Zuckerman & Dyck 1986, Ivezi_ & Elitzur 1995), this parameter is expected to characterize a star's propensity to lose mass (see also the next section).

4.3.3 K - [60] Color

As a rough means of comparing the relative rates of mass loss, we have calculated the *K - [60]* colors for each of the three types of both Mira and non-Mira stars. This is consistent with the previous investigations of stellar mass loss by Young *et al.* (1993) (circumstellar shells resolved by IRAS), Jura & Kleinmann (1989) (dust-enshrouded AGB stars), Claussen *et al.* (1987) (carbon stars, variable & non-variable), and Jura (1988) (S stars). It is our intent with this analysis to investigate *relative* mass loss rates, rather than absolute rates; in conjunction with our effective temperature data, we may provide context for the evolutionary progression of these stars. Although other investigations have utilized other colors - e.g. Jura's (1986) *K - [12]* investigation of carbon stars; Gehrz & Woolf (1971) used *[3.5] - [11]* for characterize stellar mass loss in general; Jura (1988) utilized *K - [25]* colors to investigate S stars - we have selected the *K - [60]* colors in order to more closely compare relative mass loss rates. Colors utilizing the shorter IRAS wavelength bands risk weighting bias from resonance effects due to the differing compositions of the mass lost from each type of star - carbon-rich, oxygen-rich or S-type. Investigations of mass loss of varying chemical compositions (e.g. astronomical silicate, crystalline olivine, graphite, SiC & amorphous carbon) indicate that the longer wavelength bands serve well in minimizing these effects (Ivezi_ & Elitzur 1995). For the Mira variable stars for which we have obtained multiple epochs of observational data, average values for both T_{EFF} and *K - [60]* were computed. Also, from the T_{EFF} calculated for each star, we may compute an expected blackbody $(K - [60])_{BBR}$ color; the *K - [60]* excess is thus obtainable from these two values:

$(K - [60])_{EXCESS} = K - [60] - (K - [60])_{BBR}$. Any amount of $K - [60]$ excess should be indicative of stellar mass loss.

Table 4.4. General trends of effective temperatures and radii.

	Mira	type difference	Ref	non Mira	type difference	Ref	Mira / non Mira difference
Effective Temperatures (K):							
oxygen-rich	2686 ± 298		2	3336 ± 196		3	650
		317			263		
S type	2370 ± 169		1	3073 ± 213		1	704
		208			184		
carbon	2162 ± 239		1	2889 ± 222		4	727
Radii ($R_\odot$):							
oxygen-rich	376 ± 86		2	160		3	216
		150			138		
S type	526 ± 138		1	298 ± 93		1	228
		122			102		
carbon	648 ± 171		1	400		4	248

References:

1 This paper, 2 van Belle *et al.* 1996, 3 Dyck *et al.* 1996a, 4 Dyck *et al.* 1996b.

Notes:

1 Oxygen-rich non-Mira temps from stars later than M4 in Dyck *et al.* 1996a.

2 Oxygen-rich non-Mira radii from M7 estimate & Dyck *et al.* 1996a.

4.4 Analysis

4.4.1 General Observations

Given the small sample size of the carbon and S-type Mira subsets, investigation of these variable stars in a phase-dependent manner is not possible. However, since there is a reasonable spread in the represented phases, from maximum to minimum light, we may establish general parameters for effective temperature and linear radius for these stars. Without neglecting the tendency for the Mira variables to have variability in temperature and radius, we can begin to establish a framework in which oxygen rich, S-type, and carbon stars fit relative to one another, within the context of the more complete data sets presented in our previous papers (as discussed in §4.3). Table 4.4 presents the general results discussed in this section.

Temperature. For the Mira variables, an average effective temperature T_{EFF} and standard deviation σ was calculated for each star for which multiple epochs of observational data had been obtained. The degree of variation in T_{EFF} was established by calculating the σ's of difference between the maximum and minimum T_{EFF} for those stars. For the oxygen-rich Mira variables, the largest variations observed were 4-5σ (R Peg, R Aql); however, the carbon Miras exhibited less variation, with the largest variation being 1.8-2σ (U Cyg, V Cyg), and the S-type Miras presented the least variability, with the largest variation being 1.5σ (R Cyg). We note that the carbon and S-type Miras, while having a smaller number of stars in each sample, had a greater amount of multiple epoch sampling than the oxygen-rich Mira sample. The average σ was on order 6-7% T_{EFF} for

each of the three samples.

A second interesting contrast between the oxygen-rich, S-type and carbon star samples, for both the Mira and non-Mira subsets is a tendency for the effective temperature to decrease in progression from oxygen-rich to S-type to carbon. For each of the 6 subsets, an average effective temperature was computed, with the standard deviation of the temperatures being utilized as a reasonable error bar; the non-Mira oxygen-rich star mean temperature was computed from the giant stars later than spectral class M4 found in Dyck *et al.* (1996a), with the expectation that these objects were the closest analogs to the oxygen-rich Miras, which tend to be of the later M spectral types. The non-Mira carbon star mean temperature excluding the three lowest temperature points (S Aur, TW Oph, CIT 13), which are most likely either temperatures significantly affected by the presence of circumstellar shells (S Aur, CIT 13) or interstellar reddening (TW Oph) (see Dyck *et al.* 1996b for a discussion of both effects). For both Mira and non-Mira stars, there is a difference of approximately ΔT_{EFF} _ 300K between the oxygen-rich and S-type stars, while ΔT_{EFF} is roughly 200K between the S-type and carbon stars. Between the Mira and non-Mira stars of all three types, there is also a consistent ΔT_{EFF} of approximately 700K between types.

Size. Just as there is a progressive decrease in effective temperature among the types, there is a corresponding progressive increase in linear radius from oxygen-rich to S-type to carbon. As with the temperatures, an average R was computed for each subset with the error σ_R being taken from the standard deviation of the radii in the subset. We

note that the non-Mira oxygen-rich radius was estimated from Dyck *et al.*'s (1996a) M4 estimate and from the suggestion that a factor of two in size resulted from every decrease of 500K in effective temperature; the resulting size of 160 $R_{\odot}$ is consistent with a spectral type of M7-M8, this estimate being reasonable for the late spectral-type oxygen-rich Mira variable stars. For both Mira and non-Mira stars, there is a difference of approximately ΔR _ 140-150 $R_{\odot}$ between the oxygen-rich and S-type stars, while ΔR is roughly 100-120 $R_{\odot}$ between the S-type and carbon stars. Between the Mira and non-Mira stars of all three types, there is also a consistent ΔR of approximately 230 $R_{\odot}$ between types.

As noted in §4.3.1, for the non-oxygen-rich stars atmospheric extension has the potential to affect values established for angular size, and hence linear radius. For certain stars observed, the angular size measured can potentially be of a non-photospheric nature, being substantially affected by the presence of a circumstellar shell. Two likely candidates for this effect are CIT 13 and S Aur; we shall re-examine these objects further in the subsequent discussion.

4.4.2 Effective Temperature vs. Mass Loss

We have plotted effective temperature as a function of *K - [60]* color for each of the three types of non-Mira and Mira variable stars in our sample in Figure 4.1. Also plotted for comparison is the *K - [60]* color as a function of temperature for a generic black body radiator. We note that plots of the *K - [12]*, *K - [25]* and *L - [12]* colors (discussed in §4.3.4) are in general agreement with trends found for the *K - [60]*.

Non-Mira stars. As seen in Figure 4.1, the supergiants and oxygen-rich giants lie on the *K - [60]* blackbody curve down to a temperature of approximately 3200-3400 K; below this temperature, particularly among the giants, the average $(K - [60])_{EXCESS}$

Figure 4.1. Effective temperature versus mass loss for Mira and non-Mira stars.

becomes positive and there is a turnoff redward from the blackbody curve. This trend is continued by the S-type stars and carbon stars, which are all off to the mass loss side of the blackbody curve; the coolest carbon stars (S Aur, CIT 13) also exhibit the largest values of $(K - [60])_{EXCESS}$. One carbon star, TW Oph, has an unusually low temperature in conjunction with nearly a zero value of $(K - [60])_{EXCESS}$; this has been addressed in more detail in Dyck *et al.* (1996b). There is substantial overlap between the oxygen-rich giants and the carbon stars; the S-type stars occupy a region overlapping the oxygen-rich and the carbon stars, but this region is not the exclusive domain of the S stars. Although this could be interpreted as evidence for the suggestion by de Jong (1989) that some stars are bypassing the S stage, we shall see no evidence of overlap in the next section when examining P_r / P_g as a function of $K - [60]$. Unlike the oxygen-rich giants, the supergiants do not appear to have a subset below the 3200-3400 K turnoff from the blackbody curve; only one star, α Ori, is significantly redward of the $K - [60]$ blackbody curve.

Mira variable stars. Mass loss associated with Mira variable stars has been observed via a variety of techniques: CO line profiles (e.g. Knapp *et al.* 1982, Knapp & Morris 1985), OH line profiles (e.g. Baud & Habing 1983), in addition to infrared observations (e.g. Herman *et al.* 1986). Mass loss has been associated individually with the oxygen-rich, S type and carbon Mira types (see Jura & Kleinmann 1992, Jura 1988, and Jura 1986, respectively).

All three types of Mira are found redward of the blackbody $K - [60]$ curve in the

mass loss region of Figure 4.1. The S stars once again are intermediary to the oxygen-rich and carbon stars, but within the confines of small number statistics, form a more complete 'boundary' between the two other types than do their non-variable counterparts. Also noteworthy in the presence of such a boundary is the lack of overlap between the oxygen-rich and carbon Miras. Although indicative of *some* Miras passing through a S-type stage prior to becoming carbon Miras, these data do not rule out the possibility of some Miras transitioning directly from oxygen-rich to carbon stages of evolution.

4.5 Conclusion

The IOTA program of observations of highly evolved stars has resulted in the establishment of effective temperatures and linear radii for both Mira variable and non-Mira stars, of oxygen-rich, S-type and carbon chemical abundance types. Our results indicate that significant mass loss begins for stars of all types below and effective temperature of 3400-3200K. Investigation of tendency for mass loss as characterized by P_r / P_g and actual rates of loss indicates an increased mass loss with increased P_r / P_g, as would be expected; specific features in the relationship between mass loss and P_r / P_g have been observed but remain unexplained. Pulsation, when present in giant stars, appears to be a significant mechanism in driving mass loss in those stars.

CHAPTER V

K & M GIANTS & SUPERGIANTS

5.1. Introduction

One of the last observational problems in stellar atmospheres is the detailed study of the surface structure of a star. The lowest-order measurable parameter of surface structure, the overall size, is necessary for the determination of the stellar effective temperature. In the H-R diagram, the coolest region is the least well constrained by observation. K - M luminosity class I - III stars are common and potentially useful in galactic structure studies, as distance indicators, so that their properties ought to be well understood. Two decades ago began a renaissance in the study of stellar angular diameters, with the development of speckle interferometry, lunar occultation studies and Michelson interferometers. Significant steps were made to delineate the effective temperature scale for cool stars by Ridgway *et al.* (1980), DiBenedetto & Rabbia (1987), DiBenedetto & Ferluga (1990) and DiBenedetto (1993), using observations made primarily at near-infrared wavelengths. Forty-four stars were used in these analyses.

In 1990 we began a program to measure angular diameters for a large sample of cool stars. To date, the only results which have been published are for α^1 Her (Benson *et al.* 1991), for α Ori (Dyck *et al.* 1992) and for RX Boo and RS Cnc (Dyck *et al.* 1995). Owing to the completion of the first phase of construction of IOTA (the Infrared Optical Telescope Array) and to improvements in the operating efficiency, we are now in a

position to increase this sample manyfold. Here, we report new observations of 34 K0 - M8 stars of luminosity class I, II and III and we rediscuss data for an additional three stars already published. We are concentrating our observations at near-infrared wavelengths for several reasons. First, these stars radiate most of their energy at the longer wavelengths. Second, it allows us to compare our results more directly to the previous determinations of effective temperature, referenced above, and thus provide a more homogeneous set for understanding the astrophysical parameters for these stars. Third, and most important, it is well known that many stars of this late type show the observational effects of circumstellar dust shells. Tsuji (1978) pointed out that the dust is often hard to separate from the photosphere, making a determination of the photospheric diameter problematic. At optical wavelengths, the dust particles can scatter the stellar radiation while in the thermal infrared the dust reradiates absorbed stellar energy. Light at near-infrared wavelengths, on the other hand, will penetrate to the stellar photosphere.

The selection of sources was governed by expected angular size, based upon blackbody calculations, and availability. The stars observed here are mostly in the spring and summer parts of the sky. We did not include in the sample any known Mira variables or stars with optically thick circumstellar shells. The sources are listed in Table 5.1, where we give the *Bright Star Catalog* number (Hoffleit 1982), an alternate designation, the adopted spectral type, the source for that spectral type, the assumed interstellar reddening and the bolometric flux.

Using the data reported in this paper, along with the published occultation and Michelson interferometry data, we assemble a sample of 80 independent observations of

Table 5.1. IOTA observations of K & M giant & supergiant stars.

BS	Name	Spectral Type	Ref	A_V	F_{TOT} (W cm^{-2})
2061	α Ori	M1-2Ia-Ib	1	0.46	1.15×10^{-11}
3639	RS Cnc	M6III(S)	2	0.46	8.47×10^{-13}
4909	TU Cvn	M5-III	1	0.0	2.21×10^{-13}
5299	BY Boo	M4.5III	1	0.0	2.55×10^{-13}
5340	α Boo	K1.5III	1	0.34	5.83×10^{-12}
....	RX Boo	M7.5-8	1	0.0	8.85×10^{-13}
5512	HD130144	M5IIIab	2	...	3.82×10^{-13}
....	τ^4 Ser	M5IIIa	1	0.0	4.20×10^{-13}
....	ST Her	M6-7III(S)	1	...	3.72×10^{-13}
....	X Her	M7	3	0.0	6.05×10^{-13}
6056	δ Oph	M0.5III	1	0.0	7.58×10^{-13}
6146	g Her	M6-III	1	0.0	1.08×10^{-12}
6406	α^1 Her	M5Ib-II	1	0.0	4.34×10^{-12}
6702	OP Her	M5IIb-IIIa	4	0.0	1.64×10^{-13}
6705	γ Dra	K5III	1	0.0	9.06×10^{-13}
7009	XY Lyr	M4.5-5+II	1	0.0	2.26×10^{-13}
7139	δ^2 Lyr	M4II	1	0.0	5.79×10^{-13}
7157	R Lyr	M5III	2	0.0	1.23×10^{-12}
7525	γ Aql	K3II	1	0.37	5.53×10^{-13}
7536	δ Sge	M2II	2	0.0	4.32×10^{-13}
7635	γ Sge	M0-III	1	0.0	3.24×10^{-13}
7645	VZ Sge	M4IIIa	2	...	2.30×10^{-13}
7735	31 Cyg	K4Ib	5	0.0	1.75×10^{-13}
7751	32 Cyg	K5Iab	5	0.0	2.11×10^{-13}
7886	EU Del	M6III	1	0.0	5.03×10^{-13}
7941	U Del	M5II-III	6	0.0	2.83×10^{-13}
7951	EN Aqr	M3III	1	0.0	2.52×10^{-13}
8062	HD200527	M4.5III(S)	1	0.0	8.42×10^{-14}
8079	ξ Cyg	K4.5Ib-II	1	0.34	2.91×10^{-13}
....	V1070 Cyg	M7III	7	...	3.07×10^{-13}
8262	W Cyg	M5IIIa	2	0.0	5.88×10^{-13}
8308	ε Peg	K2Ib-II	1	0.58	7.83×10^{-13}
....	TW Peg	M6-7	8	...	3.18×10^{-13}
....	SV Peg	M7	8	...	2.78×10^{-13}
....	RX Lac	M6	8	...	2.27×10^{-13}
8698	λ Aqr	M2.5III	1	0.0	4.03×10^{-13}
8775	ß Peg	M2.5II-III	1	0.0	1.63×10^{-12}

References for spectral types used in Table 5.1: (1) Keenan & McNeil (1989), (2) Hoffleit (1982), (3) Lockwood (1972), (4) Keenan (1963), (5) Wright (1970), (6) Keenan (1942), (7) Moore & Paddock (1950), (8) Kukarkin *et al.* (1969).

K and M giant and supergiant stars, with spectral classes extending to M8. We show that the effective temperature scales previously established are correct and extend them

to later spectral types. For the first time, we have enough stars to assess the spread in effective temperatures within a spectral subtype and evaluate the natural width of the effective temperature scale for a given spectral type. The comparison of effective temperature scales for giants and supergiants is readdressed (Dyck *et al*. 1992), with the conclusion that supergiants are indeed systematically cooler at a given spectral type. Finally, we look at the linear radii for the few stars which have accurate parallax data.

5.2. Observations

The new data reported in this paper were obtained in the K (λ = 2.2 μm, $\Delta\lambda$ = 0.4 μm) filter with IOTA. The interferometer, detectors and data reduction procedures have been described more fully by Carleton *et al*. (1994) and Dyck *et al*. (1995). IOTA is presently operated in a two-telescope configuration and infrared observations were made on 31 nights during 1993, 1994 and 1995. Completion of the vacuum delay system during the summer and fall of 1994 has made possible the use of all available baselines, although only two, 21 m and 38 m, were used for the observations reported herein. We sweep the optical delay line past the white light fringe position at a rate which produces an interferogram with a fringe frequency of 100 Hz. The data-collection window is sufficiently long that all of the interference pattern from a source (the interferogram) is recorded as the optical delay line sweeps past the white light position. The beams from the two telescopes are combined onto a beamsplitter, producing a reflected and transmitted component for each telescope. Thus, two independent interference signals may be recorded simultaneously for each object observed. Improvements made to the

data-taking computers and software during 1994-95 routinely allow us to obtain 1500-2000 interferograms in each data channel in an 8-hour night.

The interferograms are digitally filtered with a 100 Hz square bandpass filter and normalized by the total flux from the source. For a perfect optical system, the amplitude of this normalized interferogram (called the visibility amplitude or simply the visibility) is directly related to the angular diameter of a partially resolved stellar disk, in the sense that smaller visibility amplitudes correspond to larger angular sizes. An unresolved source will have unit visibility. However, alignment errors and other system aberrations will reduce this point source response below unity. Therefore, observations of program stars are interleaved with observations of unresolved calibration stars in order to determine the interferometer point-source response and to minimize the effects of its variations. Stellar calibration sources were chosen on the basis of blackbody calculations from the star's known spectral type and observed flux. We tried to restrict our selection to sources with visibilities greater than 90%, so that errors in these estimates, that propagate to the program star visibilities, would be minimized. The amplitude of a filtered source interferogram is determined and divided by the corresponding amplitude for a calibrator interferogram, to remove the point source response of the instrument. The resulting ratio is the properly calibrated visibility amplitude for the source. In Table 5.2 we list the observed data, where we give the date of the observation, the interferometer projected baseline, the mean visibility amplitude in each of the two detector channels, obtained from multiple interferograms, and the standard deviation of

the mean for each channel.

Table 5.2. Calibrated visibilities in the two data channels.

Star	UT Date	B(m)	V_0	ε_0	V_1	ε_1
γ Aql	95Jun09	35.74	0.508	0.001	0.454	0.004
γ Aql	95Jun10	35.80	0.616	0.028	0.600	0.023
γ Aql	95Jun11	36.07	0.710	0.067	.....	.....
γ Aql	95Jun12	36.14	0.782	0.033	0.612	0.021
λ Aqr	95Jul11	31.12	0.604	0.076	.....	.....
EN Aqr	95Jul08	36.32	0.777	0.025	0.781	0.062
α Boo	94May19	21.14	.....	.....	0.329	0.035
α Boo	94May20	21.14	.....	.....	0.259	0.005
BY Boo	95Jun03	37.36	0.713	0.001	0.700	0.010
BY Boo	95Jun04	37.23	0.641	0.009	0.593	0.013
BY Boo	95Jun05	37.29	0.692	0.001	0.616	0.016
RX Boo	94Jan21	21.13	0.239	0.019	0.238	0.013
RX Boo	94Apr19	21.21	0.443	0.018	0.381	0.018
RX Boo	94May05	21.15	0.509	0.026	0.472	0.038
RX Boo	94May19	21.21	.....	.....	0.253	0.029
RX Boo	94May20	21.12	.....	.....	0.165	0.002
RX Boo	94Jun02	21.19	.....	.....	0.259	0.017
RX Boo	94Jun03	21.12	.....	.....	0.316	0.005
RS Cnc	93Dec10	21.21	0.713	0.032	0.701	0.024
RS Cnc	94Jan14	21.21	0.436	0.029	0.512	0.027
RS Cnc	94Jan20	21.21	0.528	0.057	0.402	0.053
RS Cnc	94Jan21	21.21	0.417	0.041	0.422	0.016
TU CVn	95Jul10	37.40	0.564	0.041	0.642	0.049
W Cyg	95Jun02	36.84	0.270	0.028	0.369	0.050
W Cyg	95Jun05	36.75	0.179	0.003	0.171	0.002
ξ Cyg	95Jul10	37.82	0.499	0.033	0.680	0.019
V1070 Cyg	95Jun04	37.21	0.584	0.003	0.655	0.009
V1070 Cyg	95Jun05	36.76	0.573	0.001	0.584	0.001
31 Cyg	95Jul10	37.42	0.671	0.0601	0.7943	0.066
32 Cyg	95Jul10	37.29	0.647	0.057	0.776	0.069
EU Del	95Jun10	36.90	0.372	0.018	0.437	0.010
EU Del	95Jun11	36.99	0.346	0.069	.....	.....
EU Del	95Jun12	36.93	0.394	0.004	0.483	0.014
U Del	95Jul06	36.84	0.570	0.009	.....	.....
U Del	95Jul07	36.60	0.562	0.001	0.604	0.009
γ Dra	95Jun02	36.73	0.596	0.011	0.533	0.008
γ Dra	95Jun03	36.68	0.409	0.001	0.371	0.008
γ Dra	95Jun04	36.76	0.407	0.018	0.465	0.022
γ Dra	95Jun05	36.66	0.325	0.0122	0.252	0.015
g Her	95Apr28	20.84	0.493	0.025	0.414	0.024
g Her	95Apr29	20.68	0.584	0.011	0.532	0.024
g Her	95Apr30	20.67	0.644	0.039	0.573	0.030
g Her	95May01	20.82	0.535	0.018	0.462	0.016
OP Her	95Jun04	37.44	0.775	0.003	0.797	0.019
OP Her	95Jun05	37.50	0.753	0.007	0.779	0.005
ST Her	95Jun03	36.90	0.481	0.005	0.462	0.013
ST Her	95Jun04	36.92	0.431	0.011	0.387	0.011

Star	UT Date	B(m)	V_0	ε_0	V_1	ε_1
ST Her	95Jun05	36.89	0.435	0.016	0.436	0.011
X Her	95Apr29	20.44	0.687	0.018	0.671	0.002
X Her	95May01	20.25	0.687	0.004	0.594	0.003
X Her	95Jun03	37.50	0.193	0.002	0.180	0.003
X Her	95Jun04	37.18	0.220	0.001	0.220	0.008
RX Lac	95Jul10	37.40	0.622	0.038	0.821	0.046
δ^2 Lyr	94Apr19	21.12	0.895	0.039	0.772	0.044
δ^2 Lyr	94May05	21.23	0.862	0.039	0.997	0.048
δ^2 Lyr	95Jun05	37.63	0.370	0.006	0.356	0.008
δ^2 Lyr	95Jul09	37.26	0.372	0.011	0.373	0.001
R Lyr	95Apr29	20.70	0.572	0.012	0.482	0.015
R Lyr	95Apr30	20.71	0.689	0.006	0.610	0.001
R Lyr	95May01	20.53	0.704	0.031	0.618	0.026
XY Lyr	95Jun02	37.59	0.590	0.007	0.647	0.015
XY Lyr	95Jun03	37.00	0.663	0.010	0.660	0.011
XY Lyr	95Jun04	37.10	0.676	0.003	0.712	0.016
δ Oph	95Jun13	35.82	0.477	0.028	0.488	0.028
δ Oph	95Jul12	29.97	0.598	0.027	0.575	0.039
ß Peg	93Dec10	21.18	0.485	0.033	0.489	0.036
ß Peg	94Jun09	21.21	0.689	0.038	0.510	0.032
ε Peg	95Jun12	36.70	0.622	0.022	0.559	0.042
ε Peg	95Jul06	36.64	0.618	0.015	.....	.....
ε Peg	95Jul07	36.52	0.664	0.021	0.696	0.005
SV Peg	95Jul10	37.13	0.460	0.030	0.603	0.048
TW Peg	95Jul09	37.38	0.447	0.008	0.491	0.012
δ Sge	95Jun07	36.86	0.653	0.016	0.650	0.011
δ Sge	95Jun09	36.79	0.560	0.015	0.531	0.016
δ Sge	95Jun10	36.86	0.514	0.013	0.578	0.013
ν Sge	95Jun11	36.99	0.835	0.042	.....	.....
VZ Sge	95Jun12	36.81	0.856	0.025	0.985	0.061
τ^4 Ser	95Jun07	35.75	0.437	0.001	0.480	0.006
τ^4 Ser	95Jun09	35.78	0.410	0.004	0.401	0.002
τ^4 Ser	95Jun10	35.91	0.389	0.010	0.430	0.007
BS5512	95Jun10	36.62	0.587	0.006	0.600	0.021
BS5512	95Jun13	36.52	0.589	0.004	0.542	0.004
BS8062	95Jul10	37.62	0.925	0.052	0.987	0.080

We noted earlier (Dyck *et al.* 1995) that the interferometer internal consistency on a given night was better than that for repeated observations over more than one night. We now have a sufficient body of repeated nightly observations to quantify that difference: For a source which is about 50% resolved, the standard deviation for the

combined result of all observations for a single night in one data channel is ±0.072. Although we do not yet fully understand the reasons for the differences, they apparently arise from small changes in the instrument response which are incompletely calibrated out by the observation of unresolved sources. Because these night-to-night, external, errors are larger than the errors listed in Table 5.2, we adopt them as a better estimate of the true precision of the visibility observations. For the purpose of computing the angular diameters and effective temperatures, we have averaged the visibility data in Table 5.2 and assigned an error based upon the formula

$$\varepsilon_V = \pm \frac{0.072}{\sqrt{(Number\ of\ Nights)\,x\,(Number\ of\ Data\ Channels)}} .$$

We computed average baselines and unweighted mean visibilities and assigned the standard errors based upon this formula. In Table 5.3, we list the uniform disk angular diameter, θ_{UD}, in milliarcseconds (mas), computed by fitting the Bessel function J_1 to the mean visibility at the baseline. When stars were observed on more than one baseline (i.e., when there was more than about 5% difference in the baseline), angular diameters and errors were computed for each baseline and only the weighted mean angular diameter and its weighted error are given in Table 5.3. We have also included previously published data for α^1 Her (Benson *et al.* 1991), α Ori (Dyck *et al*. 1992) and RS Cnc (Dyck *et al*. 1995). RX Boo is also repeated because new observations were obtained in 1994.

There are six stars -- α Boo, γ Dra, R Lyr, β Peg, 31 Cyg and 32 Cyg -- which have been measured both at IOTA and at CERGA, but with different approaches to the

fringe visibility detection. A comparison of the uniform-disk angular diameters is shown plotted in Figure 5.1. From the plot, one can see that the measurements of the three stars with $\theta_{UD} \leq 10$ mas agree well. However, the measurements of the three

Table 5.3. Angular diameters and effective temperatures measured with IOTA.

Star	θ	σ	θ	T_{eff}	σ
α Ori	44.2	0.2	45.2	3605	43
RS Cnc	14.8	0.5	15.1	3246	67
TU CVn	7.4	0.6	7.6	3281	139
BY Boo	6.8	0.3	6.9	3547	89
α Boo	19.1	1.0	19.5	4628	133
RX Boo	18.4	0.5	18.8	2943	53
BS5512	7.9	0.4	8.1	3641	102
τ^4 Ser	9.8	0.3	10.0	3348	65
ST Her	9.3	0.3	9.5	3334	67
X Her	12.1	0.4	12.4	3300	67
δ Oph	9.3	0.5	9.5	3983	117
g Her	14.9	0.5	15.2	3438	71
α^1 Her	33	0.5	33.7	3271	46
OP Her	5.4	0.5	5.5	3565	170
γ Dra	9.6	0.3	9.8	4099	80
XY Lyr	6.8	0.3	6.9	3442	86
δ^2 Lyr	9.6	0.4	9.8	3665	88
R Lyr	13.3	0.6	13.6	3759	96
γ Aql	7.6	0.3	7.8	4072	94
δ Sge	7.8	0.3	8.0	3779	85
γ Sge	4.6	1.1	4.7	4579	550
VZ Sge	3.2	1.1	3.3	5039	868
31 Cyg	5.9	0.6	6.0	3466	181
32 Cyg	6.2	0.6	6.3	3543	176
EU Del	9.7	0.4	9.9	3520	84
U Del	7.9	0.5	8.1	3378	114
EN Aqr	5.5	0.7	5.6	3933	255
BS8062	2.3	1.1	2.4	4624	1107
ξ Cyg	7.5	0.6	7.7	3491	146
V1070 Cyg	7.6	0.4	7.8	3515	101
W Cyg	11.5	0.4	11.8	3361	71
ε Peg	7.3	0.4	7.5	4532	135
TW Peg	8.9	0.6	9.1	3277	117
SV Peg	8.3	0.6	8.5	3281	125
RX Lac	6.1	0.6	6.2	3638	184
λ Aqr	8.9	1.0	9.1	3477	200
ß Peg	14.3	0.7	14.6	3890	106

larger stars differ, in the sense that the IOTA diameters are, on average, 90% of the CERGA diameters. For these larger stars, we have also compared the visibility measurements directly, in addition to the uniform-disk diameters and there clearly is a systematic difference between the data sets. Six stars measured in common are too few

to allow us to decide whether there is a general systematic difference or simply the statistics of small numbers at work. We note that a 10% error in the angular size results in a 5% error in the effective temperature scale.

5.3. Effective Temperatures

We have been careful to choose, where possible, stars that are classified on the MK system, preferring spectral types estimated by Keenan and his coworkers. Second choices have been spectral types from Hoffleit (1982) and Lockwood (1972), both of which correlate very well with the Keenan types. In a few cases, other alternative sources were necessary. Total flux densities were obtained from magnitudes published in references in the SIMBAD database and in Gezari *et al.* (1993). We have estimated the effects of interstellar reddening by using the observed and intrinsic colors for the spectral type (Johnson 1966, Schmidt-Kaler 1982). Reddening corrections for each wavelength were obtained from van de Hulst's theoretical reddening curve number 15 (see Johnson 1968). There is very little difference between this theoretical curve and the empirical reddening determination made by Mathis (1980). Monochromatic flux densities at each wavelength were obtained from the magnitudes using absolute calibrations by Hayes & Latham (1975), Hayes (1984) and Blackwell *et al.* (1983). Bolometric flux densities were generally computed from a simple numerical integration of the observed monochromatic flux densities from 0.45 to 5 μm. Flux contributions beyond 5 μm were estimated by integrating a Rayleigh-Jeans distribution, normalized to the 5 μm flux density. For eight stars, not enough data were found to carry out a complete bolometric

flux density integration. In this case the mean relationship

Figure 5.1. A comparison of the uniform disk angular diameters determined with IOTA and CERGA, for six stars measured in common. The dashed line delineates the equal-diameter locus.

between flux density at K (2.2 μm) and total flux as a function of spectral type (Dyck, Lockwood & Capps 1974) was used to estimate the bolometric flux density.

In order to compute the effective temperature, it is necessary to convert the uniform-disk angular diameters to limb-darkened diameters through the use of model atmospheres. It has been noted that these corrections are generally small in the infrared, so that errors will not greatly affect the results (see, for example, DiBenedetto 1993). As we have done in the past (Dyck *et al.* 1995), we used the models of Scholz & Takeda (1987) to compute these numerical correction factors. Following the suggestion of Scholz (1985) we compute a fictitious angular diameter, θ_R, corresponding to the level in the atmosphere where the Rosseland mean opacity is unity. These corrections are nearly independent of spectral type over the range of temperatures and luminosity classes considered here and have a mean value $\theta_R \approx 1.022\ \theta_{UD}$. We have adopted this conversion for all stars observed in this study. This correction factor is approximately the same as those used for the CERGA and occultation results, so that our results and theirs may be directly compared.

The effective temperatures, T_{EFF}, and their errors, ε_T are listed in Table 5.3, where we have computed the effective temperature from

$$T_{EFF} = 1.316 \times 10^7 \left[\frac{F_{TOT}}{\theta_R^2} \right]^{1/4} \quad K \ .$$

F_{TOT} is the bolometric flux, corrected for interstellar reddening (in W cm^{-2}) and θ_R is the Rosseland mean stellar angular diameter (in mas). The error in T_{EFF} is obtained from the errors in the total flux, ε_F, and in the angular diameter, ε_θ, through the relationship

$$\frac{\varepsilon_T}{T_{EFF}} = \left[\frac{1}{16} \left(\frac{\varepsilon_F}{F_{TOT}} \right)^2 + \frac{1}{4} \left(\frac{\varepsilon_\theta}{\theta_{UD}} \right)^2 \right]^{1/2} .$$

The errors in the angular diameters are listed in Table 5.3. The error in the bolometric flux density was assumed to be an average for the entire sample of stars, dependent upon several factors. First, there are errors which depend upon the photometric system and upon the intrinsic variability of the stars observed. Most of our program stars are small-amplitude variable stars. We attempted to establish a reasonable level for the variability (and dispersion for different observers) from infrared data compiled by Gezari *et al.* (1993) for similar kinds of stars, but not necessarily the same ones observed for this program. This was necessitated by the fact that, often, very few repeated observations existed in the *Catalog of Infrared Observations* for our program stars. From a sample of 268 repeated 2.2 μm observations of nine small-amplitude variable K and M giants and supergiants, we determined the relative error in the flux density to be ±0.08. Second, there are errors caused by misestimates of the reddening which may result from errors in the measured color, errors in the assigned spectral type or errors in the intrinsic color scale. We tried to evaluate this source of error by scrutinizing those stars in our sample that lie at galactic latitude $b \geq 40^o$, where interstellar reddening should (statistically) be small. Seven stars in our sample satisfied this criterion, for which we computed the color difference $\Delta = (B\text{-}V) - (B\text{-}V)_o$. The mean value of the difference was 0.01, confirming that the mean color excess for the group is low, and the *rms* value was 0.09. Thus, we adopt an uncertainty of 0.1 in the reddening, and have not applied any corrections to the observed fluxes for stars with

$E(B-V) \leq 0.1$. Third, there are uncertainties resulting from errors in the flux calibration. Following Blackwell & Lynas-Gray (1994), we estimate the error from this source to by ±0.05. Summing all three contributions together in quadrature yields ±0.14; we adopt ±0.15 as a conservative average for the sample.

A few of the stars in our sample are not very well resolved and these tend to have large errors in the effective temperatures. However, there are 34 stars listed in Table 5.3 with estimated errors less than about 250 K; twenty-nine of these are giants of luminosity class II or III and the remaining five are supergiants. In Figure 5.2 we have plotted the 29 highest-precision giant star effective temperatures as a function of spectral type, where the data are shown as filled diamonds (♦). For comparison, we have included the temperatures measured at CERGA, represented by open squares (□), and the mean effective temperature relationship determined by Ridgway *et al*. (1980), shown as a dotted line. The first conclusion from this study is that results from all three methods agree very well. Our detailed comparison of the combined mean Michelson interferometry data with the Ridgway *et al*. scale, indicates that there is an *rms* difference of about 2% over the entire range, but that the difference is substantially greater than the dispersion in the Michelson data only at two spectral types. We conclude that the agreement between the combined Michelson interferometry temperatures and the occultation temperatures is essentially perfect.

The agreement indicated in Figure 5.2 suggests that we may reasonably compare all the available effective temperature estimates from occultations and Michelson

interferometry. We have taken the 20 best-determined stars (errors ≤ 250 K) from Ridgway *et al*. (1980) and added to them additional published results from the Kitt Peak occultation program. Restricting this latter sample to stars which have spectral types assigned by Morgan & Keenan (1973), Keenan & McNeil (1989) or the *Bright Star Catalog*, we obtain 8 additional stars (6 of which are giants) with errors ≤ 250 K, the parameters for which are summarized in Table 5.4. The bolometric fluxes for the stars in Table 5.4 were determined in approximately the same manner as those in Table 5.1, except in many cases new, unpublished photometry were obtained. We could, in principle, also add the optical wavelength data from the Mark III interferometer (e.g., Hutter, *et al*. 1989, Mozurkewich *et al*. 1991), but effective temperatures were not published for those angular diameter measurements.

Table 5.4. Supplemental occultation angular diameters and effective temperatures.

BS	Star	Spectral Type	F_{TOT} (W cm^{-2})	θ_R (mas)	ε_θ (mas)	T_{EFF} (K)	ε_T (K)
1407	75	K1III	4.15E-14	2.36	0.25	3866	210
1845	119	M2Iab-Ib	5.4E-13	9.83	0.07	3598	45
3357	θ	K5III	7.23E-14	3.27	0.13	3773	87
3461	δ	K0IIIb	1.01E-13	2.55	0.27	4645	250
....	SW	M7III:	7.46E-13	17.00	0.11	2966	36
....	HD1	M1.5III	5.94E-14	2.67	0.17	3976	135
6134	α	M1.5Iab-Ib	8.73E-12	45.65	2.75	3348	108
8850	γ	M3III	2.51E-13	6.07	0.16	3780	67

We have combined together the 66 occultation and near-infrared Michelson interferometry temperature determinations for giant stars to determine the "best" estimates for the mean effective temperatures as a function of spectral type. The

procedure was to bin the data in spectral subclasses and form an unweighted mean value. Within each bin, we kept track of the values of the differences, ΔT, between individual temperature determinations and the mean. Then, in order to smooth the data,

Figure 5.2. A plot of the effective temperature measurements for K and M giant stars, made by IOTA and CERGA, as a function of spectral type. For comparison, the effective temperature scale determined by Ridgway *et al.* (1980) is show as a dotted line.

we performed a boxcar averaging operation across the spectral types, taking ±1 spectral subtype as the width of the boxcar filter. The results of this averaging and smoothing procedure are listed in Table 5.5, where we have also listed the older effective temperature scales of Ridgway *et al*. (1980) and DiBenedetto & Rabbia (1987). Determining precise errors for each spectral subtype mean temperature is difficult because of the smoothing procedure. However, we may obtain a reasonable estimate of the average error by considering the distribution of differences, ΔT, which we find to be approximately Gaussian. Taking the *rms* value of the 53 differences, we find $\Delta T_{rms} \approx 145$ K. There is an average of 2.4 stars per spectral type bin, so that an average error for each effective temperature estimate may be taken to be $\varepsilon_T = \Delta T_{rms}/\sqrt{2.4} \approx 95$ K. We adopt 95 K as the uncertainty at each spectral type for our new, mean effective temperature scale.

The natural spread in the effective temperatures at a given spectral class is astrophysically interesting. We measure $\Delta T_{rms} \approx 145$ K, which must consist of at least three components: (1) The natural dispersion; (2) The observational error in measuring the effective temperature; and (3) The observational error in determining the spectral class. We may estimate the second of the errors listed above by taking the *rms* value of the errors assigned to each individual effective temperature determination. For the stars in the combined sample this results in about ±120 K. Trying to estimate the error in the spectral class is more difficult. Gliese (1973) has looked at the variation in MK spectral classification for K dwarf stars in the literature and has found a dispersion of ±0.6. For

the sake of further analysis, we assume that this value is representative of the classification errors for the stars presently under consideration. The average slope for the K and M giants is roughly 120 K/spectral class, so that a dispersion of ±0.6 spectral types would correspond to a dispersion of temperature of about ±70 K. Subtracting these last two sources of error in quadrature from the measured dispersion, we find that the natural dispersion in the effective temperature could be as small as about ±40 K. In fact, the errors in spectral type are undoubtedly smaller than the value we have used, since the types have come from one principal source. If there were no errors at all in the spectral type, then the natural dispersion would be about ±80 K. The true value probably lies between these two estimates.

Table 5.5. The mean effective temperature scale.

Spectral Type	Mean Effective Temperature Scale (K)		
	This Work	Ridgway *et al.* (1980)	DiBenedetto & Rabbia (1987)
K1III	4510	4610	....
K2III	4370	4450	....
K3III	4230	4270	4280
K4III	4090	4095	4115
K5III	3920	3980	4000
M1III	3835	3810	3715
M2III	3740	3730	3685
M3III	3675	3640	3630
M4III	3595	3560	....
M5III	3470	3420	....
M6III	3380	3250	....
M7III	3210	....	....

Note to Table 5.5: The estimated uncertainty for the effective temperatures determined in this paper is ±95 K for each spectral type.

There are fewer stars among luminosity classes I and I-II, so that a detailed analysis is not justified. However, in Figure 5.3 we compare the available supergiant effective temperature data to the mean relation for giants just established. It is clear that most of the supergiants lie well below the mean giant data, with the one exception being ε Peg. The second conclusion of this work is to confirm our previous results (Dyck *et al.* 1992) for the higher luminosity stars, namely that they are cooler at a given spectral type than their giant counterparts. Further, one can see a general decline of the temperature difference with advancing spectral type. Combining the IOTA and CERGA data, there are four K supergiants with spectral types between K4 and K5 (averaging slightly warmer than K4.5); taking mean values, we find T_{EFF} = 3588 K at this spectral type. From our mean relationship at K4.5, we find an average effective temperature T_{EFF} = 4005 K. Thus, the luminosity class I stars are roughly 400 K cooler than their luminosity class III counterparts at spectral type K4.5. Between spectral types M1 and M2, there are three supergiants in the IOTA and supplemental occultation sample, which average slightly cooler than M1.5. Our relationship predicts a mean giant temperature of 3760 K, about 240 K warmer than the three supergiants. Our lone supergiant at M5, α Her, is 200 K cooler than the M5 giants, but only lies about 1.5 times the combined errors away from the mean value for the giants. At present we have no explanation for the position of ε Peg in the H-R diagram. We have checked the spectral type and there seems to be no possibility of a misclassification in luminosity. Further, if there were an unseen double star in the field of view of the interferometer, the effect would be to

reduce the visibility, increase the angular diameter and lower the effective temperature, opposite to the observed effect. This star will require more detailed study to understand the observations.

Figure 5.3. A comparison of the supergiant effective temperatures to the mean effect temperature vs. spectral type relationship for giant stars. The line simply connects the mean points for the giant temperature scale but has no other significance.

5.4. Linear Radii

With the newly-determined angular diameters, it is tempting to hope that there are existing parallax data which would allow one to compute linear radii. In fact, the supergiants are beyond the range of classical ground-based astrometric capabilities and very few of the giants have well-determined parallaxes. Nevertheless, we have correlated the angular diameter data from IOTA, CERGA, the Mark III and occultations with the best parallaxes in the *General Catalogue of Trigonometric Stellar Parallaxes* (Jenkins 1963). Twenty-two stars were found with parallaxes, $\pi \geq 3\ \varepsilon_\pi$, where ε_π is the measurement error. Because many of these parallaxes are only 3-4 times the error, we have binned the observations into spectral type ranges K0-K2 (mean K1), K3-K5 (mean K4), K7-M0.5 (mean M1) and M2-M6 (mean M4). The estimated error for each mean spectral type is the standard deviation of the mean of all values within the spectral type range. The results are listed in Table 5.6 as $R_*/R_\odot$, the ratio of the stellar radius to the Solar radius. We note, as expected, that there is a general increase of the size of giants as one progresses toward the cooler types, with about a factor of two increase in size for each decrease of 500 K in the effective temperature. We have compared our estimates of stellar sizes to those given by Schmidt-Kaler (1982) and find the agreement reasonable at the hotter types. To our knowledge there have been no published estimates of linear radii for giants later than early M. However, when the Hipparchos data are available there should be a dramatic increase in high-quality parallaxes, so that linear stellar scale sizes will be well-determined to at least M8.

Table 5.6. Estimates of mean linear radii.

Spectral Type	R*/R⊙
K1III	16 ± 2
K4III	31 ± 6
M0III	40 ± 2
M4III	83 ± 19

5.5. Estimating Apparent Angular Diameters

In this paper we have focused on the determination of stellar effective temperatures based on measured angular diameter and photometry. It is often desired to invert this process and estimate the angular diameter based on photometry and T_{EFF} calibrations. A convenient procedure is to use published compilations of spectrophotometry to estimate the bolometric flux and to use a T_{EFF} versus spectral type calibration along with equation (14) to compute the limb-darkened diameter. We have carried out this calculation and present the results in Table 5.7 in the form of Rosseland mean angular diameter (in mas) for a star of K magnitude zero. For convenient reference, we have carried out this calculation for earlier spectral types as well as those discussed in this paper. The types earlier than G are based on intensity interferometry results (Hanbury Brown, Davis & Allen 1974). The G stars are based upon the results in Ridgway *et al*. (1980) and the K0 through M7 stars are based upon the T_{EFF} calibration presented in this paper. Stars later than M7 are merely an extrapolation of the latter calibration and are only included as preliminary estimates which may be useful in planning observations.

Table 5.7. Rosseland mean angular diameters versus spectral type for K=0.

Spectral Type	θ_R (mas)	Spectral Type	θ_R (mas)
B0	1.92	M0	5.64
A1	3.21	M1	5.78
F0	3.61	M2	5.87
F8	4.35	M3	5.95
G8	4.68	M4	5.98
K0	4.75	M5	6.10
K1	4.98	M6	6.60
K2	5.22	M7	7.11
K3	5.32	M8	(7.9)
K4	5.47	M9	(8.4)
K5	5.54	M10	(8.8)

In order to predict an observational result from Table 5.7, it will be necessary to multiply the Rosseland mean angular diameter by a limb-darkening correction to yield an appropriate uniform disk angular diameter. The correction will be wavelength dependent, but typically in the range 0.8-1.0. We expect that the apparent diameters estimated in this way will be useful as guides and may not be accurate to more than about 10% over the visible and near-infrared parts of the spectrum.

5.6. Conclusion

We have shown that it is possible to amass a large quantity of angular diameter data for K and M giants and supergiants, using existing ground-based interferometers. Approximately one-third of such stars available to IOTA have now been observed and new effective temperatures computed. From an analysis of the statistics of these temperatures, we do not believe that further observations in the spectral interval K0III to M7III will add much new astrophysical information. A more fruitful investigation would

be to concentrate observations on those small-amplitude giant variables with spectral types later than M7, and to push the effective temperature scale to its' ultimate limit in the H-R diagram.

CHAPTER VI

CARBON STARS

6.1. Introduction

From a statistical analysis of the distribution and mass-loss properties of carbon stars, Claussen *et al.* (1987) inferred that these stars probably originated from F stars in the mass range 1.2 to 1.6 $M_{\odot}$. Early observations by Mendoza V. & Johnson (1965) and Richer (1971) indicated that this group of stars occupied a region of the H-R diagram populated by the K and M giants. Yet very little fundamental information exists for the carbon star group. Only nine stars were listed in the White & Feierman (1987) catalog, having previously-published lunar occultation angular diameters. Quirrenbach *et al.* (1994) have measured the angular size of UU Aur, Y CVn and TX Psc using the Mark III interferometer and, using additional published lunar occultation diameters and photometry, estimated the effective temperature for nine carbon stars. From their own measured spectrophotometry and published angular diameters, Lázaro *et al.* (1994) have estimated the effective temperatures for four stars.

The effective temperature scale is not very well established owing to these small numbers. In Mendoza V. & Johnson (1965), the temperature estimates range between 2270K and 5500K. Cohen (1979) adopted a temperature scale, as a function of Yamashita (1972, 1975) spectral class, which ranged from 3240K at C2 to 2230K at C9. Quirrenbach *et al.* (1994) compared their effective temperature

scale with the scale set by Tsuji (1981a) based upon matching observed fluxes and colors to model atmospheres (the infrared flux method) and found that temperatures determined from angular diameter measurements are about 100K cooler than those determined from model atmospheres. Goebel *et al.* (1993) have argued that differences of a few hundred K for the effective temperature of TX Psc will determine whether or not the chemical composition is consistent with the existence of a deep envelope. Certainly the atomic line and molecular band strengths in the complex spectra are highly dependent upon the star's surface temperature (Tsuji 1981b). Thus, more angular diameter determinations will help to improve our understanding of the atmospheric properties of this class of stars. Effective temperatures are also an important parameter for understanding the flux spectrum from circumstellar shells surrounding these stars. Rowan-Robinson & Harris (1983) show that the model spectra seem to indicate that the atmospheric temperatures for the earlier types are around 2500K and for the later types around 2000K.

It is the purpose of this paper to report new angular diameter measurements of 15 carbon stars made with the IOTA (Infrared Optical Telescope Array) interferometer. Two of these, TX Psc and Y CVn, are common with lunar occultation and Mark III interferometry while 13 are measurements of new stars. We report the first observation of CIT 13, one of the original "infrared stars" (Ulrich *et al.* 1966). We find that there are significant differences in the estimated

reddening that, depending upon the method of estimation, will limit the accuracy of the effective temperatures determined from the measured diameters. When we combine our best observations with the sample analyzed by Quirrenbach *et al.* (1994), we obtain effective temperatures for a sample of 16 stars ranging in Yamashita spectral types from C5 to C9. We obtain the result that the temperatures increase slightly over this range of spectral types, counter to the original hopes for the spectroscopic classification schemes. This result confirms previous conclusions by Tsuji (1981a) and Ridgway *et al.* (1981) based upon the infrared flux method.

6.2. Observations

The data reported here were obtained at IOTA between April and October 1995. Two telescopes on baselines of 21 and 38 meters and a *K* filter ($\lambda = 2.2$ μm, $\Delta\lambda = 0.4$ μm) were used for all observations. The interferometer and details of the data-taking and reduction process have been described more fully by Carleton *et al.* (1994) and Dyck *et al.* (1995). Briefly, the incoming wavefront is divided by the two telescopes and propagated through the interferometer as an afocal beam. Optical delay differences are compensated by fixed and variable delays and the beams are recombined onto a beamsplitter which produces two complementary interference signals. These are monitored by two independent, single-element InSb detectors. In our mode of operation, we drive the variable delay line past the zero-path position at a rate which produces an interferogram with a fringe frequency of 100 Hz. The amplitude of the interferogram at the zero-path position for partially-resolved circular disks is related to the source fringe visibility amplitude, with lower amplitudes corresponding to larger diameter sources. The response of the interferometer plus atmosphere is calibrated by observation of stars known to be unresolved and observations of calibrators are alternated with observations of program sources to minimize the effects of variations of the interferometer and atmosphere. The observed fringe visibility of the source divided by the average fringe visibility of calibrators measured before and after the source results in the normalized fringe visibility for the source. The data for the two independent detector channels have then been averaged. These averaged,

normalized visibilities are listed in Table 6.1, along with their standard deviations, the date of the observation, the number of interferograms obtained and the interferometer baseline.

Table 6.1. IOTA observations of carbon stars.

Star	UT Date	B (m)	N	$V \pm \varepsilon_V$
AO And	95 Oct 08	38.26	100	0.863±0.099
VX And	95 Oct 05	36.90	100	0.681±0.058
V Aql	95 Jul 12	31.13	98	0.511±0.017
S Aur	95 Oct 05	37.15	34	0.478±0.053
WZ Cas	95 Oct 04	34.73	100	0.777±0.051
Y CVn	95 Apr 28	20.50	159	0.702±0.052
Y CVn	95 Apr 29	20.58	158	0.643±0.013
Y CVn	95 May 01	20.60	196	0.655±0.009
Y CVn	95 Jun 03	37.71	25	0.251±0.009
Y CVn	95 Jun 04	37.69	169	0.220±0.007
Y CVn	95 Jun 05	37.68	398	0.200±0.004
RS Cyg	95 Oct 08	38.22	98	0.849±0.130
RV Cyg	95 Oct 08	38.24	100	0.577±0.084
V460 Cyg	95 Jul 10	37.08	76	0.704±0.051
W Ori	95 Oct 07	32.94	99	0.501±0.057
RT Ori	95 Oct 07	34.46	100	0.866±0.130
SY Per	95 Oct 04	34.98	100	0.895±0.009
SY Per	95 Oct 05	36.41	50	0.938±0.158
Z Psc	95 Oct 08	38.21	97	0.810±0.123
TX Psc	95 Jul 08	36.90	28	0.320±0.029
TX Psc	95 Oct 06	33.20	50	0.514±0.122
TX Psc	95 Oct 07	34.09	50	0.478±0.091
CIT 13	95 Jul 09	37.59	269	0.252±0.005
CIT 13	95 Jul 10	36.95	56	0.336±0.013

Our observing strategy for measuring stellar disk diameters is to measure one visibility at one telescope separation, corresponding to a single spatial frequency. Neglecting the effects of surface structure and limb darkening, a single spatial frequency will allow a unique determination of the angular diameter. The procedure involves finding the best-fitting uniformly-bright, circular disk visibility function (the Bessel

function J_1) to the observed datum to yield the uniform-disk angular diameter, θ_{UD}. For a source of unknown geometry, more than one spatial frequency point is required to understand that geometry. However, for stellar disks, a single visibility measurement in the range $0.15 \leq V \leq 0.80$ should provide sufficient accuracy for the project described in this paper.

If a source was observed on more than one night, the visibilities and baselines were averaged when the baselines differed by no more than 10%. For Y CVn and TX Psc, observations were made at baselines which differed by more than 10%. Uniform disk diameters were computed for each baseline and the final value for each star was the weighted mean of the independent determinations.

We feel that 2.2 μm is a good choice of wavelengths for the observations because 1) it lies near, but on the Rayleigh-Jeans side of, the flux spectrum peak wavelength and 2) the effects of circumstellar dust on the determination of the atmospheric angular diameter will be minimized. The second assumption is based upon the following arguments, first put forward by Tsuji (1978): Small circumstellar dust particles generated by the star will absorb, scatter and thermalize the photospheric radiation. Owing to their small size, the absorption and scattering efficiencies decrease with increasing wavelength. Hence, longer wavelengths are better than shorter ones from this point of view. However, as the wavelength increases, the thermal re-emission spectrum of the grains becomes increasingly more important. If the grain temperatures are less than about 1000K (Rowan-Robinson & Harris 1983), then the peak of the re-emission

spectrum will be at wavelengths longer than about 3 μm, with shorter wavelengths lying on the steeply declining exponential part of the spectrum. Hence, 2.2 μm seems to be an ideal wavelength.

However, all of the stars in our sample have measurable mass loss, with rates dM/dt greater than about 10^{-7} $M_{\odot}$ yr^{-1} (Claussen *et al.* 1987). This implies the existence of a circumstellar shell which may affect our determination of the effective temperatures. Judging from the models of Rowan-Robinson & Harris (1983), we believe that most of the stars in our sample (as we shall see later, there are two or three important exceptions) will have 2.2 μm optical depths much less than 0.1. We will discuss the possible effects of shells on our angular diameters in a later section.

The sample of stars selected depended upon brightness, availability and variability class. We have restricted the sample discussed in this paper to semi-regular and irregular variable stars. Mira variables have been specifically excluded from the discussion, although we have observed a number of these, and they will be the subject of a future paper. Most of the observations reported here were made on a single night, with 50-100 interferograms typically obtained for an observation. Our previous experience (Dyck *et al.* 1996) has shown us that this is sufficient in a statistical sense to characterize the angular diameter of bright stars with visibilities near 50%. The errors listed for the angular diameters, however, were based upon the rms fluctuations in the visibility of stars observed repeatedly over many nights. We have found that this error better characterizes the uncertainty in the visibility and, hence, the angular diameter than

does the standard deviation listed in Table 6.1. The formula for assigning this "external" error to the visibilities is

$$\varepsilon_V = \pm \frac{0.051}{\sqrt{\text{number of nights}}} .$$

The interested reader should see Dyck *et al.* (1996) for a more complete description.

As we have previously noted (Dyck *et al.* 1996), there appears to be a systematic difference between the uniform-disk diameters determined at IOTA compared to those determined at the same wavelength with the I2T interferometer at CERGA. The difference is in the sense that stars with diameters in the range 10 - 20 milliarcsec (mas) are about 10% smaller measured with IOTA than with CERGA. For stars with smaller diameters, there appears to be no measurable difference. A 10% difference in the angular diameter corresponds to a 2.5% difference in the effective temperature scales for the two interferometers.

6.3. Effective Temperatures

To compute the effective temperatures we need the bolometric flux, F_{BOL}, corrected for reddening, and the angular diameter which corresponds to the average radiating surface for the star, θ_R. Then, we use the relationship

$$T_{EFF} = 1.316 \times 10^7 \left(\frac{F_{BOL}}{\theta_R^2} \right)^{1/4} \text{K} ,$$

where F_{BOL} is measured in W cm^{-2} and θ_R is measured in mas.

Previous estimates of the effective temperature and luminosity for carbon stars (Mendoza V. & Johnson 1965, Richer 1971) have indicated that these stars have

properties close to the K and M giants. Hence, atmospheric extensions ought to play a relatively small role in the determination of the effects of limb darkening. As before, we have used the model atmospheres of Scholz & Takeda (1987) to evaluate limb darkening effects, and have adopted the surface where the Rosseland mean opacity is unity as the appropriate surface for computing an effective temperature. The conversion from uniform disk angular diameters to Rosseland mean angular diameters is a small multiplicative factor with small dispersion for the models computed by Scholz & Takeda (1987). Following Dyck *et al.* (1996), we have adopted

$$\theta_R = 1.022 \; x \; \theta_{UD} \; .$$

Tsuji (1981a), on the other hand, has suggested that the carbon stars have temperatures that are lower and luminosities that are higher than the normal M giant sequence, so that some atmospheric extension may be important. From our investigation of the Scholz & Takeda (1987) models, we estimate that the limb-darkening corrections could be no more than 10% different from our correction factors (i.e., the correction from uniform-disk diameters to Rosseland mean diameters). This could lead to a systematic error of 5% in the effective temperature scale; we shall return to this point.

The Rosseland mean opacity surface has the advantage that the effective temperatures will not be dependent upon the wavelength of the observation. For other limb-darkening corrections, the temperatures computed will be corrected for center-to-limb brightness variations but will still be a function of wavelength since the brightness profiles at each wavelength will, in general, correspond to different altitudes in the atmosphere. The different altitudes will lead to a wavelength-dependent limb-darkened

angular diameter and, hence, an effective temperature which is a function of wavelength.

To compute the bolometric flux densities, we have made extensive use of the data compiled by Gezari *et al.* (1993) for wavelengths longer than 1 μm. Shorter wavelength data were obtained from Mendoza V. & Johnson (1965), Johnson *et al.* (1966), Eggen (1967) and Richer (1971). We converted magnitudes from filters *B* through *L* into absolute fluxes and performed a simple numerical integration over this wavelength range. Fluxes beyond 3.5 μm were estimated by taking a Rayleigh-Jeans integration, normalized to the flux in the *L* passband. Variability is noted for these carbon stars but, from an inspection of the average infrared variation for our stars given in Gezari *et al.* (1993), we believe that the bolometric flux generally changes by no more than 10%. In cases where photometry is missing, we have used mean colors for the spectral type, tied to the observed *K* magnitude. For the purposes of estimating the errors from the bolometric flux, we have assumed a conservative 15% for variability and errors in the absolute calibration, unless significant photometry was not available. For this case, we have explored the extremes of the colors versus spectral types and computed corresponding extreme values of the bolometric flux. Differences in the effective temperatures obtained from these extreme flux values were added in quadrature to other sources of error to obtain the final estimates of the error in the temperature.

Reddening may also be important and, in some cases, different estimates thereof vary wildly. We have compared the reddening determinations made by Richer (1971) at optical wavelengths with those made by Claussen *et al.* (1987) at near-infrared

wavelengths. Each determination rests upon a different set of assumptions and in many cases the results agree well. For example, for TX Psc, Richer obtains $A_V = 0.25$ while Claussen *et al.* obtain $A_V = 0.22$. On the other hand, reddening estimates for VX And are very discrepant, with Richer (1971) obtaining $A_V = 6.1$ and Claussen *et al.* obtaining $A_V = 0.8$! When two estimates of the reddening were available, we computed values of the bolometric flux using each. Differences in the effective temperatures from these reddening values were added quadratically to the other sources of error to obtain total errors in the effective temperatures.

We have listed our new effective temperature determinations in Table 6.2, where we have given the name of the star, the Yamashita spectral type, the uniform-disk angular diameter, the error in the measured diameter, the Rosseland mean angular diameter, the adopted bolometric flux, the effective temperature, the error in the effective temperature, the mass-loss rate from Claussen *et al.* (1987) and the major source of the error in the effective temperature. In addition to our new observations, we have compiled the limb-darkened angular diameters discussed by Quirrenbach *et al.* (1994) in Table 6.3 and computed their effective temperatures after redetermining the bolometric flux (it is not clear how Quirrenbach *et al.* dealt with the reddening). These stars bring the total number in the sample to 22.

6.4. Discussion

Four of the stars listed in Tables 6.2 and 6.3 have estimated errors in the

Table 6.2. Effective temperatures from the IOTA interferometry.

Star	F_{bol} (W cm^{-2})	$\theta_{UD} \pm \varepsilon_\theta$ (mas)	θ_R (mas)	$T_{EFF} \pm \varepsilon_T$ (K)	Sp Type	dM/dt ($M_\odot$ yr^{-1})	Error Source
VX And	1.87×10^{-13}	6.6±0.6	6.75	3332±598	C4.5	1.2×10^{-7}	R
AQ And	7.12×10^{-14}	4.0±0.8	4.09	3362±394	C5.4	2.5×10^{-7}	R=D
V Aql	4.36×10^{-13}	10.1±0.7	10.32	3328±480	C5.4	1.3×10^{-7}	R
S Aur	6.36×10^{-14}	8.9±0.6	9.10	2191±219	---	6.8×10^{-7}	F
WZ Cas	1.14×10^{-13}	5.8±0.7	5.93	3140±193	C9.2	6.8×10^{-8}	D
Y CVn	3.62×10^{-13}	11.6±0.3	11.86	2964±52	C5.5	1.1×10^{-7}	R=D=F
RS Cyg	7.84×10^{-14}	4.3±0.8	4.39	3321±312	C8.2	1.0×10^{-7}	D
RV Cyg	1.21×10^{-13}	7.6±0.5	7.77	2784±97	C6.4	2.2×10^{-7}	D
V460 Cyg	1.45×10^{-13}	6.3±0.6	6.44	3200±157	C6.3	1.6×10^{-7}	D
W Ori	3.34×10^{-13}	9.7±0.6	9.91	3177±306	C5.4	1.3×10^{-7}	R
RT Ori	4.38×10^{-14}	4.4±0.9	4.50	2839±292	C6.4	1.4×10^{-7}	D
SY Per	3.57×10^{-14}	3.4±0.8	3.47	3069±363	C6.4	8.9×10^{-8}	D
Z Psc	8.84×10^{-14}	4.8±0.7	4.91	3240±239	C7.2	9.3×10^{-8}	D
TX Psc	3.18×10^{-13}	11.2±0.3	11.44	2921±60	C7.2	7.2×10^{-8}	D=F
CIT 13	3.39×10^{-14}	10.8±0.4	11.04	1700±37	---	2.8×10^{-6}	?

Table 6.3. Supplemental effective temperature data.

Star	F_{bol} (W cm^{-2})	$\theta_{LD} \pm \varepsilon_\theta$ (mas)	$T_{EFF} \pm \varepsilon_T$ (K)	Sp Type	dM/dt ($M_\odot$ yr^{-1})	Error Source

Y Tau	1.42E-13	8.4±1.0[1]	2787±169	C6.4	2.2×10^{-7}	D
UU Aur	3.43E-13	12.1±0.2[2]	2899±82	C6.4	1.3×10^{-7}	R
X Cnc	1.11E-13	8.2±0.6[1]	2653±102	C5.4	1.0×10^{-7}	D
Y CVn	3.62E-13	14.8±0.5[2]	2655±52	C5.5	1.1×10^{-7}	R=D=F
TW Oph	7.59E-14	10.4±0.5[1]	2147±58	C5.5	1.1×10^{-7}	D=F
SZ Sgr	3.05E-14	3.3±0.2[1]	3009±84	C7.3	1.8×10^{-7}	D
AQ Sgr	1.3E-13	6.0±0.5[1]	3234±257	C7.4	1.4×10^{-7}	R
RT Cap	2.47E-13	8.0±0.2[1]	3274±580	C6.4	9.5×10^{-8}	R
TX Psc	3.18E-13	9.3±0.8[1]	3239±136	C7.2	7.2×10^{-8}	D
TX Psc	3.18E-13	11.2±1.0[2]	2953±136	C7,2	7.2×10^{-8}	D

Notes to Table 6.3: [1] Angular diameter obtained from lunar occultation. [2] Angular diameter obtained from the Mark III interferometer. See Quirrenbach *et al.* (1994) for details.

effective temperature which are larger than about 400K; these are VX And, AQ And, V Aql and RT Cap. It is interesting to note that, for these four stars, uncertainties in the interstellar reddening dominate the error in the effective temperature. We have excluded these four from further analysis. We begin our discussion with a comparison of the effective temperatures computed for TX Psc and Y CVn, stars that have angular diameter measurements made with a variety of techniques. It has been noted from repeated measures of TX Psc that there may be a substantial variation in the angular diameter which is correlated with the visual magnitude (Quirrenbach *et al.* 1994). We note that our effective temperature agrees very well with the value obtained from the average Michelson interferometry carried out by Quirrenbach *et al.* but disagrees substantially with the lunar occultation determinations (Lasker *et al.* 1973, de Vegt 1974, Dunham *et al.* 1975). The sense of the disagreement with the lunar occultations is that the IOTA effective temperature estimate is lower than the one made from the occultations. Most of this disagreement appears to be the result of the time variations noted for TX Psc. On the other hand, our observations of Y CVn indicate a smaller angular diameter than does the optical wavelength interferometry of Quirrenbach *et al.* Our effective temperature determination for this star is about 300K higher than theirs. Thus, we see no consistent pattern in the measurements made in common, but there may be as much as a few hundred K scatter among the effective temperatures determined from lunar occultations, the Mark III optical interferometer and the IOTA (near-infrared) interferometer.

There are sixteen stars in the sample with errors in the effective temperature less than about 400K and that have Yamashita spectral types, intended to be a temperature sequence following suggestions by Keenan & Morgan (1941). Our stars range in spectral class from C5 to C9, where Cohen has suggested effective temperatures ranging from 2750K down to 2230K, respectively. We have plotted the effective temperatures for these sixteen stars, as a function of spectral type, in Figure 6.1. One sees in this figure that the average effective temperature for the group is slightly less than 3000K and that there is only a weak dependence upon spectral type. Furthermore, the dependence is opposite to that desired from the spectroscopic classification, namely, that the temperature actually increases toward the "later" spectral types. This behavior has been previously noted by Tsuji (1981a,b) from effective temperature calculations based on the infrared flux method. Since the Yamashita spectral sequence is based largely upon the strengths of diatomic molecular bands, perhaps the large dispersion in band strengths implies the existence of different levels of mixing, as suggested by Goebel *et al.* (1993), rather than a change in effective temperature.

Our temperature scale is warmer than the one adopted by Cohen (1979) by about 250K at the early types to about 750K at the later types; compared to the temperature scale adopted by Rowan-Robinson & Harris (1983) our scale is 500 - 1000 K warmer. For nine stars in common, our effective temperature scale is about 200K warmer than Tsuji's (1981a) scale. Note that, in Figure 6.1, there is one star which seems to have a much lower temperature than all the others: TW Oph, classified C5, has an effective

temperature of about 2150K. Its angular diameter was determined by lunar occultation methods (Ridgway *et al.* 1982). We will return to this star later in the discussion.

Figure 6.1. A plot of the effective temperatures versus Yamashita (1972, 1975) spectral type for the carbon stars discussed in this paper.

In Table 6.4, we have summarized the average temperature for each spectral class, along with the estimated dispersion at each spectral type. At spectral class C5, we have excluded TW Oph. Where only one temperature exists, we have taken the rms error for all the multiple observations in the other spectral classes. Note that the averages vary from about 2900K for type C5 up to about 3150K at type C9. The mean over all spectral types C5-C9 (excluding TW Oph) is about 3000±200K (rms variation).

Table 6.4. Mean effective temperatures versus Yamashita spectral class.

Spectral Type	$T_{EFF}\pm\varepsilon_T$ (K)
C5	2880±156
C6	2928±69
C7	3130±62
C8	3321±96
C9	3140±96

There are three stars in Tables 6.2 and 6.3 which have significantly lower temperatures than the remainder of the sample. These are S Aur, CIT 13 and TW Oph, of which only TW Oph has a Yamashita classification. It is possible that undetected circumstellar emission or scattering will affect the determination of the effective temperature and it will generally be in the sense of lowering the temperature. The argument is the following: A measurable presence from a circumstellar shell will appear as an angular diameter which is larger than the stellar surface. The increase in size will depend upon the ratio of circumstellar to stellar flux and, hence, on the dust optical depth of the shell. An increase in

angular size for a given flux will correspond to a lower temperature.

In order to investigate the possibility that the undetected presence of circumstellar dust has affected the temperature determinations, we have correlated the temperatures in Tables 6.2 and 6.3 with the mass loss rates determined by Claussen *et al.* (1987). A higher mass loss rate will generally correspond to a larger shell optical thickness and, hence, to a larger fractional flux observed from shell emission and scattering. Although the mass loss rates determined by these authors are total rates obtained by assuming a constant gas-to-dust ratio, they have been determined from the excess far-infrared flux and correspond essentially to properties of the dust. In Figure 6.2 we have plotted the data for all 22 stars observed on this program. There are three important points to note about the figure. First, there is a clustering of stars near effective temperature 3000K and mass loss rate $dM/dt = 1 \times 10^{-7}\ M_{\odot}\ yr^{-1}$. We propose that this group of stars is unaffected by circumstellar shells. Second, there are two stars (S Aur and CIT 13) with significantly higher estimated mass loss rates than this first group which also have significantly lower effective temperatures. We believe that our temperature estimates have been corrupted by the presence of circumstellar shells for these two stars. Third, TW Oph with a low mass loss rate also has a significantly lower temperature than stars in the first group.

We believe that the low temperature for this star is not affected by the

presence of a circumstellar shell. It also appears unlikely that TW Oph represents an isolated example of a rare group of carbon stars with higher luminosity since the circumstellar CO expansion velocity is only a modest 9 km/sec (Loup *et al.* 1993; but see the discussion of carbon star luminosities by Zuckerman, Dyck & Claussen 1986). Perhaps this star is a member of a class of lower temperature carbon stars; this point may be

Figure 6.2. A plot of the estimated mass loss rates from Claussen *et al.* (1987) versus the effective temperatures. Note that there is a group of stars which cluster at about T_{EFF} = 3000K and dM/dt = 10^{-7} $M_{\odot}$ yr^{-1}. The two stars with the highest mass-loss rates are S Aur and CIT 13. The remaining star with very low effective temperature is TW Oph, discussed more fully in the text.

addressed by observation of a much larger sample of carbon stars. On the other hand, it was emphasized to us by the referee that TW Oph lies in the direction of the Galactic Center, where reddening may be very important. Our assumed reddening was $A_V = 0.77$, obtained from Claussen *et al.* (1987). In order to raise the effective temperature of this star to the average of the other C5 stars the visible reddening would have to be of order $A_V \sim 5.7$. This difference, with respect to Claussen *et al.*, is of the same order as noted above for VX And and cannot be ruled out at this time.

One of the important conclusions of this research is that there is a relatively small range of effective temperatures for most of the stars observed in our sample. This temperature, approximately 3000K in the mean, is about 200K cooler than the M7 luminosity class III stars recently discussed by Dyck *et al.* (1996). This confirms the result of Tsuji (1981a,b) that the carbon stars were cooler than the earlier M giants.

Claussen *et al.* (1987) assumed that galactic carbon stars have the same narrow range of absolute K magnitudes which are observed for carbon stars in the Magellanic Clouds (Frogel, Persson & Cohen 1980) and infer a mean bolometric luminosity of 10^4 $L_\odot$. If we take this mean luminosity and couple it with our mean effective temperature, we deduce a mean radius for C5-C9 carbon stars of about 400 $R_\odot$. This may be compared to the mean radius 80 $R_\odot$ determined from parallax data for the M4 giants (Dyck *et al.* 1996). On the other hand, van Belle *et al.* (1996) have shown from statistical distance arguments that the oxygen-rich Mira variables have near-infrared radii

averaging 376 $R_{\odot}$; the effective temperatures for this sample of Miras average 2700 K. Taking radii and effective temperatures together, carbon stars observed in the present program are closer to the Mira variables than to the M giants among the oxygen-rich stars. This finding is consistent with, for example, the evolutionary sequence for carbon stars suggested by Willems (1987). In his picture, the non-Mira carbon stars are the direct descendants of evolving oxygen-rich Mira variables in which pulsations have been largely quenched.

The large radii present a potential problem for our previous assumptions about the conversion from uniform-disk diameters to Rosseland mean diameters. In van Belle *et al.* (1996), it was found that the conversion factor ranged from 0.98 to 1.11 for Mira stars of effective temperature near 3000K, depending upon whether the star was near maximum or minimum light. If the limb-darkening correction were at either of these extremes it could result in a 5% error in the effective temperature scale, in either direction. Specifically, if the angular diameter correction factor were 1.11, then our scale would be depressed by about 150K, agreeing more closely with the infrared flux method scale (Tsuji 1981a,b). These differences in temperature scale may become clearer with additional model atmospheres calculations.

6.5. Conclusion

In this paper we have discussed new interferometric determinations of angular diameters for 15 carbon stars. We have combined these data with lunar occultation and Michelson interferometry data for 7 other stars found in the literature. Coupling the angular diameters with bolometric fluxes we have computed effective temperatures for 22 stars. Using the statistical luminosity determinations from Claussen *et al.* (1987), we infer the mean radius for the sample. We find the following:

1. There is a small range of effective temperatures for stars classified C5-C9 (Yamashita 1972, 1975), with a tendency for later spectral types to be hotter stars. The mean temperature, excluding three peculiar examples is 3000±200K.;

2. There is generally no evidence for the effects of undetected circumstellar shells upon the effective temperature determinations, except for two stars (S Aur and CIT 13). For these two stars, that have mass loss rates near 10^{-6} $M_{\odot}$ yr^{-1}, the effective temperatures are significantly lower than the ones described in point 1. above;

3. The statistical mean radius for 20 stars in the sample (S Aur and CIT 13 excluded) is 400 $R_{\odot}$. This radius makes the carbon stars as extended as the average Mira variable discussed by van Belle *et al.* (1996). A consequence of the extension is that there may be a systematic error of ±150K resulting from an incorrect choice of limb-darkening correction; and

4. There is one star (TW Oph) which has an anomalously low effective temperature, which may indicate a relatively rare occurence of lower temperature carbon stars or may simply indicate a very significant error in the reddening estimate.

CHAPTER VII

MIRA VARIABLE STARS

7.1 Introduction

The recent development of interferometric methods at optical and infrared wavelengths has provided the astronomical community with more than an order of magnitude increase in spatial resolution over direct imaging techniques. Using the Infrared Optical Telescope Array (IOTA, see Carleton *et al.* 1994 and Dyck *et al.* 1995), we have recently begun a program of high resolution, K band observations of Mira variable stars. Mira variables figure prominently in our observing strategy, since these stars are large and bright at infrared wavelengths. Using crude estimates of surface temperatures and the observed total fluxes it is estimated that more than 70 such stars have black body angular diameters in excess of 5 milliarcseconds (mas), easily resolvable targets for the current generation of Michelson interferometers. However, only six *JHK* band diameters for five of these stars have been published in the literature (Ridgway *et al.* 1992, Di Giacomo *et al.* 1991, Ridgway *et al.* 1979); the data on the 18 stars presented in this paper more than triple the existing sample of measured angular diameters for Mira variables at near-infrared wavelengths. More importantly, this large sample allows for more detailed analyses of the behavior of these stars.

Recent models of Mira variables have attempted to resolve important questions regarding the pulsation mode, mass loss and evolution of these stars. The pulsation mode remains a currently-unresolved issue; depending upon initial assumptions, models

supporting both fundamental mode oscillation (Willson & Hill 1979; Hill & Willson 1979; Wood 1990) and first overtone oscillation (Wood 1974; Tuchman *et al.* 1979; Perl & Tuchman 1990) have been constructed. Attempts to reconcile the models with observations have produced results in support of both fundamental mode (Cannizzo *et al.* 1990) and first overtone pulsation (Tuchman 1991, Barthès & Tuchman 1994; Haniff, Scholz & Tuthill 1995). In addition to addressing the question of oscillation mode, stellar evolution questions, such as the connection of Mira variable star mass loss rates to planetary nebula formation, have also been explored (Tuchman *et al.* 1979).

It is by means of *direct observation* of the angular sizes of Mira variables that we may be able to provide unique insight into these questions. For example, recent studies at optical wavelengths (Haniff, Scholz & Tuthill 1995, hereafter HS&T) have attempted to infer the mode of pulsation from the diameter data. Additional information in the form of bolometric flux estimates will yield further information, such as effective temperature, the scale for which is not particularly well established for this class of stars. Also, our angular size measurements and derived quantities have implications regarding the nature of mass loss and evolution among Mira variables. An investigation of mass loss evolution by Bowen & Willson (1991) used indirectly-inferred values for stellar radius and effective temperature, both of which are more directly obtained in this investigation.

Carbon-rich, oxygen-rich and S-type Miras are all being observed at IOTA as a part of our ongoing high resolution program; in this paper we present only the

observations of the oxygen-rich variety. Operations at IOTA producing these results are discussed in §7.2, detailing source selection and observation. In §7.3 the procedures used in establishing the stellar parameters for the stars observed are discussed; the parameters include phase, spectral type, bolometric flux, angular size, effective temperature and linear radius. These parameters are in turn examined for significant interrelationships in the discussion of §7.4. Under the assumption of the validity of the period-mass-radius relations developed by Ostlie & Cox (1986), the IOTA data collected on the Mira variables observed in this program do not strongly indicate a particular oscillation mode. This result differs substantially from the results of a comparable study by HS&T, who conclude that Mira variables are first-overtone pulsators; we discuss the implications of these differences in §7.4.

7.2 Observations

The data reported in this paper were obtained in the *K* band ($\lambda = 2.2$ μm, $\Delta\lambda =$ 0.4 μm) at IOTA, using the 38 meter baseline. Use of IOTA at 2.2 μm to observe Mira variables offers three advantages: First, effects of interstellar reddening are minimized, relative to the visible ($A_K = 0.11\ A_V$; Mathis 1990); Second, the effects of circumstellar emission are minimized shortward of 10 μm (Rowan-Robinson & Harris 1983), and; Third, the *K* band apparent uniform-disk diameter of Mira variables is expected to be close to the Rosseland mean photospheric diameter (see the discussion in §7.3.3). The interferometer, detectors and data reduction procedures have been described more fully by Carleton *et al.* (1994) and Dyck *et al.* (1995). As was previously reported in these

papers, starlight collected by the two 0.45 m telescopes is combined on a beam splitter and detected by two single element InSb detectors, resulting in two complementary interference signals. The optical path delay is mechanically driven through the white light fringe position to produce an interferogram with fringes at a frequency of 100 Hz. Subsequent data processing locates the fringes in the raw data and filters out the low and high frequency noise with a square filter 50 Hz in width. Recent software and hardware upgrades to the computers driving the interferometer and collecting the data have resulted in a improved data collection rate to 1500-2000 fringe packets per night. On the best nights we can observe 20 science sources and an equal number of calibrators.

Observations of target objects are alternated with observations of unresolved calibration sources to characterize slight changes in interferometer response, due to both seeing and instrumental variations. Raw visibilities are determined from the amplitude of the interferogram at the white light fringe position, normalized by the incoherent flux from the star. An estimate of the noise is obtained from a similar measurement made in the data string outside the region of coherence; the noise estimate is used in obtaining a weighted average of the visibility data, which is typically taken in sets of 50 interferograms. The raw visibilities of the target objects are then calibrated by dividing them by the measured visibilities of the calibration sources, using the calibration sources as samples of the interferometer's point response. Calibration sources were selected from *V* band data available in *The Bright Star Catalog, 4th Revised Edition* (Hoffleit 1982) and *K* band data in the *Catalog of Infrared Observations* (Gezari *et al.* 1993),

based upon angular sizes calculated from estimates of bolometric flux and effective temperature; calibration source visibility was selected to be at least 90% and ideally greater than 95%, limiting the effect of errors in calibrator visibility to a level substantially below measurement error.

Mira variables observed for this paper were selected based upon a number of criteria. Stars needed to be bright enough in V and K to be detected by both the star trackers and the InSb detectors; the current limits of the IOTA interferometer dictate $V <$ 8.0 mag and $K < 5$ mag (though for observations at all airmasses and seeing conditions, we require $K < 2.5$ mag). The Mira variables needed to be at a declination accessible to the mechanical delay available for a given evening. This is because the difference in delay between the two apertures, which can range from -30 m to +20 m, depends upon source declination and hour angle. Since only 4.6 m of this range is accessible at any time, observing is constrained to a specific declination bin about 10^{o} wide on any given night. The stars also needed to be of sufficient estimated angular size to be resolved by IOTA. Mira phase was not a factor in target selection; hence, our targets represent Miras at a variety of phases, from visible light maximum to minimum.

Eighteen oxygen-rich Mira variables were observed at IOTA during three observing runs in June, July and October of 1995. The visibility data for the two detector channels have been averaged and are listed in Table 7.1, along with the date of the observation, the interferometer projected baseline, the stellar phase and the derived uniform disk angular size; the latter two points are discussed further in §7.3. Our

experience with the IOTA interferometer (Dyck *et al.* 1996) has demonstrated that the night-to-night RMS fluctuations in visibility data generally exceed the weighted statistical error from each set of interferograms; we have characterized these fluctuations and use the empirical formula

$$\varepsilon_V = \pm \frac{0.0509}{\sqrt{number\ of\ nights}}$$

to assign the "external" error. The interested reader should see Dyck *et al.* (1996) for a more complete discussion. Finally, visibility data were fit to uniform disk models to obtain an initial angular size θ_{UD}. These uniform disk diameters and their estimated errors, derived from the uncertainty in the visibilities, are also listed in Table 7.1.

We note that typically a single point was utilized in calculating the uniform disk diameter θ_{UD}. For the stars in our sample, the visibility data were all at spatial frequencies, x, shortward of the first zero of the uniform disk model, $|2\ J1(x)/x|$. HS&T noted that the uniform disk model was not a particularly good model for visible-light data for Mira variables; rather, the data were a better fit to a simple Gaussian. Although we do not currently have multiple spatial frequency data for any Mira variables, we expect that the departures from a uniform disk model will not be as great at 2.2 μm as it is at visible wavelengths. This expectation is based upon our unpublished 2.2 μm data for α Her, a supergiant star expected to have the same order of atmospheric extension as do the Mira variables. A comparison of our data with visible α Her data (Tuthill 1994) indicates that the departures from a uniform disk visibility curve are present in the visible but not the infrared. Thus we assume that to first order, a uniform disk model will also

fit the Mira data; a slight correction to the derived angular sizes to account for this assumption will be discussed in §7.3.3. In this case, a single spatial frequency point will uniquely and precisely determine the angular diameters for visibilities in the approximate range $0.25 \leq V \leq 0.75$. If there are significant differences between the

Table 7.1. IOTA observations of Mira variable stars.

Star	P [d]	Date	B_p [m]	V^1	φ	θ_{UD} [mas]
R Aql	283.4	95 Jun 10	36.24	0.3255	0.90	10.76±0.61
		95 Jun 11	35.76	0.3437		
		95 Oct 06	33.85	0.1657	0.31	13.62±0.72
R Aqr	387.8	95 Jul 11	31.51	0.1404	0.34	14.95±0.93
		95 Jul 11	29.48	0.2125		
		95 Oct 07	33.19	0.1540	0.57	14.06±0.72
R Aur	457.4	95 Oct 03	35.16	0.3050	0.08	11.06±0.58
		95 Oct 04	34.91	0.3522		
		95 Oct 05	35.92	0.3146		
R Cas	430.8	95 Oct 04	35.27	0.1245	0.81	13.55±0.95
		95 Oct 05	36.30	0.1273		
T Cas	445.0	95 Oct 04	35.33	0.1835	0.30	12.81±0.66
S Her	308.5	95 Jul 07	36.50	0.7914	0.81	4.85±1.17
		95 Jul 08	36.96	0.8630		
U Her	406.4	95 Jun 10	36.84	0.2998	0.03	10.65±0.79
		95 Jun 13	36.94	0.3797		
X Oph	331.6	95 Jul 07	35.53	0.1289	0.37	12.97±0.60
		95 Jul 08	36.59	0.1535		
		95 Oct 07	34.11	0.2571	0.75	12.30±0.76
S Ori	413.4	95 Oct 06	33.86	0.3313	0.56	10.54±0.68
		95 Oct 07	32.96	0.5149		
U Ori	371.4	95 Oct 08	38.24	0.2480	0.97	11.08±0.57
R Peg	377.3	95 Jul 07	36.65	0.3909	0.90	10.18±0.40
		95 Jul 08	36.84	0.3109		
		95 Oct 06	34.49	0.4199	0.13	9.72±0.67
		95 Oct 07	34.50	0.5116		
S Peg	320.0	95 Jul 08	36.58	0.5766	0.28	7.90±0.72
		95 Oct 06	34.01	0.7294	0.56	6.32±0.95
		95 Oct 07	34.00	0.7712		
U Per	322.4	95 Oct 04	35.55	0.7763	0.55	5.84±0.78
		95 Oct 05	36.02	0.7358		
R Ser	355.4	95 Jul 07	36.50	0.4873	0.32	8.56±0.58
		95 Jul 08	36.89	0.5429		
X Aur	164.0	95 Oct 04	34.98	1.1506	0.62	Unresolved
Z Cet	185.2	95 Oct 06	32.87	0.9998	0.92	Unresolved
RY Lyr	326.6	95 Oct 08	38.26	1.0858	0.37	Unresolved
R Per	210.1	95 Oct 05	37.00	1.1585	0.03	Unresolved

1. Standard nightly error is $\varepsilon_V = 0.0509$.

brightness profiles for supergiants and for Mira variables then this assumption will be invalid; this point may only be addressed by detailed multiple spatial frequency observations of the visibility curves.

7.3 Stellar Parameters

7.*3.1 Phase*

The phases of the Mira variables observed were established by means of two sources. Periods were initially obtained from *The General Catalog of Variable Stars, 4th Edition* (*GCVS*, Kholopov *et al.* 1988). However, since the zero phase date in the *GCVS* at the epoch of the observations was no less than 11 cycles old for our sample stars, visual brightness data available from the Association Francaise des Observateurs d'Etoiles Variables (AFOEV) was utilized in estimating a recent zero phase date (Schweitzer 1995); for one star (R Peg), data from the American Association of Variable Star Observers (AAVSO) was utilized for this purpose (Mattei 1995).

As an additional cross-check, Fourier analysis (as discussed in Scargle, 1982 and Horne & Baliunas, 1986) of the AFOEV data also provided period information, but using light curve data which was more recent than that found in the *GCVS*. The periods from the *GCVS* and the AFOEV analysis agreed at the 1% level, corresponding to an average difference in period of 1d4. With the agreement in periods, the zero phase

estimate was the larger uncertainty in phase determination, although this uncertainty was still small, averaging 6^d with a median of 3d5. Periods, determined from Fourier analysis of the AFOEV data, and phases, from AFOEV and AAVSO data, for each of the Mira variables are presented in Table 7.1.

7.3.2 Spectral Type & Bolometric Flux

Bolometric fluxes (F_{BOL}) of the Mira variable stars were estimated from a relationship between F_{BOL}, 2.2 μm flux (F_K) and spectral type, as established by Dyck, Lockwood & Capps (1974). In order to obtain bolometric fluxes, *K* magnitudes were first estimated from the incoherent flux levels present in the IOTA data. We obtained our standard star photometric calibrations using the *K* band measurements found in the *Two Micron Sky Survey* (Neugebauer & Leighton 1969) for our non-variable point-response calibration sources. No airmass corrections were applied since the calibrators were observed at nearly identical airmasses as the Mira variables. In all cases the bolometric fluxes were obtained from the absolute *K* fluxes through the observed relation between $log\ (F_K/F_{BOL})$ and spectral type (Dyck, Lockwood & Capps 1974), a relationship that requires the phase dependent spectral type for the star. We note that the $log\ (F_K/F_{BOL})$ - spectral type relationship also has a firm theoretical basis and may be seen in the "infrared flux method" calculations carried out by Blackwell & Lynas-Gray (1994). No reddening corrections were applied to obtain the bolometric fluxes. These were deemed unnecessary since the typical magnitude of the corrections, $\Delta \underline{m}_K \approx 0.10$

mag (calculated from the empirical reddening determination of Mathis, 1990), is less than the RMS K band error, σ_K = 0.15 mag. The spectral types for the Miras were obtained from the mean observational data of Lockwood & Wing (1971) (henceforth referred to as L&W) and Lockwood (1972); the cycle-to-cycle repeatability of the phase dependent spectral types was examined and found to be roughly ±0.25 of a subclass. Spectral types, *K* magnitudes and bolometric fluxes are given in Table 7.2. The errors in the *K* magnitudes are the standard deviations of the individual measurements on a given night. From the observed scatter in the F_K/F_{BOL} relationship we estimate an rms error of ±13% in F_{BOL} from the use of the *K* magnitude; we estimate a further uncertainty of ±5% in the absolute calibration (Blackwell & Lynas-Gray 1994). The estimated error for F_{BOL} in Table 7.2 is the quadrature sum of these contributions.

Table 7.2. Mira variable bolometric fluxes and spectral types.

Star	Date	$K \pm \varepsilon_K$	$F_{BOL} \pm \varepsilon_F$	Spectral Type
R AOL	95 Jun 10	-0.84±0.04	383.0±55.5	M6.5
	95 Oct 06	-0.77±0.03	316.4±45.1	M8.2
R AOR	95 Jul 11	-1.01±0.10	399.2±68.5	M8?
	95 Oct 07	-0.74±0.30	311.3±103.0	M8?
R AUR	95 Oct 03	-0.79±0.02	365.8±51.5	M6.5
X AUR	95 Oct 04	3.83±0.14	5.3±1.1	M6
R CAS	95 Oct 04	-1.29±0.13	447.4±85.2	M9.8
T CAS	95 Oct 04	-0.98±0.06	411.4±62.4	M7
Z CET	95 Oct 06	2.97±0.05	12.5±1.8	M5
S HER	95 Jul 07	1.47±0.11	43.1±7.6	M7
U HER	95 Jun 10	-0.43±0.02	240.8±33.9	M7.5
RY LYR	95 Oct 08	2.79±0.09	12.4±2.1	M7.5
X OPH	95 Jul 07	-1.03±0.10	402.0±68.9	M8.2
	95 Oct 07	-1.05±0.10	414.2±71.0	M8
S ORI	95 Oct 06	0.11±0.01	130.5±18.2	M9
U ORI	95 Oct 08	-0.52±0.02	233.2±32.8	M8.8
R PEG	95 Jul 07	0.50±0.06	98.2±14.9	M8.2
	95 Oct 06	-0.18±0.08	208.6±33.5	M6.5
S PEG	95 Jul 08	1.36±0.51	50.5±26.7	M6.5
	95 Oct 06	1.45±0.04	40.9±5.9	M8.2
R PER	95 Oct 05	4.02±0.19	4.8±1.1	M5
U PER	95 Oct 04	0.97±0.05	64.4±9.5	M8
R SER	95 Jul 07	-0.15±0.07	186.1±29.0	M7.5

References for spectral types in Table 7.2 are from Lockwood & Wing (1971) and Lockwood (1972).

It is also worthwhile to point out that over the range of spectral types in question (M5-M9.8), the $log(F_K/F_{BOL})$ vs. spectral type relationship is nearly flat, making the determination of F_{BOL} robust despite possible inaccuracies in spectral type. An error of two full subclasses results in only a 14% difference in the determined F_{BOL}; we shall see (in §7.3.4) that this results in only a 4% difference in the determined effective temperature. A good example of this is R Aqr, which, at phases of 0.34 and 0.57, did not have a spectral type listed in Lockwood (1972); the range of phases covered for that star in that paper only runs from 0.00-0.16. Stars showing similar phase-spectral type behavior in the Lockwood paper at the phase range of 0.00-0.16 (R Aql, T Cas, RU

Cyg, X Oph) exhibit a spectral type of roughly M8±1 at a phase of 0.58. Hence, even though a spectral type was not directly available for R Aqr at the phase at which it was observed, a reasonable estimate for its F_{BOL} was still possible.

7.3.3 True Angular Diameter

In order to estimate effective temperatures, the uniform disk diameters in Table 7.1 needed to be converted to stellar diameters corresponding to the non-uniform extended atmospheres of the Mira variables. For our purposes here, we used the model Mira atmospheres discussed in Scholz & Takeda (1987) (henceforth referred to as S&T). We note that the S&T models do not account for the time for both shock compressed material and material expanding between shocks to return to radiative equilibrium. These regions, with $T > T_{RadEq}$ and $T < T_{RadEq}$, respectively, can alter the brightness distribution profile and consequently alter the 'true' angular sizes derived from the uniform disk diameters. Dynamical atmosphere calculations have the potential to resolve these concerns (e.g. Bowen 1988, Bowen & Willson 1991); however, center-to-limb brightness profiles are not yet available for such calculations. The missing physics in the models has the potential to make for poor agreement between angular sizes derived at different wavelength bands; as we shall see in §7.4.5, this is indeed the case. Noting these concerns, for our purposes here we shall use the S&T models as a sufficient expectation of the intensity distribution across the disk of a Mira variable.

Using the disk intensity distributions given in S&T for their X3500 and X3000 models, visibility curves were computed for these model stars and compared to

visibilities for uniform disks. The X3500 and X3000 models of S&T are one solar mass, solar element abundance Mira variable stars with maximum temperatures of 3500K and 3000K, respectively. Other intermediate-temperature models were referred to in S&T (X3350 & X3200) but, since intensity distributions for these models are not explicitly given, they were not utilized in our analysis. In their discussion of model Mira atmospheres, S&T adopt a radius corresponding to the altitude at which the Rosseland mean opacity equals unity, a convention that shall also be used in this paper.

Our procedure, then, is to convert our uniform disk angular diameters to the corresponding Rosseland mean angular diameters. First, a 2.2 μm uniform- to limb darkened-disk scaling factor, R_{LD}/R_{UD}, was calculated by comparing visibility curves of uniform-disk and S&T's limb darkened-disk intensity distributions; R_{LD}/R_{UD} typically resulted in an increase (on average 23%) in calculated size. Second, a limb darkened- to Rosseland disk scaling factor, R_R/R_{LD}, was given in S&T; R_R/R_{LD} typically resulted in an decrease (on average 17%) in calculated size. For 2.2 μm uniform disk diameters, the net R_R/R_{UD} scaling factor is close to unity; this result is consistent with theoretical expectations (Willson 1986). The R_R/R_{UD} scaling factor has been computed for each of the four Mira models used from S&T (X3000 & X3500, minimum & maximum for each).

Stars between a phase of 0.25 to 0.75 were considered to be at minimum; stars between 0.00 to 0.25, and 0.75 to 0.99 were considered to be at maximum. Since, as we shall see in §7.3.4, there was not a clear separation between the derived temperatures,

the X3000 and X3500 scaling factors were averaged together. For the maximum light models, the X3500 and X3000 R_R/R_{UD} values were 0.97 and 0.99, respectively, (a negligible difference) which were averaged to a maximum light scaling factor of 0.98. For the minimum light models, the R_R/R_{UD} values were 1.05 and 1.17, resulting in a scaling value of 1.11; we note that a full difference of 0.06 (the difference between 1.11 and the R_R/R_{UD} values for the two minimum light models) in scaling factor results in only a 3% change in the resultant value of T_{EFF}. The corrected angular diameters are listed in Table 7.3, along with the assumed multiplicative factor to convert uniform disk diameters to Rosseland mean diameters and the S&T models from which they were derived.

Table 7.3. Mira variable effective temperatures.

Star	Date	Model	Scaling	$\theta_R \pm \varepsilon_\theta$ [mas]	$T_{EFF} \pm \varepsilon_T$ [K]
R AOL	95 Jun 10	MAX	0.98	10.54±0.60	3189±147
	95 Oct 06	MIN	1.11	15.12±0.80	2539±113
R AOR	95 Jul 11	MIN	1.11	16.59±1.03	2568±136
	95 Oct 07	MIN	1.11	15.61±0.80	2489±215
R AUR	95 Oct 03	MAX	0.98	10.84±0.57	3109±137
R CAS	95 Oct 04	MAX	0.98	13.28±0.93	2954±174
T CAS	95 Oct 04	MIN	1.11	14.22±0.73	2795±128
S HER	95 Jul 07	MAX	0.98	4.76±1.15	2749±354
U HER	95 Jun 10	MAX	0.98	10.43±0.78	2855±146
X OPH	95 Jul 07	MIN	1.11	14.40±0.66	2762±134
	95 Oct 07	MAX	0.98	12.06±0.74	3041±160
S ORI	95 Oct 06	MIN	1.11	11.70±0.75	2313±110
U ORI	95 Oct 08	MAX	0.98	10.86±0.56	2776±121
R PEG	95 Jul 07	MAX	0.98	9.98±0.39	2333±100
	95 Oct 06	MAX	0.98	9.53±0.66	2881±153
S PEG	95 Jul 08	MIN	1.11	8.77±0.80	2107±295
	95 Oct 06	MIN	1.11	7.02±1.05	2235±186
U PER	95 Oct 04	MIN	1.11	6.49±0.87	2604±199
R SER	95 Jul 07	MIN	1.11	9.50±0.64	2804±144

The largest scaling factor, R_R/R_{UD}(MIN) = 1.11, results in only a 5% change in the resultant value of T_{EFF}. Thus, introduction of the uniform disk/Rosseland mean disk scaling factors constitutes merely a perturbation upon the final effective temperature; however, for completeness, they have been included in this study. The analyses found in the next section have been performed with the size scaling noted in this subsection. However, as a cross-check, each analysis was repeated without the scaling prescribed by the S&T models, and the gross trends found in the results were unchanged (see §7.4.3 for an illustration of this point).

We also note that some consideration was given to the possibility of departures from spherical symmetry in these variable stars. As has been observed in visible light observations of Mira variables (Karovska *et al.* 1991, Haniff *et al.* 1992, Wilson *et al.* 1992), these stars can be considerably elongated, possessing up to a 20% difference between semi-major and semi-minor axes. However, this effect appears to diminish at longer wavelengths: In Karovska *et al.*, a 18% difference at 533 nm is accompanied by only a 7% difference at 850 nm. These observations, which were made with a 4-m telescope, will have marginal resolution at the longest wavelength so that the observed decrease in the asymmetry may be the result of loss of resolution. Since the symmetric or asymmetric nature of these stars has at this time not been specifically quantified at 2.2 μm, we have been unable to specifically account for it. The reader should be aware of the potential for this effect to introduce spread in our sample of angular sizes, though it is our expectation that its magnitude will be less than the errors in the data set. We

will return to possible effects of asymmetries in §7.4.5.

7.3.4 Effective Temperature

The stellar effective temperature, T_{EFF}, is defined in terms of the star's luminosity and radius by $L = 4\pi\sigma R^2 T_{EFF}^4$. Rewriting this equation in terms of angular diameter and bolometric flux, a value of T_{EFF} was calculated from the flux and Rosseland diameter using

$$T_{EFF} = 2341 \; x \left[\frac{F_{BOL}}{\theta_R^2} \right]^{1/4} ;$$

the units of F_{BOL} are 10^{-8} erg/cm^{2}s, and θ_R is in mas. The error in T_{EFF} is calculated from the usual propagation of errors applied to equation (20). The measured T_{EFF}'s are given in column 6 of Table 7.3, and are found to fall in the range between 2100 K and 3200 K.

7.3.5 Linear Radius

As with many types of variable stars, Mira variables exhibit a period-luminosity relationship, as first suggested by Gerasimovic (1928). Later work confirmed this relationship (e.g. Clayton & Feast 1969), although in the visible the relationship shows a lot of scatter. To overcome this handicap, methods for determining Mira variable luminosity have been expanded to include both the visible and the infrared (Celis 1980, 1981, 1984; Cahn & Wyatt 1978, Wyatt & Cahn 1983; Robertson & Feast 1981; Feast *et al.* 1989; Jura & Kleinmann 1992, henceforth J&K). Distances to the Miras in our sample could be estimated by a number of statistical approaches: The period-mass-luminosity relationship developed by Cahn & Wyatt; The infrared period-luminosity relationship developed by Feast *et al.* as modified by J&K and; The color-absolute

magnitude relation of Celis as applied by Young. J&K (1992) give no estimates of the errors in the distances. Using the uncertainties in the constants for the infrared period-luminosity relationship given by Feast *et al.* (1989), we established an average uncertainty of 19% in the J&K distances. For the Wyatt & Cahn (1983) distances, we adopt an uncertainty of 10% in these distances, following the authors' suggestion. For distances from the method of Celis, Young (1995) adopted an uncertainty of 19%; we have adopted this error estimate as well. In Table 7.4 we have summarized the distances from the three methods and given our adopted distance and estimated error. The final estimated distance and its error is an average of the independent estimates tabulated, weighted by the errors just discussed.

Table 7.4. Mira variable linear radii.

Star	Date	$\theta_R \pm \varepsilon_\theta$ [mas]	D [pc][1]	D [pc][2]	D [pc][3]	$D \pm \varepsilon_D$ [pc]	$R \pm \varepsilon_R$ [$R_\odot$]
R Aql	95 Jun 10	10.54±0.60		200	190	198±17	224±24
	95 Oct 06	15.12±0.80		200	190	198±17	321±33
R Aqr	95 Jul 11	16.59±1.03	200	230		222±20	396±43
	95 Oct 07	15.61±0.80	200	230		222±20	372±38
R Aur	95 Oct 03	10.84±0.57		260		260±26	303±34
R Cas	95 Oct 04	13.28±0.93		180	230	187±17	267±30
T Cas	95 Oct 04	14.22±0.73		240	350	253±23	386±40
S Her	95 Jul 07	4.76±1.15	590			590±112	302±93
U Her	95 Jun 10	10.43±0.78		350	360	352±31	395±46
X Oph	95 Jul 07	14.40±0.66			270	270±51	418±82
	95 Oct 07	12.06±0.74			270	270±51	350±70
S Ori	95 Oct 06	11.70±0.75		410	480	422±37	530±58
U Ori	95 Oct 08	10.86±0.56		260	240	255±23	298±31
R Peg	95 Jul 07	9.98±0.39	400	410		408±36	437±42
	95 Oct 06	9.53±0.66	400	410		408±36	418±47
S Peg	95 Jul 08	8.77±0.80	640	610		616±55	580±74
	95 Oct 06	7.02±1.05	640	610		616±55	465±81
U Per	95 Oct 04	6.49±0.87		440		440±44	307±51
R Ser	95 Jul 07	9.50±0.64	330	390		373±33	381±42

[1] Jura & Kleinmann (1992); [2] Wyatt & Cahn (1993); [3] Young (1995)

For the Feast *et al.* (1989) distances taken from J&K, we note two concerns: First, following the suggestion of Wood (1990) concerning LMC versus Milky Way metallicities, J&K argue that local stars are intrinsically fainter at K by 0.25 mag, and modify Feast *et al.*'s M_K - P relationship accordingly; and Second, Feast *et al.*'s single line fit for the M_K-P data ignores an 'elbow' in the data at approximately $\log P = 2.6$, a corner which is also evident in LMC Mira data of Hughes & Wood (1990). Explicit examination of the Feast *et al.* data indicates that true K magnitudes for the longer period variables, including those at the corner, are potentially brighter than those indicated by the simple single line fit. For Mira variables with $\log P = 2.57$, which is the average value for the stars in our data set, the actual K magnitudes are potentially brighter by 0.25 mag. Countering the first concern is the argument by Willson, Bowen & Struck (1996) that the assumption that local Mira variables are fainter is incorrect. However, the net effect of these two concerns is to cancel each other out, and they are listed herein merely for the sake of completeness. Considering the possibility of these two concerns not completely canceling, the worst case would be a change in K magnitude of the full 0.25 mag, resulting in a difference of 12% in distance, well within the error bars already assigned to the Feast *et al.* distance estimates.

We note that we will ultimately be addressing the question of the pulsation mode (see §7.4) for the Mira variables in our sample. Two of the methods for computing the distance (the period-mass-luminosity and the infrared period-luminosity relationships) are dependent upon initial assumptions about the pulsation mode; however the mean color

method developed by Celis is not. Where there is overlap among the methods, it may be seen from Table 7.4 that the agreement of the three methods is good. The rather unrelated methods of Celis and Wyatt & Cahn shows an average *random* difference of 20%, comparable to the errors given, with a maximum difference of 46% in the T Cas estimates. Hence, for the purpose of further discussion, we assume that the effect of an assumption about the pulsation mode produces only minor changes in the distance scale.

Once distances to these stars were established, linear radii were then calculated by means of simple geometry. The sizes estimated for these stars are consistent with grossly extended stars in their postgiant evolutionary stage and are in the expected 200-600 $R_{\odot}$ range (see Hill & Willson 1979, Tuchman *et al.* 1979, Wood 1974). Not listed in Tables 3-5 are two stars which were unresolved, X Aur and Z Cet. Unsurprisingly, the distances for these stars are much greater than for the resolved sources, both being at approximately 950 pc. The mean Mira size, 376 $R_{\odot}$, would be only 3.7 *mas* at a distance of 950 *pc*, well below the smallest observed angular size of 4.85 *mas*. Even the maximum observed size, 580 $R_{\odot}$, would still be only partially resolved (5.7 *mas*) with the projected baselines at which these stars were observed.

7.3.6 Previously-published Data

As mentioned in the introduction (§7.1), six infrared angular size measurements for five stars have been published. We have applied the same reduction procedure discussed in §7.3 to the previously published data and have listed the results in Table 7.5. Errors are not listed in Table 7.5 but are of the same order as the our own data. Stellar

parameters derived from these observations are in good agreement with our own results. For specific stars, there are the following pertinent points:

o Cet (Mira). Observations of this star with the IR Michelson Array (IRMA) were published as a single epoch measurement (Ridgway *et al.* 1992), but for the purposes of this paper, we have separated the data into two epochs: 8/21/90 (φ = 0.85) and 9/19/90 (φ = 0.94). We note that the phases calculated for these two epochs were incorrectly listed in Ridgway *et al.* (1992). Spectral type and K band flux for Mira was estimated from phase-dependent values given in L&W. Size scaling of the star's uniform disk angular diameter θ_{UD} to Rosseland diameter θ_R was calculated as discussed in §7.3.3; this scaling is different than the scaling applied in Ridgway *et al.* (1992), but is consistent with expected scaling (Ridgway 1996, Haniff 1996). Distances for Mira can be found from trigonometric parallax (van Altena, Lee & Hoffleit 1991) and also from the other indirect estimates (Wyatt & Cahn 1983, Jura & Kleinmann 1992); a weighted average of these measurements was utilized as a reasonable estimate of the true distance of Mira.

R Leo. This star was observed by Di Giacomo *et al.* (1991) via lunar occultation. Spectral type was determined from phase-dependent values given in L&W and the K band magnitude was estimated from Gezari *et al* (1993). A distance estimate to R Leo was computed by taking a weighted average of values found in Wyatt & Cahn (1983), Celis (1984), van Altena, Lee & Hoffleit (1991) and Jura & Kleinmann (1992). We note that T_{EFF} and R were determined from the published θ_{UD} by the methods presented in

§7.3; compared to the values determined independently by Di Giacomo *et al.*, they agree to within 1% and 5%, respectively.

S Psc, U Ari, VV Sgr. The angular diameters for these stars were determined by Ridgway *et al.* (1979) by lunar occultation, with VV Sgr being observed twice (24 Aug 1977 & 24 May 1978). Determination of the phase of VV Sgr was not possible; light curve data was not available, and the zero epoch date in the *GCVS* was 50+ cycles old. Spectral types for S Psc and U Ari were determined from phase-dependent values given

Table 7.5. Previous angular size observations of Mira variable stars.

Star	Date	P (d)	φ	Spectral Type	Ref	K	Ref	F_{BOL} [10^{-8} erg/cm^{2}s]	θ_{UD} [mas]	Ref	λ [μm]	$\Delta\lambda$ [μm]	Scaling	θ_R [mas]	T_{EFF} [K]	D [pc]	R [$R_\odot$]
o CET	08/21/90	331.8	0.85	M8.5	1	-2.20	1	1387.44	37.04	4	2.20	0.40	0.98	36.30	2371	89	346
o CET	09/19/90	331.8	0.94	M6.5	1	-2.60	1	2668.17	35.93	4	2.20	0.40	0.98	35.22	2835	89	336
R LEO	05/02/90	313.7	0.21	M7	1	-2.65	3	1592.99	33.00	5	2.16	0.04	1.11	36.63	2443	101	398
S PSC	12/02/76	411.1	0.92	M6.5	2	2.44	3	12.93	3.84	6	2.23	0.14	0.98	3.76	2288	918	371
U ARI	09/03/77	372.0	0.49	M8	2	1.48	3	38.57	6.11	6	1.62	0.42	1.00	6.11	2360	620	407
VV SGR	08/24/77	401.5				1.97	3	30.51	5.21	6	1.62	0.42	1.00	5.21	2410	700	392
VV SGR	05/24/78	401.5				1.97	3	30.51	4.99	6	2.17	0.03	1.00	4.89	2488	700	375

1. Lockwood & Wing (1971); 2. Lockwood (1972); 3. Gezari *et al.* (1993); 4. Ridgway *et al.* (1992); 5. Di Giacomo *et al.* (1991); 6. Ridgway *et al.* (1979)

in L&W and Lockwood (1972); the K band magnitude for each of the three stars was estimated from values in Gezari *et al.* (1993). The U Ari observations were in the J band; a 1.6 μm θ_{UD} to θ_R scaling factor was calculated using the pertinent data from S&T, using the method discussed in §7.3.3. For both of the observations of VV Sgr, a scaling factor of 1 was employed since determination of phase was not possible. A distance estimate to S Psc was found in Onaka, De Jong & Willems (1989), who used their method of modeling dust shell spectra; distance estimates to U Ari are in Wyatt & Cahn (1983), Jura & Kleinmann (1992). A distance estimate to VV Sgr can be found in Nguyen-Q-Rieu *et al.* (1979), who utilized the period-mean maximum visual absolute magnitude relationship found in Clayton & Feast (1969) and Foy, Heck & Mennessier (1975); however, the indicated value of 1375 pc results in a linear diameter more than a factor of 2 larger than diameters for other Mira variables of the same type. Alternatively, we may estimate its distance from the distances derived for the other stars in the sample, under the crude assumption that all Miras have equal *K* luminosities. This method results in a distance of 700 pc which produces a more consistent value for the radius; we adopt this value for the remainder of the discussion.

7.4 Discussion

7.4.1 Relationships among the Derived Quantities

Now that we have established values for the basic properties of phase, spectral type, bolometric flux, effective temperature and radius for the Mira variables we observed, we will investigate possible relationships between these basic stellar

parameters. We must stress that treating the Mira variables as identical stars is a crude assumption; however, we are attempting to investigate the gross behavior of these similar stars. We also note that, aside from radius, these parameters are the direct result of observational data and do not make any assumptions about the pulsation mode of the stars. As we mentioned above, two of the approaches for deriving distances, and hence linear radii, presume to varying extents fundamental mode pulsation; however, we reiterate that the third approach of Celis avoids such assumptions and produces numbers in rough agreement with the first two methods.

7.4.2 Effective Temperature Versus Spectral Type

In a previous paper (Dyck *et al.* 1996), we used angular size measurements from the IOTA interferometer to investigate the dependence of T_{EFF} upon spectral type for a large sample (66) of giant and a smaller sample (11) of supergiant stars. Our results refined the mean T_{EFF}-spectral type relationship for giant stars from the spectral types K1 through M7. The data set on luminosity class I and I-II stars in our sample indicated that they are roughly 400 K cooler than their giant counterparts at a spectral type of K4.5; the data suggested that the effective temperature difference between supergiants and giants approaches zero as the spectral type approaches to M6. In contrast, the Mira variables observed for this paper are considerably cooler than their giant counterparts at spectral types *later* than M6.

For stars with effective temperature errors less than 250 K we have plotted the spectral type and effective temperature data in Figure 7.1, where we have included, for

comparison, the earlier results obtained for K and M giants and supergiants. The mean value of the effective temperature as a function of spectral subclass is listed in Table 7.6 for those Mira variables shown in Figure 7.1. The errors listed were obtained from the standard deviation of the temperatures at each spectral subtype. For the undersampled spectral subclasses M7.0 and M7.5, the error listed in Table 7.6 has been estimated from the average error for better-sampled spectral subclasses (M6.5, M8.0, M8.2), and scaled by $\sqrt{5}/2$ to account for differences in sample size. The data from subclasses M8.2-M9.0 has been collected together for a single estimate of T_{EFF} at subclass M8.5.

Table 7.6. Mira variable mean effective temperatures.

Spectral Type	Mean $T_{EFF}\pm\varepsilon_T$ (K)	Fitted $T_{EFF}\pm\varepsilon_T$ (K)[2]
M6.5	2900±270	2910
M7.0	2770±410[1]	2770
M7.5	2830±410[1]	2640
M8.0	2580±225	2500
M8.5	2520±280	2380

1. Error estimate (see §7.4.3).
2. T_{EFF} = (M subclass) * (-273 ± 40) + (4690 ± 530) *K*.

Although the errors listed in T_{EFF} listed in Table 7.6 are sizable, a great deal of the spread could be due to inaccuracies in determination of spectral subclass for the Miras observed. Since the spectral classifications were inferred rather than directly determined contemporaneously, the possibility of slight misclassification exists. Examining the multiple epoch data of L&W and Lockwood (1972), there appears to be approximately a half to full subclass of spread in the classification for stars as they pass through a given phase point. As a consequence, the errors on spectral type were

assumed to be ±0.33 for the stars in our sample,

Figure 7.1. A plot of effective temperatures versus spectral type for the Mira variables observed, and corresponding giant/supergiant data from Dyck *et al*. (1996).

except for R Aqr, which as noted in §7.3.2 was assumed to be ±1.0. A rudimentary line fit to our T_{EFF} -spectral type data (accounting for errors in both spectral type and T_{EFF}) results in a fit of T_{EFF} = (M subclass) * (-273 ± 40) + (4690 ± 530) *K*, with a reduced χ^2 = 2.47. As evidenced by the χ^2, the fit is indeed rudimentary, but the gross result is that a change on one spectral subclass would affect a change of roughly $\Delta T_{EFF} \approx$ 300K. Contemporaneous spectral typing thus has the potential to greatly reduce the scatter in T_{EFF} -spectral type relationship.

Note that the Mira variables are substantially cooler than the giant stars of the same spectral type. At spectral type M7 the Mira scale is offset to lower temperatures by nearly 400 K; at M8 the Mira scale is about 350 K cooler than the temperature of RX Boo, an M8 giant. These results are a general extension of the earlier finding that the more luminous stars are systematically cooler than the less luminous ones (Dyck *et al.* 1996).

7.4.3 Effective Temperature Versus Phase

We expect from the photometric and spectroscopic studies that the effective temperature of a Mira variable will change during its cycle of variability. As described in §7.3.1 and §7.3.4, phase and temperature as a function of phase have been determined for each of the Mira variables observed at IOTA. We have plotted the data for all the stars in Figure 7.2, where clearly there is a lot of scatter resulting from the poor assumption that the stars are all identical. Nevertheless, we may see a clear trend when the data are averaged into phase bins; this is shown in the figure as a solid line.

As a comparison we have taken the L&W and Lockwood (1972) observations of

Figure 7.2. Effective temperature as a function of phase, including data obtained on this program and data previously published for 5 other Mira variables. Bin size for both the observed Mira variables and the predicted Mira variable behavior is 0.2 of a period. The predicted temperatures have been estimated from the T_{EFF}-spectral type relation illustrated in Figure 7.1 and the phase-dependent spectral type data of Lockwood & Wing (1971) and Lockwood (1972).

the spectral types of several of the stars we observed (R Aql, o Cet, S Her, U Her, X Oph, R Peg) made over several cycles, converted them to effective temperatures using the linear relation described in §7.4.2, averaged the results and plotted the averages in Figure 7.2 as a dashed line. One may see that the expected variation of the effective temperature, based upon the L&W and Lockwood (1972) data, is such that it peaks slightly after maximum visible light (at phase ≈ 0.1) and has its minimum near phase 0.6-0.7; the amplitude of the variation is about 400 K, ranging from 2500 K to 2900 K. Averages of our heterogeneous data are consistent with these patterns; we note that the greatest deviation between the two sets of T_{EFF} data is at a phase of 0.7, where our data is the most sparse.

As was mentioned in §7.3.3, our analysis was repeated for temperatures obtained without the use of angular size scaling. A plot of these temperatures, not repeated here, showed the same level of scatter and trends as the temperatures determined from the Rosseland-scaled diameters so that the effective temperatures are insensitive to this level of size scaling. This is consistent with expectation that near infrared uniform disk diameters should be reasonable as direct indicators of the true photospheric diameters of Mira variables (Willson 1986).

7.4.4 Radius Versus Effective Temperature

It is also of interest to plot radius versus effective temperature, which we have done in Figure 7.3. Although there is considerable spread with the uncertainty shared between T_{EFF} error and the error in distance measurements, to first order the relation appears linear. For the purpose of further discussion, an error-weighted two

Figure 7.3. Mira variable radius versus effective temperature. To first order these parameters appear to be linearly interrelated for these stars. Initial multi-epoch data supports the hypothesis that these stars are varying along this line over the course of their periods.

dimensional linear least squares fit was performed upon the sample, with the following result:

$$R = 405 \pm 16 \ R_{\_} - 0.233 \pm 0.004 \ \frac{R_{\_}}{K} \ x \ (T_{EFF} - 2500K),$$

with a reduced chi-square of 0.94.

Suppose that Miras variables, to first order, over the course their cycles oscillate along the line segment fit to the data, with their amplitudes limited by the observed locus of data points. We can use our line fit to specify surface area as a temperature dependent quantity; the product of that area and the Planck function gives the total power at any wavelength for a given temperature. The range of temperatures can be estimated from the observed phase-dependent variation; in §7.4.3 the variation was indicated to be approximately 400 K, between 2500 K and 2900 K. The fit of equation (21) indicates a size range of 405 $R_{\odot}$ to 310 $R_{\odot}$ from minimum temperature to maximum temperature, a variation of roughly 25%, which is consistent with our observed radius variations. Under this hypothesis, three features are predicted to be seen in Mira variable observational data as the temperature varies. First, the visible light flux reaches extremes at either edge of the temperature range, maximizing at a temperature of about 2900 K and minimizing at about 2500 K. The difference in flux over the course of the cycle corresponds to a factor of 2.9, or approximately 1.2 mag. Second, the K flux peaks at about 2500 K, and reaches minimum value at about 2900 K. In this wavelength band, the difference in flux corresponds to a factor of 1.1, or about 0.14 mag. Third, since the two wavelength bands peak at separate temperatures, the V and K band maxima exhibit

a phase shift relative to one another during a Mira's cycle. A cursory examination of our result indicates that the value of the phase lag is approximately 0.5.

Each one of these three predicted characteristics of Mira variables is in gross agreement with the actual observed behavior of Mira variables. The observed variation of a Mira variable in the V band ranges from ΔV _ 2.5 mag up to ΔV _ 6 mag for the more extreme Mira variables (e.g. R Cas). Examining the K band light curves presented in L&W, we find a diminished K band variability relative to the V band variability. The K band variation seen in the limited L&W infrared data is in the ΔK _ 1 mag range. Also, the delay of maximum with increasing wavelength is a well-known characteristic of Mira variables (Pettit & Nicholson 1933; L&W; Barnes 1973); L&W observed the K band lag to be approximately 0.1-0.2. For each of the three light curve characteristics expected from our simple hypothesis, there is poor *specific* agreement between the observations and the expectations (e.g. $\Delta K_{observed}$ _ 1 mag vs. $\Delta K_{predicted}$ _ 0.14 mag) ; however, the gross agreement (e.g. phase lag prediction, diminished *K* variability) indicates that to first order the simple line fit begins to explain the behavior of the stars. Higher order perturbations upon the line fit have the potential to refine the agreement between the specific numeric predictions and the observed data; such perturbations will be calculatable when further multiple epoch data becomes available.

As an observational check of this hypothesis, the sample of two-epoch data we have at present (R Aql, R Aqr, X Oph, R Peg, S Peg and the o Cet data from Ridgway *et al.* 1992) can be plotted on a similar illustration as Figure 7.3; the changes observed in

the effective temperatures and radii for these stars is entirely consistent with this hypothesis and can be seen in Figure 7.4. For the stars observed at IOTA, there is an average $\Delta\varphi = 0.31$ (range 0.23-0.41), whereas Ridgway *et al.*'s o Cet data has $\Delta\varphi = 0.09$.

7.4.5 Oscillation Mode

The results presented in this paper have the potential to constrain the ongoing debate regarding the pulsation of Mira variables. Specifically, the common lament is for improved values for effective temperatures and radii (see Ostlie & Cox 1986, Perl & Tuchman 1990). As an initial evaluation using our data, we examine the period-mass-radius (PMR) relations developed by Ostlie & Cox (1986, henceforth O&C) by means of a linear pulsation study. For fundamental mode and first overtone pulsators, respectively:

$$\log P = -1.92 - 0.73 \log M_0 + 1.86 \log R,$$
$$\log P = -1.60 - 0.51 \log M_1 + 1.59 \log R.$$

From these two relations, estimates of the oscillation mode can be calculated for a star of known mass, given observations of period and radius, with the caution that these relations generally apply to a mean radius for the star. We have plotted our radius and period data in Figure 7.5 along with the O&C relationships for fundamental and first-overtone pulsations; stellar mass is listed as a parameter for each of the pulsation modes. Shown for comparison are the visible HS&T results, and the infrared data for the other 5 stars taken from the literature (as discussed in §7.3.6). Results from other PMR relations developed by Fox & Wood (1982) and Wood (1990) were also

Figure 7.4. As Figure 7.3, but for the five stars for which multiple epoch data has been obtained. Multiple epoch data on o Cet from Ridgway *et al.* (1992) have also been plotted. For the stars observed at IOTA, approximately one third of a period has elapsed ($\Delta\varphi$ = 0.31, range 0.23-0.41), whereas Ridgway *et al.*'s o Cet data has $\Delta\varphi$ = 0.09.

evaluated, producing essentially the same results.

Using the O&C relations to determine the oscillation mode of a Mira variable requires that an acceptable range of masses for the stars be specified. These are generally established by statistical arguments based upon numbers, galactic distribution and expected lifetimes. There is not general agreement for the Mira variables: Willson (1982), Wood (1982) and Willson (1986) favor a mass range $0.8\ M_{\odot} < M < 3.0\ M_{\odot}$ while HS&T prefer $1.0\ M_{\odot} < M < 1.5\ M_{\odot}$ based upon arguments about mass loss (Knapp & Morris 1985). The choice of mass range has interesting consequences. In Figure 7.5 we designate by lines the regions for the two mass limits which support first overtone and fundamental oscillation modes. In this figure we have plotted our data as well as the visible light data from HS&T. For the wider mass range cited above, we find that our infrared data lie in *both* the first overtone and fundamental oscillation mode regions. For the narrow mass ranges, we see that our data lie primarily *between* the regions indicating fundamental and first overtone modes. Also, since a certain amount of spread in our radius data could be due to distance errors and potential stellar asymmetries, we can attempt to circumvent these effects by examining our data set as a whole. The unweighted average radius is $376\pm86\ R_{\odot}$, and the unweighted average period is 363±51 days (unweighted since the dominant source of radius error is typically a 20% distance error); the indicated mass and mode of this composite data point could be taken to be either fundamental mode, on the high end (~ $3.0\ M_{\odot}$), or first overtone, on the low end of masses (~ $0.8\ M_{\odot}$). For these reasons we favor the larger range of

masses.

Note that the HS&T radii lie within our sample but all at the high end of the

Figure 7.5. A plot of the derived Mira variable radius and period data. Overplotted is the visible-light Mira data of Haniff, Scholz & Tuthill (1995) and the previously-published infrared data for the 5 other stars discussed in the text. Lines indicate regions for fundamental and first overtone masses for both 0.8-3.0 $M_{\odot}$ (dash) and 1.0-1.5 $M_{\odot}$ ranges (dot), as determined by the period-mass-radius relations of Ostlie & Cox (1986). Mass increases with radius for a given mode and period.

range of the radii. The mean radius from the HS&T study is 443 $R_{\odot}$ and from our study is 376 $R_{\odot}$ (with unweighted standard deviations of 43 $R_{\odot}$ and 86 $R_{\odot}$, respectively); that is, the HS&T radii are 18% larger than ours in the mean. In contrast to our finding of either/neither oscillation mode, dependent upon the mass range chosen, HS&T's results strongly indicated first overtone oscillation, due to the larger indicated diameter from their visible light data. As a verification of our interferometric data, the other infrared size data was examined for significant deviations from our results; the mean of 368 $R_{\odot}$, with a standard deviation of 39 $R_{\odot}$, is entirely consistent with our observations. The conclusion of HS&T strongly indicated that a narrow mass range is appropriate for Mira variables; the different conclusions between our study and that of HS&T is troubling and may be examined further.

We note that the data of HS&T incorporates, for each star, multiple epochs of data without any apparent discrimination for the proximity of these stars to maximum or minimum. Hence, the radii determined by HS&T are in certain cases averaged, in the presence of even coverage throughout the cycle. A net result would be the reduction of overall spread in their data set, indicating a 1.0 $M_{\odot} < M < 1.5\ M_{\odot}$ mass range, narrower than the range indicated by our single epoch data. While an *average* Mira radius might actually be more appropriate for establishing stellar mass within the context of PMR relations, we note that our data set average is outside the narrow mass range for either fundamental or first overtone pulsation, as discussed above.

An important source of errors arises from the lack of geometrically determined

distances. This is likely to scale the whole set of radii, rather than to move the HS&T sample selectively with respect to ours. In §7.3.3, we noted that observations of o Cet (Karovska *et al.* 1991) indicated up to a 20% asymmetry in the photospheric extension, a difference coincidentally close to the difference in mean radii between our study and the HS&T study. Could this be the cause of the difference between our observations and the optical wavelength data of HS&T? If this were to be the case, we would need to observe the minor axis preferentially and HS&T the major axis preferentially, an unlikely circumstance.

Independent of the distance estimates, however, we can compare angular diameters of stars common to both data sets. There are three stars common to the two data sets: R Aql, R Cas, and U Ori. The angular diameters of these stars derived by HS&T are systematically larger than ours by a factor of 1.76±0.16. Although small-number statistics could produce a systematic difference for the three stars, one clearly expects some larger and some smaller radii if the result is purely statistical. We may also examine the relative angular diameters for the three stars, normalizing the values to the radii of R Aql presented in our respective data sets; we find:

$$R\,Cas : U\,Ori : R\,Aql = \left\{ \begin{array}{c} 1.42 \pm 0.27 : 1.06 \pm 0.26 : 1.00 \pm 0.30\ HS\ \&T, \\ \\ 1.26 \pm 0.11 : 1.03 \pm 0.08 : 1.00 \pm 0.08\ This\ paper. \end{array} \right\}$$

We note that the 'E model' θ_R values that HS&T preferred have been used in the comparison; also, our φ = 0.90 R Aql data has been used in the comparison, which is consistent with HS&T's φ = 0.06 R Aql data (both data points are at maximum light);

also, the R Cas and U Ori data are at maximum light for both HS&T and the data presented in this paper. This result, which is more or less scaling independent, is indicative of the general *observational* agreement between our data sets and that more appropriate Rosseland mean scaling factors would produce closer final results. As was noted in §7.3.3, the lack of existing models to account for certain aspects of the stellar pulsation physics has the potential for poor agreement between Rosseland diameters derived from differing wavelengths; the general observational agreement between HS&T's and our data sets is a strong indication that more complete Mira variable models are necessary for achieving complete agreement between the two data sets.

Comparison of the two data sets to the recent dynamic atmospheres models of Bowen (1988, 1996), also indicates that the models utilized are incompletely describing the brightness profiles of these stars. Close agreement of the P-L relationship from the Bowen models with the observed P-L data (Willson, Bowen & Struck 1996) strongly suggests that dynamic models are necessary for reconciling not only the two data sets, but observational data in general with theoretical expectations. Comparing the Bowen P-L relation (in the form of a P-R relation) to both our data and HS&T's (Willson 1996), both sets derive radii in excess of that expected from the Bowen models. From the expected size at an average period of $\log \underline{P}=2.56$, the HS&T E model data are too large by an average 160 $R_{\odot}$, while our data at $\log \underline{P} = 2.57$ are too large by an average 94 $R_{\odot}$. The agreement of the Bowen models with the observed P-L data, and the disagreement of our data and HS&T's, suggest that brightness profiles from dynamic pulsation models

will be necessary to reduce the interferometric data with greater accuracy. Additional evidence arises from the fact that the S&T models are unable to yield the same Rosseland mean radius for each of the wavelengths used in the HS&T study (Tuthill 1996).

One further concern regarding use of relations such as those derived by O&C is the argument by Ya'ari & Tuchman (1996) that pulsation features of long-period variables cannot be predicted by linear analysis, but only by full, nonlinear hydrodynamic models. PMR relations, or any similar relations accessible to the data in our sample set, unfortunately do not yet exist for nonlinear models.

In spite of the many possibilities for uncertainty, we are encouraged by the lower limit of the PMR data. None of our lowest mass fundamental mode-indicated oscillators dip below the 0.8 $M_{\odot}$ lower edge. We note that an extension of the upper end of the Mira variable mass range to 4.0 $M_{\odot}$ would include all but two of our stars in the fundamental mode (S Ori, S Peg being the exceptions), though at this point the regions occupied by two modes begins to overlap seriously.

7.5 Conclusions

The IOTA program of observing Mira variable stars has resulted in a much greater number of near-infrared angular size measurements for Miras; previous results were available for only five of these stars. Determinations of T_{EFF} and radius are possible with the caveat that the radii depend upon poorly-known distances; we have established an effective temperature-spectral type relationship for the range M6.5-M8.5. The

period-dependent temperature and radius variations of these stars are interrelated, as would be expected. The atmospheric models that are utilized in reducing the visibility data clearly play a significant role in the results obtained; the inability of current models to describe the complex extended atmospheres of these stars precisely at all wavelengths is highlighted by the disagreement between our infrared results and HS&T's visible results. Although our data indicate that Mira variables may oscillate in both fundamental and first-overtone modes, depending upon the star, the disagreement with the HS&T results indicates that it may be premature to draw firm conclusions about the oscillation mode from the angular diameter data. However, our data would appear to agree with estimates that the mass range for Mira variables is 0.8 - 3.0 $M_{\odot}$.

CHAPTER VIII

CONCLUSION

8.1 Summary of Results

The most significant contribution of this dissertation is in the refinement (and in certain cases, establishment) of certain basic stellar parameters:

- Effective temperatures and linear sizes were defined & refined for oxygen-rich, S-type and carbon stars, for both Mira variables and non-Miras (§4).
- For K & M giants and carbon stars, effective temperature was correlated with spectral type (§5,6).
- For oxygen-rich Mira variables, the periodic nature of linear size and effective temperature was established (§7).

Utilization of these basic parameters opened the door to more complicated investigations of stellar physics, including:

- oxygen-rich Mira variable pulsation mode (§7.4), and
- relative mass loss rates between the chemical abundance types (§4.4).

8.2 Future Research

There are two specific areas of further research possible with the IOTA interferometer: First, continuing investigations into the objects examined in this dissertation; and Second, investigations into new classes of objects accessible to the instrument through system upgrades. On the first score, while the initial research of this dissertation is complete, additional research will advance the results obtained. For

Table 8.1. General results of the dissertation: effective temperatures and radii for highly evolved stars.

	non-Mira	*Mira*
Effective Temperature (*K*)		
oxygen-rich	3300 ± 200[1]	2700 ± 300
S type	3100 ± 200	2400 ± 200
carbon	2900 ± 200	2200 ± 200
Radii ($R_{\odot}$)		
oxygen-rich	160 ± 50[2]	380 ± 90
S type	300 ± 90	530 ± 140
carbon	400 ± 110	650 ± 170

1. Estimated from data for M4 and later giant stars.

2. Estimate for M7 giants.

example, the measurement of angular size for an individual variable star over many cycles would provide improved insight into the nature of variability in size and temperature.

Secondly, the IOTA system is slated for a series of upgrades that will open up a number capabilities of the instrument, including:

· visible light fringe detection,

· infrared star tracking,

· improved infrared fringe sensitivity, and

· a third aperture.

Of these, the first - the visible light detector system - has already finished engineering tests and is expected to start producing scientific results over the course of this year. This upgrade provides a factor of four of improvement in resolution, in addition to sampling a physically different region of stellar atmospheres. Use of IOTA in the visible has the potential to resolve a number of main sequence stars, the 'middle-aged' precursors to the highly evolved stars examined in this dissertation. Both infrared tracking and improved infrared sensitivity will make young stellar objects (YSOs) observable by IOTA. YSOs are the precursors to main sequence stars, and observations of these objects would make research on the complete sequence of stellar evolution accessible to IOTA - from stellar birth to mid-life to death. Finally, a third aperture would allow for retrieval of closure phase information, and hence, image reconstruction with the interferometer.

REFERENCES

Chapter I

Abell, G.O., Morrison, D. & Wolff, S.C., 1987, Exploration of the Universe, 5th ed., (Philadelphia: Saunders College Publishing).

Angel, J.R.P., 1990, in Modern Technology and its Influence on Astronomy, Wall, J.V. & Boksenberg, A., eds., (New York: Cambridge), 143.

Baldwin, J.E., Beckett, M.G., Boysen, R.C., Burns, D., Buscher, D.F., Cox, G.C., Haniff, C.A., Mackay, C.D., Nightingale, N.S., Rogers, J., Scheuer, P.A.G., Scott, T.R., Tuthill, P.G., Warner, P.J., Wilson, D.M.A., Wilson, R.W., 1996, *A&A*, **306**, 13.

Barr, L.D., ed., 1990, *Advanced Technology Optical Telescopes IV*, *Proc. SPIE*, **1236**.

Black, D.C., 1995, *BAAS*, **187**, 93.04.

Born, M., Wolf, E., 1980, Principles of Optics, 6th ed. (Oxford, London, New York : Pergamon Press)

Carleton, N.P., Traub, W.A., Lacasse, M.G., Nisenson, P., Pearlman, M.R., Reasenberg, R.D., Xu, X., Coldwell, C., Panasyuk, A., Benson, J.A., Papaliolios, C., Predmore, R., Schloerb, F.P., Dyck, H.M., Gibson, D., 1994, *Proc. SPIE,* **2200,** 152.

Chandler, J.F. & Reasenberg, R. D., 1990, in Inertial Coordinate System on the Sky, Proc. IAU Symp. 141, (Dordrecht, Kluwer), p. 217-228.

Coulman, C.E., 1985, *ARAA*, **23**, 19.

Currie, D.G., Knapp, S.L., Liewer, K.M., 1974, *ApJ*, **187**, 131.

Dainty, J.C., 1981, in Symposium on Recent Advances in Observational Astronomy, Johnson, H.L. & Allen, C., eds., (Mexico), p. 95.

Davis, J., Tango, W.J. (eds.), 1979, Proc. of IAU Colloq. No. 50, "High Angular Resolution Stellar Interferometry", (Australia: University of Sydney).

Davis, J. , Tango, W.J., 1986, *Nature*, **323**, 234.

Davis, J. 1994, in Very High Angular Resolution Imaging, Proc. IAU Symp. 158, ed. J.G. Robertson and W.J. Tango (Dordrecht, Kluwer), p. 135.

Dyck, H.M, Howell, R.R., 1983, *PASP*, **95**, 786.

Dyck, H.M., Kibblewhite, E.J., 1986, *PASP*, **98**, 260-267.

Dyck, H.M., Benson, J.A. & Ridgway, S.T., 1993, *PASP*, **105**, 610-615.

Dyck, H.M., Benson, J.A., Carleton, N.P., Coldwell, C., Lacasse, M.G., Nisenson, P., Panasyuk, A., Papaliolios, C., Pearlman, R.D. & Reasenberg, R.D., 1995, *AJ*, **109**, 378.

Elliot, J.L., Glass, I.S., 1970, *AJ*, **75**, 1123.

Fizeau, H., 1868, *Compt. Rend. Acad. Sci. Paris*, **66**, 934.

Fried, D.L., 1966, *JOSA*, **56**, 1372.

Gay, J., Mekarnia, D., 1988, *Proc. NOAO-ESO*, **29**, 811.

Gezari, D.Y., Labeyrie, A., Stachnik, R.V., 1972, *ApJL*, **173**, L1.

Glass, I.S., Elliot, J.L., 1972, *AJ*, **77**, 523.

Hanbury Brown, R., Twiss, R.Q., 1954, *Phil. Mag.*, **45**, 663-82.

Hanbury Brown, R., Twiss, R.Q., 1956, *Nature*, **178**, 1046.

Hanbury Brown, R., Twiss, R.Q., 1957, *Proc. Roy. Soc. London*, **A 242**, 300-24.

Hanbury Brown, R., Twiss, R.Q., 1957, *Proc. Roy. Soc. London*, **A 243**, 291-319.

Hanbury Brown, R., Twiss, R.Q., 1958, *Proc. Roy. Soc. London*, **A 248**, 199-221.

Haniff, C.A., Buscher, D.F., 1992, *JOSA A*, 9, 203.

Haniff, C.A., Mackay, C.D., Titterington, D.J., Sivia, D., Baldwin, J.E. & Warner, P.J., 1987, *Nature*, 328, 694.

Hutter, D.J., Elias, N.M., II, Hindsley, R.B., Hummel, C.A., Armstrong, J.T., Buscher, D.F., Mozurkewich, D., Johnston, K.J., Westerhout, G. & White, N.M., 1993, *BAAS*, **183**, 73.07.

King, H.C., 1979, The History of the Telescope, (New York: Dover).

Kulagin, E.S., 1970, *Soviet Astronomy*, **13**, 1023.

Korff, D., 1973, *JOSA*, **63**, 971

Labeyrie, A., 1970, *A&A*, **6**, 85.

Labeyrie, A., 1978, *ARAA*, **16**, 77.

McAlister, H.A., 1992, in A Lunar Optical-Ultraviolet-Infrared Synthesis Array (LOUISA), (New Mexico Univ.), p. 18-34.

McCarthy, D.W., Low, F.J., 1975, *ApJL*, 202, L37.

McCarthy, D.W., Low, F.G. & Howell, R.R., 1977, *ApJL*, 214, L85.

McCarthy, D.W., Low, F.G. & Howell, R.R., 1977, *Opt. Eng.*, 16, 569.

Merrill & Anderson, 1920, *ApJ*, **51**, 263.

Michelson, A.A., 1890, *Phil. Mag.*, (5th Series), **30**, 1.

Michelson, A.A., 1891, *Nature*, **45**, 160.

Michelson, A.A., Pease, F.G., 1921, *ApJ*, **53**, 249-259.

Nakajima, T., Kulkarni, S.R., Gorham, P.W., Ghez, A.M., Neugebauer, G., Oke, J.B., Prince, T.A. & Readhead, A.C.S., 1989, *AJ*, 97, 1510.

Pease, F.G., 1931, *Ergeb. Exaten Naturwiss.*, **10**, 84.

Shao, M., Staelin, D.H., 1980, *App. Opt.*, **19**, 1519.

Shao, M., Colavita, M.M. & Staelin, D.H., 1986, *Proc. SPIE*, **628**, 250.

Shao, M., 1992, in A Lunar Optical-Ultraviolet-Infrared Synthesis Array (LOUISA), (New Mexico Univ.), p. 109-113.

Shao, M., Livermore, T.R., Wolff, D.M., Yu, J.W., Colavita, M.M., 1995, *BAAS*, **187**, 71.03.

Stèephan, 1873, *Compt. Rend. Acad. Sci. Paris*, **76**, 1008.

Stèephan, 1874, *Compt. Rend. Acad. Sci. Paris*, **78**, 1008.

Tango, W.J., 1979, Proc. of IAU. Colloq. No. 50, "High Angular Resolution Stellar Interferometry", (Australia: University of Sydney), 13-1.

Townes, C.H., Danchi, W.C., Sadoulet, B. & Sutton, E.C., 1986, *Proc. SPIE*, **628**, 281.

Twiss, R.Q., Tango, W.J., 1977, *Revista Mexicana de Astr. Astrofísica*, **3**, 35.

Weiler, E., Kaplan, M., Thronson, H., 1995, *BAAS*, **187**, 71.01.

Chapter II

Hanbury Brown, R., Davis, J., Lake, R.J.W. & Thompson, R.J., 1974, *MNRAS*, **167**, 475

Hecht, E., 1990, *Optics*, (Reading, MA: Addison-Wesley Publishing Co., Inc.)

Meyer-Arendt, J.R., 1972, *Introduction to Classical and Modern Optics*, (Englewood Cliffs, NJ: Prentice-Hall, Inc.)

Michelson, A.A., 1890, *Phil. Mag.*, (5th Series), **30**, 1

Schroeder, D.J., 1987, *Astronomical Optics*, (San Diego: Academic Press, Inc.)

Steward, E.G., 1983, *Fourier Optics: An Introduction*, (New York: Halsted Press)

Chapter IV

Baud, B. & Habing, H.J., 1983, *A&A*, **127**, 73.

Bieging, J.H. & Latter, W.B., 1994, *ApJ*, **422**, 765-782.

Carleton, N.P., Traub, W.A., Lacasse, M.G., Nisenson, P., Pearlman, M.R., Reasenberg, R.D., Xu, X., Coldwell, C., Panasyuk, A., Benson, J.A., Papaliolios, C., Predmore, R., Schloerb, F.P., Dyck, H.M., Gibson, D., 1994, *Proc. SPIE,* **2200,** 152.

Celis, S.L., 1980, *A&A*, **89**, 145.

Chan, S.J. & Kwok, S., 1988, *ApJ*, **334**, 362-396.

Claussen, M.J., Kleinmann, S.G., Joyce, R.R. & Jura, M., 1987, *ApJS*, **65**, 385-404.

Cohen, M., 1979, *MNRAS*, **186**, 837.

de Jong, T., 1989, *A&A*, **223**, L23-L26.

Dyck, H.M., Lockwood, G.W. & Capps, R.W., 1974, *ApJ*, **189**, 89.

Dyck, H.M., Benson, J.A., Carleton, N.P., Coldwell, C., Lacasse, M.G., Nisenson, P., Panasyuk, A., Papaliolios, C., Pearlman, R.D. & Reasenberg, R.D., 1995, *AJ*, **109**, 378.

Dyck, H.M., Benson, J.A., van Belle, G.T. & Ridgway, S.T., 1996a, *AJ*, **111**, 1705-1712.

Dyck, H.M., van Belle, G.T. & Benson, J.A., 1996b, *AJ*, **112**, 294-300.

Feast, M.W., Glass, I.S., Whitelock, P.A. & Catchpole, R.M., 1989, *MNRAS*, **241**, 375.

Gehrz, R.D. & Woolf, N.J., 1971, *ApJ*, **165**, 285-294.

Gezari, D. Y., Schmitz, M., Pitts, P. S. & Mead, J. M., 1993, *Catalog of Infrared Observations*, NASA Reference Publication 1294.

Groenewegen, M.A.T., de Jong, T., van der Bliek, N.S., Sliijkhuis, S. & Willems, F.J., 1992, *A&A*, **253**, 150-172

Haniff, C.A., Scholz, M. & Tuthill, P.G., 1995, *MNRAS*, **276**, 640.

Herman, J., Burger, J.H. & Penninx, W.H., 1986, *A&A*, **167**, 247.

Hoffliet, D. & Jaschek, C., 1982, *The Bright Star Catalogue* (New Haven: Yale University Observatory).

Horne, J.H. & Baliunas, S.L., 1986, *ApJ*, **302**, 757.

Iben, I., Jr. & Renzini, A., 1983, *ARAA*, **21**, 271-342.

Infrared Processing and Analysis Center (IPAC), *IRAS Point Source Catalog*, 1986.

Ivezi_, Z. & Elitzur, M., 1995, *ApJ*, **445**, 415-432.

Jorissen, A. & Mayor, M., 1992, *A&A*, **260**, 115-132.

Jura, M., 1986, *ApJ*, **303**, 327-332.

Jura, M., 1988, *ApJS*, **66**, 33-41.

Jura, M. & Kleinmann, S.G., 1989, *ApJ*, **341**, 359-366.

Jura, M. & Kleinmann, S.G. 1992, *ApJS*, **79**, 105.

Kholopov, P.N., Samus', N.N., Frolov, M.S., Goranskij, V.P., Gorynya, N.A., Kireeva, N.N., Kukarkina, N.P., Kurochkin, N.E., Medvedeva, G.I., Perova, N.B. & Shugarov, S.Yu., 1988, *General Catalog of Variable Stars, 4th ed.* (Nauka Publishing House, Moscow), (GCVS).

Knapp, G.R., Phillips, T.G., Leighton, R.B., Lo, K.Y., Wannier, P.G., Wootten, H.A. & Huggins, P.J., 1982, *ApJ*, **252**, 616.

Knapp, G.R. & Morris, M., 1985, *ApJ*, **292**, 640.

Kwok, S. & Chan, S.J., 1993, *AJ*, **106**, 2140-2153.

Lang, K.R., 1992, *Astrophysical Data*, (New York: Springer-Verlag).

Little, S.J., Little-Marenin, I.R. & Bauer, W.H., 1987, *AJ*, **94**, 981.

Little-Marenin, I.R., 1986, *ApJ*, **307**, 15.

Lockwood, G.W. & Wing, R.F., 1971, *ApJ*, **169**, 63.

Lockwood, G.W., 1972, *ApJS*, **209**, 375.

Mathis, J.S., 1990, *ARA&A*, **28**, 37.

Neugebauer, G. & Leighton, R.B., 1969, *Two-Micron Sky Survey*, NASA SP-3047.

Ostlie, D. A. & Cox, A. N., 1986, *ApJ*, **311**, 864.

Rowan-Robinson, M. & Harris, S., 1983, *MNRAS*, **202**, 767-795.

Rowan-Robinson, M. & Harris, S., 1983, *MNRAS*, **202**, 797-811.

Scalo, J.M.& Ross, J.E., 1976, *A&A*, **48**, 219-234.

Scargle, J.D., 1982, *ApJ*, **263**, 835.

Scholz, M. & Takeda, Y., 1987, *A&A*, **186**, 200, (S&T).

Schweitzer, E., 1995, Observations from the AFOEV Database, private communication.

Smith, V.V. & Lambert, D.L., 1988, *ApJ*, **333**, 219.

Smith, V.V. & Lambert, D.L., 1990, *ApJS*, **72**, 387.

Thronson, H.A., Latter, W.B., Black, J.H., Bally, J. & Hacking, P., 1987, *ApJ*, **322**, 770.

Tsuji, T., 1981, *J. Astrop. Astr.*, **2**, 95-113.

Tuthill, P. G. 1994, Ph.D. dissertation, University of Cambridge.

van Belle, G.T., Dyck, H.M., Benson, J.A. & Lacasse, M.G., 1996, *AJ* (accepted).

van Altena, W.F., Lee J.T., & Hoffleit, E.D., 1991, in *The General Catalogue of Trigonometric Stellar Parallaxes (1991): a Preliminary Version,* (New Haven: Yale University Observatory).

Willems, F.J. & de Jong, T., 1986, *ApJ*, **309**, L39-L42.

Willems, F.J. & de Jong, T., 1988, *A&A*, **196**, 173-184.

Willson, L.A., 1982, in *Pulsation in Classical and Cataclysmic Variable Stars* (Eds. J.P. Cox & C.J. Hansen), 269.

Willson, L.A., 1986, in *Late Stages of Stellar Evolution* (Eds. S. Kwok & S.R.

Pottasch), Reidel Publishing Co., Dordrecht, Holland, 253.

Willson, L.A., 1988, IAU, Colloquium on the Use of Pulsating Stars in Fundamental Problems of Astronomy, 111th, Lincoln, NB, Aug. 15-17.

Willson, L.A., Bowen, G.H. & Struck, C., 1996, in *From Stars to Galaxies*, (Eds. C. Leitherer, U. Fritze-v. Alvensleben & J. Huchra), ASP Conference Series Vol. 98.

Wilson, 1953, *General Catalogue of Stellar Radial Velocities* (Washington, D.C.: Carnegie Institution of Washington) Publication 601, (GCRV).

Wing, R.F. & Yorka, S.B., 1977, *MNRAS*, **178**, 383-394.

Wood, P.R., 1982, in *Pulsation in Classical and Cataclysmic Variable Stars* (Eds. J.P. Cox & C.J. Hansen), 284.

Wyatt, J.H. & Cahn, S.P., 1983, *ApJ*, **275**, 225.

Yorka, S.B. & Wing, R.F., 1979, *AJ*, **84**, 1010-1019.

Young, K., Phillips, T.G. & Knapp, G.R., 1993, *ApJ*, **409**, 725-738.

Zuckerman, B., Palmer, P., Gilra, D.P., Turner, B.E. & Morris, M., 1978, *ApJ*, **220**, L53-L56.

Zuckerman, B. & Dyck, H.M., 1986, *ApJ*, **304**, 394-400.

Zuckerman, B. & Maddalena, R.J., 1989, *A&A*, **223**, L20-L22.

Chapter V

Benson, J. A. *et al*. 1991, *AJ*, **102**, 2091

Blackwell, D. E. *et al*. 1983, *MNRAS*, **205**, 897

Blackwell, D. E. & Lynas-Gray, A. E. 1994, *A&A*, **282**, 899

Carleton, N. P. *et al.* 1994, *Proc. SPIE*, **2200**, 152

DiBenedetto, G. P. & Rabbia, Y. 1987, *A&A*, **188**, 114

DiBenedetto, G. P. & Ferluga, S. 1990, *A&A*, **236**, 449

DiBenedetto, G. P. 1993, *A&A*, **270**, 315

Dyck, H. M., Lockwood, G. W. & Capps, R. W. 1974, *ApJ*, **189**, 89.

Dyck, H. M., Benson, J. A., Ridgway, S. T. & Dixon, D. J. 1992, *AJ*, **104**, 1982

Dyck, H. M. *et al.* 1995, *AJ*, **109**, 378

Gezari, D. Y., Schmitz, M., Pitts, P. S. & Mead, J. M. 1993, *Catalog of Infrared Observations*, NASA Reference Publication 1294

Gliese, W. 1973, *IAU Symposium No. 50*, edited by Ch. Fehrenbach & B. E. Westerlund (Reidel, Dordrecht), p. 52

Hanbury Brown, R., Davis, J. & Allen, L. R. 1974, *MNRAS*, **167**, 121

Hayes, D. S. 1984, *Calibration of Fundamental Stellar Quantities*, edited by D. S. Hayes, L. E. Pasinetti and A. G. D. Philip (Reidel, Dordrecht), p. 246

Hayes, D. S. & Latham, D. W. 1975, *ApJ*, **197**, 593

Hoffleit, D. 1982, *Catalog of Bright Stars* (Yale University Press, New Haven)

Hutter, D. J. *et al*. 1989, *AJ*, **340**, 1103

Jenkins, L. F. 1963, *General Catalogue of Trigonometric Stellar Parallaxes* (Yale University Press, New Haven)

Johnson, H. L. 1966, *ARAA*, **4**, 193

Johnson, H. L. 1968, Nebulae and Interstellar Matter, edited by B. M. Middlehurst & L. H. Aller (University of Chicago Press, Chicago), chapter 5

Keenan, P. C. 1942, *ApJ*, **95**, 461

Keenan, P. C. 1963, *Basic Astronomical Data*, edited by K. Aa. Strand (University of Chicago Press, Chicago), chapter 8

Keenan, P. C. & McNeil, R. C. 1989, *ApJS*, **71**, 245

Kukarkin, B. V. *et al*. 1969, *General Catalogue of Variable Stars, Third Edition* (Astronomical Council of the Academy of Sciences in the USSR, Moscow)

Lockwood, G. W. 1972, *ApJS*, **24**, 375

Mathis, J. S. 1980, *ARAA*, **28**, 37

Moore, J. H. & Paddock, G. F. 1950, *ApJ*, **112**, 48

Morgan, W. W. & Keenan, P. C. 1973, *ARAA*, **11**, 29.

Mozurkewich, D. *et al*. 1991, *AJ*, **101**, 2207

Ridgway, S. T., Joyce, R. R., White, N. M. & Wing, R. F. 1980, *ApJ*, **235**, 126

Schmidt-Kaler, Th. 1982, in *Landolt-Börnstein New Series, Volume 2b, Astronomy and Astrophysics - Stars and Star Clusters*, edited by K. Schaifers & H. H. Voigt (Springer-Verlag, New York)

Scholz, M. 1985, *A&A*, **145**, 251

Scholz, M. & Takeda, Y. 1987, *A&A*, **186**, 200

Tsuji, T. 1978, *PASJ*, **30**, 435

Wright, K. O. 1970, *Vistas in Astronomy*, **12**, 147

Chapter VI

Carleton, N. P. et al. 1994, *Proc. SPIE*, **2200**, 152.

Claussen, M. J., Kleinmann, S. G., Joyce, R. R. & Jura, M. 1987, *ApJS*, **65**, 385.

Cohen, M. 1979, *MNRAS*, **186**, 837.

de Vegt, C. 1974, *A&A*, **34**, 457.

Dunham, D. W., Evans, D. S., Silverberg, E. C. & Wiant, J. R. 1975, *MNRAS*, **173**, 61p.

Dyck, H. M. et al. 1995, *AJ*, **109**, 378.

Dyck, H. M., Benson, J. A., van Belle, G. T. & Ridgway, S. T. 1996, *AJ* (in press).

Eggen, O. J. 1967, *ApJS*, **14**, 307.

Frogel, J. A., Persson, S. E. & Cohen, J. G. 1980, *ApJ*, **239**, 495.

Gezari, D. Y., Schmitz, M., Pitts, P. S. & Mead, J. M. 1993, *Catalog of Infrared Observations*, NASA Reference Publication 1294.

Goebel, J. H., Goorvitch, D., Larson, H. P. & Alexander, D. R. 1993, *ApJ*, **402**, 680.

Haniff, C. A., Scholz, M. & Tuthill, P. G. 1995, *MNRAS*, **276**, 640.

Johnson, H. L., Mitchell, R. I., Iriarte, B. & Wisniewski, W. Z. 1966, *Comm. Lunar & Planetary Lab.*, **4**, 99.

Keenan, P. C. & Morgan, W. W. 1941, *ApJ*, **94**, 501.

Lasker, B. M., Bracker, S. B. & Kunkel, W. E. 1973, *PASP*, **85**, 109.

Lázaro, C., Hammersley, P.L., Clegg, R. E. S., Lynas-Gray, A. E., Mountain, C. M., Zadrozny, A. & Selby, M. J. 1994, *MNRAS*, **269**, 365.

Loup, C., Forveille, T., Omont, A. & Paul, J. E. 1993, *A&AS*, **99**, 291.

Mendoza V., E. E. & Johnson, H. L. 1965, *ApJ*, **141**, 161.

Noguchi, K., Kawara, K., Kobayashi, Y., Okuda, H., Sato, S. & Oishi, M. 1981, *PASJ*, **33**, 373.

Quirrenbach, A., Mozurkewich, D., Hummel, C. A., Buscher, D. F. & Armstrong, J. T. 1994, *A&A*, **285**, 541.

Richer, H. B. 1971, *ApJ*, **167**, 521.

Ridgway, S.T. *et al.*, 1981, "Carbon Star Effective Temperatures", in *Physical Processes in Red Giants*, I. Iben and A. Renzini, eds., (Reidel, Dordrecht, Holland), 47-50.

Ridgway, S. T., Jacoby, G. H., Joyce, R. R., Siegel, M. J. & Wells, D. C. 1982, *AJ*, **87**, 808.

Rowan-Robinson, M. & Harris, S. 1983, *MNRAS*, **202**, 797.

Scholz, M. & Takeda, Y. 1987, *A&A*, **186**, 200.

Tsuji, T. 1978, *PASJ*, **30**, 435.

Tsuji, T. 1981a, *JA&A*, **2**, 95.

Tsuji, T. 1981b, *JA&A*, **2**, 253.

Ulrich, B. T., Neugebauer, G., McCammon, D., Leighton, R. B., Hughes, E. E. &

Becklin, E. 1966, *ApJ*, **146**, 288.

van Belle, G. T., Dyck, H. M., Benson, J. A. & Lacasse, M. G. 1996, *AJ* (accepted).

White, N. M. & Feierman, B. H. 1987, *AJ*, **94**, 751.

Willems, F. J. 1987, in *Late Stages of Stellar Evolution*, S. Kwok & S. R. Pottasch, eds. (Kluwer: Dordrecht), pp. 135-138.

Yamashita, Y. 1972, *Ann. Tokyo Astron. Obs*., **13**, 169.

Yamashita, Y. 1975, *Ann. Tokyo Astron. Obs*., **15**, 47.

Zuckerman, B., Dyck, H. M. & Claussen, M. J. 1986, *ApJ*, **304**, 401.

Chapter VII

Barnes, T.G., III, 1973, *ApJS*, **25**, 369.

Barthès, D. & Tuchman, Y., 1994, *A&A*, **289**, 429.

Blackwell, D. E. & Lynas-Gray, A. E. 1994, *A&A*, **282**, 899.

Bowen, G.H., 1988, *ApJ*, **329**, 299.

Bowen, G. H. & Willson, L. A., 1991, *ApJ*, **375**, L53.

Bowen, G.H., 1996, in prep.

Cahn, J.H. & Wyatt, S.P., 1978, *ApJ*, **221**, 163.

Cannizzo, J. K., Goodings, D. A. & Mattei, J. A., 1990, *ApJ*, **357**, 235.

Carleton, N.P., Traub, W.A., Lacasse, M.G., Nisenson, P., Pearlman, M.R., Reasenberg, R.D., Xu, X., Coldwell, C., Panasyuk, A., Benson, J.A., Papaliolios, C., Predmore, R., Schloerb, F.P., Dyck, H.M., Gibson, D., 1994, *Proc. SPIE,* **2200,**

152.

Celis, S.L., 1980, *A&A*, **89**, 145.

Celis, S.L., 1981, *A&A*, **99**, 58.

Celis, S.L., 1984, *AJ*, **89**, 1343.

Clayton, M.L. & Feast, M.W., 1969, *MNRAS*, **146**, 411.

Di Giacomo, A., Lisi, F., Calamai, G. & Richichi, A., 1991, *A&A*, **249**, 397.

Dyck, H.M., Benson, J.A., van Belle, G.T. & Ridgway, S.T., 1996, *AJ*, **111**, 1705..

Dyck, H.M., Benson, J.A., Carleton, N.P., Coldwell, C., Lacasse, M.G., Nisenson, P., Panasyuk, A., Papaliolios, C., Pearlman, R.D. & Reasenberg, R.D., 1995, *AJ*, **109**, 378.

Dyck, H.M., Lockwood, G.W. & Capps, R.W., 1974, *ApJ*, **189**, 89.

Feast, M.W., Glass, I.S., Whitelock, P.A. & Catchpole, R.M., 1989, *MNRAS*, **241**, 375.

Fox, M.W. & Wood, P.R., 1982, *ApJ*, **259**, 198.

Foy, R., Heck, A. & Mennessier, M.O., 1975, *A&A*, **43**, 175.

Gerasimovic, B.P., 1928, *Proc. Natn. Acad. Sci. U.S.A.*, **14**, 963 (Harv. Reprint 54).

Gezari, D. Y., Schmitz, M., Pitts, P. S. & Mead, J. M., 1993, *Catalog of Infrared Observations*, NASA Reference Publication 1294.

Haniff, C.A., Ghez, A.M., Gorham, P.W., Kulkarni, S.R., Matthews, K. & Neugebauer, G., 1992, *Astronomical Journal*, **103**, 1662.

Haniff, C.A., Scholz, M. & Tuthill, P.G., 1995, *MNRAS*, **276**, 640, (HS&T).

Haniff, C.A., 1996, private communcation.

Hill, S. J. & Willson, L. A., 1979, *ApJ*, **229**, 1029.

Hoffliet, D., 1982, *Catalog of Bright Stars* (Yale University Press, New Haven).

Horne, J.H. & Baliunas, S.L., 1986, *ApJ*, **302**, 757.

Hughes, S.M.G. & Wood, P.R., 1990, *AJ*, **99**, 784.

Jura, M. & Kleinmann, S.G. 1992, *ApJS*, **79**, 105, (J&K).

Karovska, M., Nisenson, P., Papaliolios, C. & Boyle, R.P., 1991, *ApJ*, **374L**, 51.

Kholopov, P.N., Samus', N.N., Frolov, M.S., Goranskij, V.P., Gorynya, N.A., Kireeva, N.N., Kukarkina, N.P., Kurochkin, N.E., Medvedeva, G.I., Perova, N.B. & Shugarov, S.Yu., 1988, *General Catalog of Variable Stars, 4th ed.* (Nauka Publishing House, Moscow), (GCVS).

Knapp, G.R. & Morris, M., 1985, *ApJ*, **292**, 640.

Lockwood, G.W. & Wing, R.F., 1971, *ApJ*, **169**, 63.

Lockwood, G.W., 1972, *ApJS*, **209**, 375.

Mathis, J.S., 1990, *ARA&A*, **28**, 37.

Mattei, J.A., 1995, Observations from the AAVSO International Database, private communication.

Neugebauer, G. And Leighton, R.B. 1969, *Two-Micron Sky Survey*, NASA SP-3047.

Nguyen-Q-Rieu, M., Laury-Micoulaut, C., Winnberg, A. & Schultz, G.V., 1979, *A&A*, **75**, 351.

Onaka, T., De Jong, T., Willems, F.J., 1989, *A&AS*, **81**, 261.

Ostlie, D. A. & Cox, A. N., 1986, *ApJ*, **311**, 864, (O&C).

Pettit, E. & Nicholson, S.B., 1933, *ApJ*, **78**, 320.

Perl, M. & Tuchman, Y., 1990, *ApJ*, **360**, 554.

Ridgway, S. T., Wells, D. C., Joyce, R. R. & Allen, R. G., 1979, *AJ*, **84**, 247.

Ridgway, S.T., Benson, J.A., Dyck, H.M., Townsley, L.K. & Hermann, R.A. 1992, *AJ*, **104**, 2224.

Ridgway, S.T., 1996, private communication.

Robertson, B.S.C & Feast, M.W., 1981, *MNRAS*, **196**, 111.

Rowan-Robinson, M. & Harris, S., 1983, *MNRAS*, **202**, 767.

Scargle, J.D., 1982, *ApJ*, **263**, 835.

Scholz, M. & Takeda, Y., 1987, *A&A*, **186**, 200, (S&T).

Schweitzer, E., 1995, Observations from the AFOEV Database, private communication.

Tuchman, Y., Sack, N. & Barkat, Z., 1979, *ApJ*, **234**, 217.

Tuchman, Y., 1991, *ApJ*, **383**, 779.

Tuthill, P. G. 1994, Ph.D. dissertation, University of Cambridge.

Tuthill, P. G. 1996, private communication.

van Altena, W.F., Lee J.T., & Hoffleit, E.D., 1991, in *The General Catalogue of Trigonometric Stellar Parallaxes (1991): a Preliminary Version,* Yale University Observatory, New Haven, Connecticut.

Willson, L. A. & Hill, S. J., 1979, *ApJ*, **228**, 854.

Willson, L.A., 1982, in *Pulsation in Classical and Cataclysmic Variable Stars* (Eds. J.P. Cox & C.J. Hansen), 269.

Willson, L.A., 1986, in *Late Stages of Stellar Evolution* (Eds. S. Kwok & S.R. Pottasch), Reidel Publishing Co., Dordrecht, Holland, 253.

Willson, L.A., Bowen, G.H. & Struck, C., 1996 in *From Stars to Galaxies*, (Eds. C. Leitherer, U. Fritze-v. Alvensleben & J. Huchra), ASP Conference Series Vol. 98.

Willson, L.A., 1996, private communication.

Wilson, R.W., Baldwin J.E., Buscher D.F. & Warner P.J., 1992, *MNRAS*, **257**, 369.

Wood, P.R., 1982, in *Pulsation in Classical and Cataclysmic Variable Stars* (Eds. J.P. Cox & C.J. Hansen), 284.

Wood, P. R., 1990, in *From Miras to Planetary Nebulae : Which Path for Stellar Evolution?*, ed. M.O. Mennessier & A. Omont (Gif-sur-Yvette: Editions Frontières), 67.

Wood, P. R., 1974, *ApJ*, **190**, 609.

Wyatt, J.H. & Cahn, S.P., 1983, *ApJ*, **275**, 225.

Ya'ari, A. & Tuchman, Y., 1996, *ApJ*, **456**, 350.

Young, K., 1995, *ApJ*, **445**, 872.

A man is a small thing, and the night is very large and full of wonders. - Lord Dunsany, *The Laughter of the Gods.*

About the Author

Gerard van Belle was born in Tallahassee, FL, in 1968. One of his earliest memories is that of watching the Apollo 17 launch; that and a department store telescope purchased for him by his parents ensured that his gaze has ever since been fixed upon the heavens. After two years in the pre-engineering major with the Caltech cooperative program, Gerard switched over to Physics-Astronomy and graduated with honors from Whitman College in 1990. Three years at The Johns Hopkins University produced a master's degree in Physics and a transfer to the University of Wyoming, where he is finally wrapping up the elusive Ph.D. Future plans include working at The Jet Propulsion Laboratory (essentially, being an engineer hired by Caltech - go figure), pursuing the still-elusive pilot's license, and writing The Great American Novel.